The Development and Validation of a Finite Element Model for a Quay Wall in the Amaliahaven Project in the Port of Rotterdam

K.A.Abdel-Rahman

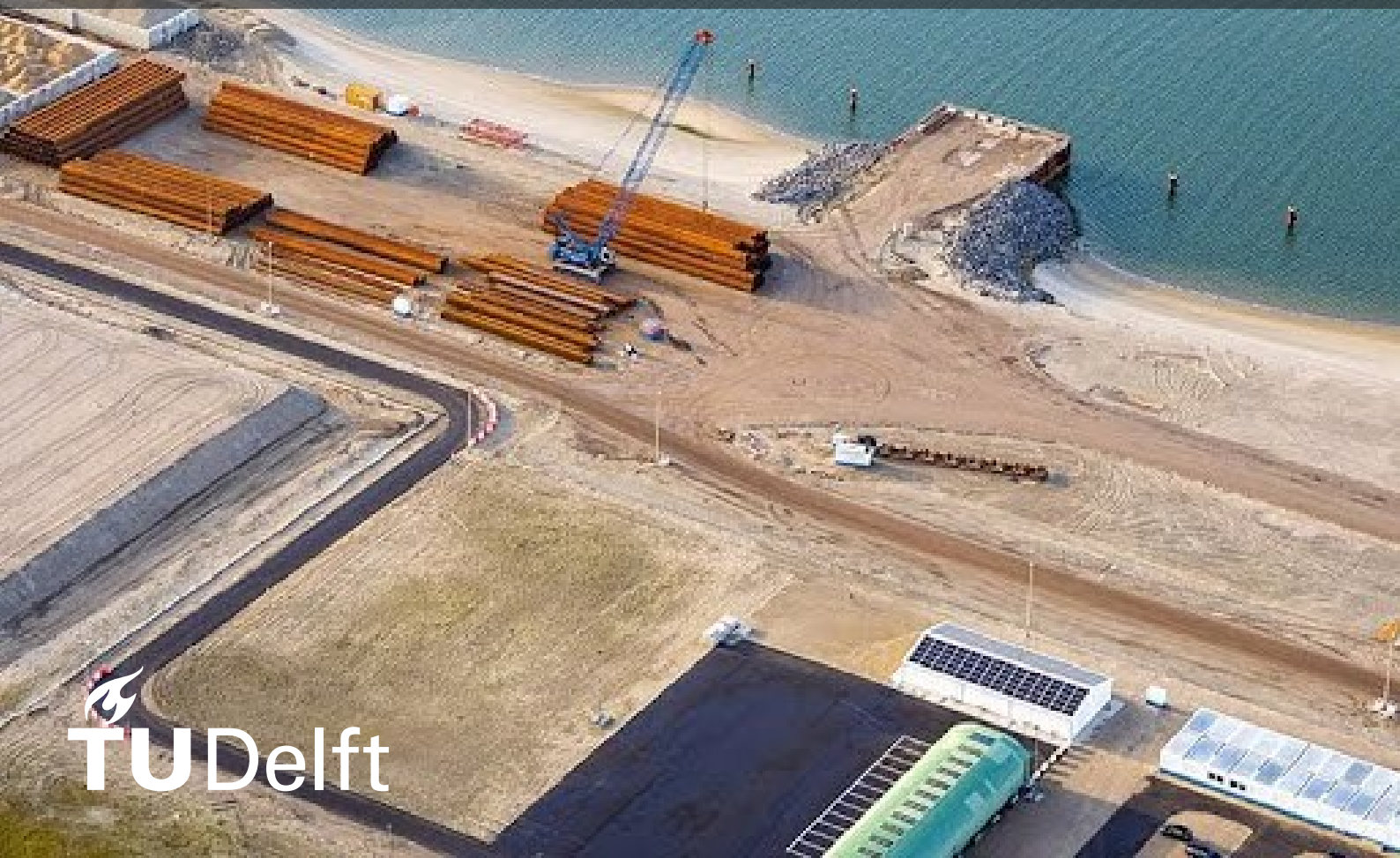

TU Delft

The Development and Validation of a Finite Element Model for a Quay Wall in the Amaliahaven Project in the Port of Rotterdam

by

K.A.Abdel-Rahman

to obtain the degree of Master of Science

at the Delft University of Technology,

to be defended publicly on Friday 29 August, 2025 at 10:00 AM.

Student number:	5957338	
Thesis Committe:	Prof. dr. ir. K.G. Gavin	TU Delft, Chair
	dr. ir. Luca Flessati	TU Delft
	dr. ir. Alex Kirichek	TU Delft
	dr. ir. Ozan Alver	TU Delft

Coverpage: Amaliahaven Quay Wall Construction. Source: Port of Rotterdam

TU Delft

Preface

This thesis, titled ”The Development and Validation of a Finite Element Model for a Quay Wall in the Amaliahaven Project in the Port of Rotterdam”, has been written to fulfill the requirements for obtaining the degree of Master of Science in Civil Engineering, with a focus in Geotechnical Engineering, at Delft University of Technology.

The aim of this research was to develop and validate a finite element model that accurately represents the behavior of a quay wall constructed as part of the Amaliahaven expansion project. This work reflects not only a technical challenge but also a deeply engaging and rewarding conclusion to an eventful and enriching two year academic journey in TU Delft.

I would like to express my sincere gratitude to my daily supervisor Dr. Ozan Alver and my main supervisor Prof. Ken Gavin for their invaluable guidance, critical feedback, and continuous support throughout the course of this work. I am also thankful to the members of my assessment committee, Dr. Luca Flessati and Dr. Alex Kirichek, for their time, insights, and constructive comments.

A heartfelt thank you goes to my family for their unwavering encouragement and support during this entire period. Their presence, even from afar, has been a steady source of motivation.

Working on this thesis has been a genuinely enjoyable experience, and I consider it a fitting conclusion to what has been a unique and fruitful chapter in my life.

K.A.Abdel-Rahman
Delft, August 2025

Abstract

Quay walls are earth-retaining structures that provide berthing for ships, enabling safe loading and unloading operations and secure mooring. As essential components of port infrastructure, they support maritime logistics, global trade, and economic growth. Increasing vessel sizes and operational demands have led to the need for quay walls capable of withstanding greater berthing depths, heavier loads, and more complex service conditions. Finite Element Modelling (FEM) has become a primary tool for investigating their mechanical behavior; however, the reliability of FEM predictions is constrained by uncertainties in soil properties, constitutive model selection, and idealized representation of construction and connection details.

To address these limitations, this study develops, calibrates, and validates a FEM of a smart quay wall in the Amaliahaven Project, Port of Rotterdam, using field monitoring data collected during staged dredging. The quay wall is instrumented with inclinometers that recorded lateral displacements during dredging. Geotechnical parameters were derived from Cone Penetration Tests (CPTs) and empirical correlations, with the Hardening Soil (HS) model adopted as the primary constitutive model. The HSsmall model was also tested to evaluate the influence of small-strain stiffness.

The research employed a staged construction simulation in PLAXIS, incorporating all relevant structural components, including the combi wall, front wall, relieving platform, anchors, and screw injection bearing piles. Initial FEM results systematically underestimated measured displacements. A grouped sensitivity analysis was conducted to identify the most influential parameters across dredging phases, revealing that the friction angles of Layers 1 and 2 and the stiffness moduli of Layers 2 and 3 had the greatest effect on wall behavior. This guided the calibration strategy, where iterative inverse analysis was used to refine stiffness and strength parameters. Calibrated results achieved agreement within the accepted engineering tolerance of ±30% for all dredging phases, with the largest improvement observed at the final stage.

A persistent discrepancy in front wall rotation behavior was traced to the assumed frictionless hinge connection between the front wall and combi wall. Modelling the connection as fixed significantly reduced deviations, achieving errors as low as 13%, and indicating that actual site behavior lies between idealized hinge and rigid conditions. Comparison of HS and HSsmall models showed that small-strain stiffness had minimal influence on predicted displacements for this case, due to the high stiffness of the sand layers and relatively small strain levels during dredging.

A parametric study assessed the effects of dredging depth, surcharge loading, and key soil parameters. Results showed that dredging beyond −21 m NAP caused a progressive increase in maximum lateral displacement, particularly between −22.5 m and −24 m NAP; surcharge loads above 40 kN/m² amplified wall movement, especially in the upper section; and variations in the key parameters identified by the sensitivity analysis produced the most significant changes in displacement magnitude and profile. In all cases, anchor forces remained well below the 2,200 kN design capacity, confirming structural safety.

This research demonstrates that combining sensitivity analysis with targeted calibration can significantly improve FEM predictive accuracy for quay walls. It also highlights the importance of realistic connection modelling and the value of parametric studies in understanding performance under varying operational and geotechnical conditions. The validated modelling framework not only bridges the gap between empirical design and numerical prediction but also provides a robust tool for evaluating future modifications, such as deeper dredging, increased operational loads, or climate-related changes in soil behavior.

Contents

List of Figures

List of Tables

1

Introduction

1.1. Thesis Context

Quay walls are earth-retaining structures that provide berthing for ships, enabling safe loading and unloading operations and secure mooring (De Gijt and Broeken, 2013) [10]. As essential components of port infrastructure, they support maritime logistics, global trade, and economic growth. Advancements in global trade and shipping have led to the increased demand for quay walls that support greater berthing depths and heavier vessel loads.

In addition, quay walls should cater for supporting heavy operational loads, resist vessel impacts, endure environmental conditions and ensure long term stability. Quay walls exhibit complex soil-structure interaction due to the presence of anchors, relieving platforms, and bearing piles.

This thesis focuses on the quay walls of the Amaliahaven Project in the Port of Rotterdam. These are considered smart quay walls because they are equipped with sensors and monitoring systems, including inclinometers that measure lateral displacements of the wall. This research focuses on simulating the dredging phase in a finite element model and validating the model against field measurements collected during dredging. The validated model is then used in a parametric study that considers surcharge loading, dredging level variation, and soil parameter variation.

1.2. Problem Definition

Current quay wall design methods still rely on experience and lack detailed analysis of quay wall behavior during construction and operation. Finite Element Modelling (FEM) has become the primary tool for investigating the mechanical behavior of quay walls. FEM relies on constitutive models to represent soil behavior. These models inherently include uncertainties due to the non-linear and heterogeneous nature of soils. Furthermore, FEM requires the idealization of the soil profile, which impacts model reliability since site soil conditions are only approximated.

To improve the reliability of FEM, it is important to reduce the uncertainties in the input parameters. One approach is to use field measurements to calibrate and validate the FEM. In this study, inclinometer data are employed to iteratively calibrate the soil parameters in the finite element model. This inverse analysis approach involves systematically adjusting input parameters until the model's predictions align with the observed field measurements, enabling the model to accurately represent the quay wall's behavior during the dredging phases.

At the moment, there is little experience with using measurement data from smart quay walls. It is unknown whether the currently collected data provides sufficient information about the behavior of smart quay walls, or if essential information is missing.

The core research problem is the lack of field-validated models that can accurately capture quay wall behavior during critical construction phases like the dredging phase. Bridging this gap is essential for developing more reliable and efficient quay wall designs, and for further enhancing the use of smart

quay walls.

1.3. Research Objective

The aim of this research is to develop, calibrate and validate a reliable finite element model for a quay wall in the Amaliahaven Project in the Port of Rotterdam, using field measurement data collected during the dredging construction phase.

To achieve this aim, a finite element model of the quay wall system was developed using PLAXIS software. The model incorporates key factors such as soil properties, groundwater levels, and the staged dredging construction process. Calibration and validation were carried out using field measurements, specifically inclinometer data, to improve the model's accuracy and reliability.

The calibration process followed a semi-probabilistic inverse analysis approach. Initial soil parameters were derived deterministically from cone penetration test (CPT) data, using the mean values of cone resistance, sleeve friction, and friction ratio for each soil layer. The model was then executed in PLAXIS and its predictions were compared with field observations.

To refine the model further, a sensitivity analysis was conducted using predefined coefficients of variation from the NEN 9997-1. This analysis identified the most influential soil parameters and layers affecting wall behavior. The insights gained guided the iterative parameter adjustments, accounting for expected variability and improving the fit between predicted and observed responses. This approach enhanced the model's reliability while incorporating practical uncertainty.

To achieve this objective, the following research question is defined:

How can a finite element model be developed, calibrated and validated to accurately simulate the behavior of a quay wall in the Port of Rotterdam?

To address this question, a set of sub questions is defined, ensuring a systematic approach to achieve the research objective:

1. What are the key structural and geotechnical factors influencing the mechanical behavior of quay walls during dredging activities?
2. What are the calibration and validation methods available to ensure the finite element model accurately represents the mechanical behavior of the quay walls?
3. How can the Finite Element Method be applied to model the interaction between the quay wall structure and the surrounding soil during dredging?
4. Which soil constitutive model will be used to represent soil behavior in the finite element model, and how will its input parameters be derived?

1.4. Outline of Thesis

In this section, the overall structure of the thesis is presented. For each chapter, the main aim and the key topics covered are summarized.

Chapter 2: Literature Review The aim of the literature review is to provide a scientific foundation by identifying key concepts, methods, and gaps in existing research. The literature review begins by examining the key structural and geotechnical parameters that influence the mechanical behavior of quay walls during dredging activities. It also explores the calibration and validation methods available to ensure that the finite element model accurately represents the mechanical behavior of the quay wall. Furthermore, the literature review investigates how the Finite Element Method can be applied to model the interaction between the quay wall structure and the surrounding soil during dredging. Finally, identifies the soil constitutive model to be used for modeling soil behavior in the finite element model and deriving the input parameters.

Chapter 3: Methodology The aim of the methodology chapter is to present the method applied to achieve the research objective of this thesis. The chapter begins in Section 3.2 with a description of the case study, which includes the geological conditions at the site, the definition of soil stratigraphy, and the development of a representative soil profile for analysis. This is followed by the determination

of the constitutive model parameters required for the FEM. The section concludes with an overview of the quay wall type under study, including its geometry and structural layout. Section 3.3 focuses on the field measurements. It discusses the dredging activities carried out at the site and presents the inclinometer data selected for use in the calibration and validation of the FEM. Section 3.4 outlines the FEM setup in PLAXIS, covering the selection of domain size, mesh size, model assumptions, model inputs, and the description of the construction stages. Section 3.5 presents the calibration and the validation methodology adopted in this study, including a discussion of the sensitivity analysis and its implementation. The purpose of the sensitivity analysis is to evaluate the influence of strength and stiffness parameters of different soil layers on the predicted lateral displacement of the quay wall. This helps identify which parameters have the greatest impact on wall behavior and should therefore be prioritized for iterative adjustment during the inverse analysis using inclinometer data.

Section 3.6 details the parametric study, which explores the quay wall's response to variations in selected strength and stiffness parameters. This study also includes the addition of two extra dredging phases, as well as the introduction and modification of surcharge loads, to investigate their effects on the overall structural response of the quay wall.

Chapter 4: Results and Discussion

The aim of this chapter is to present and interpret the results obtained from the Finite Element Method (FEM) analysis. The analysis focuses primarily on the lateral displacements of the combi wall and front wall throughout the successive dredging phases, as well as the development of anchor forces.

The results are discussed with reference to four distinct FEM scenarios:

1. The initial base model using preliminary soil parameters.
2. The calibrated model, in which parameters were refined based on the sensitivity analysis.
3. A variant model featuring a fixed connection between the combi wall and the front wall, intended to assess the influence of structural connection assumptions.
4. A model incorporating the Hardening Soil model with small-strain stiffness (HSsmall), used to evaluate the effect of enhanced stiffness behavior at low strain levels.

This chapter also presents and discusses the results of the sensitivity analysis, which was conducted to identify the influence of key soil parameters on wall displacements and to support the calibration process. In addition, the outcomes of the parametric study are included, examining how variations in soil properties, dredging stages, and surcharge loads affect the quay wall's structural response.

Finally, the chapter includes the validation process. This is done by evaluating the degree of agreement between the FEM predictions and the field measurements, particularly the inclinometer data, and assesses the reliability and limitations of the modelling approach. This chapter also highlights the implications of modelling assumptions on the overall performance of the quay wall system.

Chapter 5: Conclusion and Recommendations

The aim of this chapter is to summarize the key conclusions of the thesis and offers recommendations based on the research findings. First, the main results and insights derived from the study are discussed. Subsequently, the research sub-questions are addressed based on the outcomes of the analysis and supporting literature. This is followed by an answer to the main research question.

2

Literature Review

2.1. Introduction

The aim of this chapter is to establish the theoretical foundation for developing, calibrating, and validating a finite element model of a quay wall in the Amailahaven project in the Port of Rotterdam. The literature review serves to position this research within existing knowledge on quay wall behavior, soil–structure interaction, and numerical modelling approaches. It emphasizes the importance of addressing geotechnical uncertainties, demonstrates the role of field measurements in model validation, and draws on lessons from previous studies. In doing so, the review provides both the rationale and the methodological basis for the modelling framework adopted in this thesis.

2.2. Overview of Quay Walls

Quay walls are earth-retaining structures that provide berthing for ships, enabling safe loading and unloading operations, and provide secure mooring. The design of a quay wall should meet a set of requirements that depend on factors like the local soil conditions, water levels, and the size of ships and freight loads, (De Gijt and Broeken, 2013) [10].

2.2.1. Functional Requirements

The functional requirements of quay walls include retaining the soil behind the quay wall, providing the bearing capacity to support imposed loads from freight handling and storage, and serving as a water-retaining structure for the areas behind it during periods of high water tides, (De Gijt and Broeken, 2013) [10].

2.2.2. Development Context: Port of Rotterdam

The dimensions of ships play an important role in the design of quay walls. Over time, the dimensions and the load capacity of ships have increased, hence affected the required berthing depth, (De Gijt and Broeken, 2013) [10]. This development is particularly evident in the port of Rotterdam, which is the main focus of this study. Due to increase in the draught of ships, the port of Rotterdam had to be repeatedly deepened and the port area moved further seawards, (De Gijt and Broeken, 2013) [10]. This is clearly illustrated in Figure 2.1 which shows how the growth in ship dimensions has led to an increase in the water depth and thus the retaining height of the quay walls.

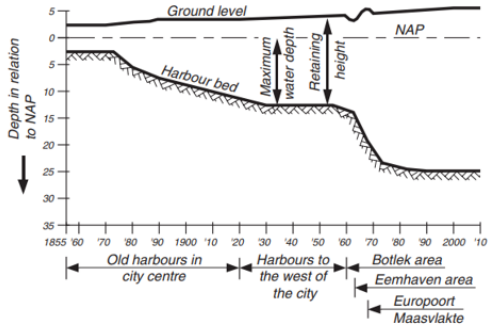

Figure 2.1: History of water depth in the port of Rotterdam [10]

2.2.3. Design and Construction Challenges

The design of quay walls is complex and primarily shaped by practical experience, developed through efforts to solve geotechnical challenges and optimize structural performance. This is particularly evident in Rotterdam, where engineers have consistently faced the challenge of designing quay walls that can support heavier loads and greater retaining heights in weak subsoil conditions, (De Gijt and Broeken, 2013) [10].

2.2.4. Types of Quay Walls

There are four basic types of quay walls namely:

- **Gravity Walls:** For this type of quay wall, the retaining function is obtained by the own weight of the structure [10].
- **Sheet Pile Walls:** For this type of wall, the retaining function is obtained from the soil pressure, combined with an anchorage system and through the bending stiffness of the wall, (De Gijt and Broeken, 2013) [10].
- **Sheet Pile Walls with Relieving Platforms:** This type of wall is similar to the above mentioned in terms of soil retaining, however a reliving platform is incorporated into the structure where its primary purpose is to reduce the lateral soil pressure acting on the wall, (De Gijt and Broeken, 2013) [10].
- **Open Berth Quays:** For this type of quay wall, the structure consists of a deck on piles that extends over a slope [10].

Figure 2.2 illustrates the types of quay walls. The selection of a quay wall type depends on several factors, including the subsoil conditions, the volume and nature of freight to be handled, and the size and type of vessels expected to berth, [10] . The main focus in this research is on sheet pile walls with relieving platforms, which is discussed in more detail in the following section.

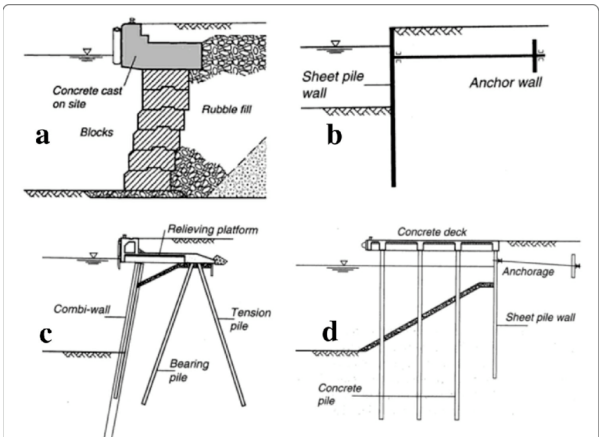

Figure 2.2: Types of Quay walls: (a) Gravity Wall, (b) Sheet Pile Wall, (c) Sheet Pile Wall with Reliving Platform and (d) Open Berth Quays [10]

2.2.5. Sheet Pile Walls with Relieving Platforms

In this type of quay wall, the horizontal load on the front wall is reduced by incorporating a relieving platform [10]. The structure features sheet pile walls on the waterside that serve both bearing and retaining functions, and a foundation system on the landside consisting of bearing piles, with tension piles included in some cases, (De Gijt and Broeken, 2013) [10]. The relieving platform forms a connection between the sheet pile wall and the pile foundation [10].

Sheet pile wall systems derive their retaining capacity and stability from the soil's fixation capacity. For greater retaining heights, it becomes necessary to anchor the upper section to resist horizontal forces. In principle, the anchored sheet pile wall behaves like a beam on two supports: passive soil pressure at the bottom and anchor forces at the top, (De Gijt and Broeken, 2013) [10].

This study focuses on sheet pile wall systems with relieving platforms, particularly those using a combined wall system. Such systems are applied when higher loads and greater retaining heights should be accommodated for.

A combined wall system consists of heavy primary elements, typically tubular piles, installed at intervals and connected by lighter secondary sheet piles. The primary elements provide both soil-retaining and vertical load-bearing functions, while the secondary sheet piles primarily transfer lateral soil pressure to the primary piles through arching action. The secondary elements may be shorter due to the redistribution of forces via this arching effect. Finally, the secondary sheet piles primarily serve to provide impermeability or to limit groundwater flow from the active side to the passive side, thereby reducing seepage forces acting on the structure.

Arching occurs because the tubular piles have significantly higher bending stiffness than the intermediate sheet piles, causing them to attract a greater portion of the horizontal forces, as described in the brochure of Arcelor Mittal (2019) [1]. Figure 2.3 illustrates the combined wall system and the corresponding soil arching behavior.

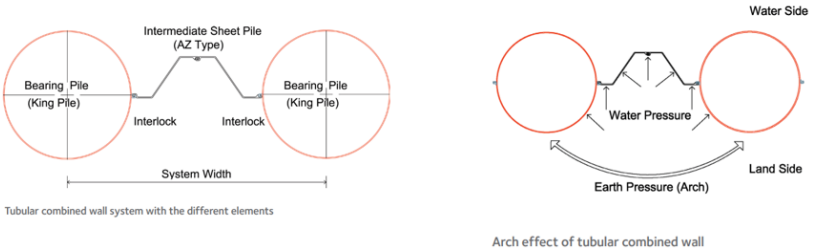

Figure 2.3: Combined wall system and the schematization of soil arching [1]

Anchorage System

Anchor systems play a critical role in providing horizontal stability to sheet pile walls. Anchor systems functions as an upper support for the sheet pile helping to resist lateral earth pressures and operational loads. There are several types of anchorage systems namely:

- **Horizontal Anchorage:** This type consists of a dead-man anchorage that is connected to the sheet piling by a tie rod with an anchor head. Horizontal anchorage systems for quay walls include bar anchors, cable anchors, and screw anchors. Bar anchors use a traditional steel bar and anchor block to transfer loads to a passive resistance wall (dead-man), while cable anchors employ high-strength steel cables, often pre-stressed, to reduce deformation during dredging. Screw anchors, made of threaded steel rods, are cost-effective but prone to deformation under cyclic loads, making them unsuitable for areas like Rotterdam where stability is critical.
- **Anchors with grout body:** This type of anchors consists of an anchor head, a tendon free length and a grout body, [24].This type of anchors includes grout anchors and screw injection anchors.
- **Tension Piles:** This type provides anchorage through a pile trestle system, closed piles, or M-V (Muller Verfahern) piles

Figure 2.4 illustrates the types of anchorage systems. The focus of this research is on anchors with a grout body, specifically screw injection anchors.

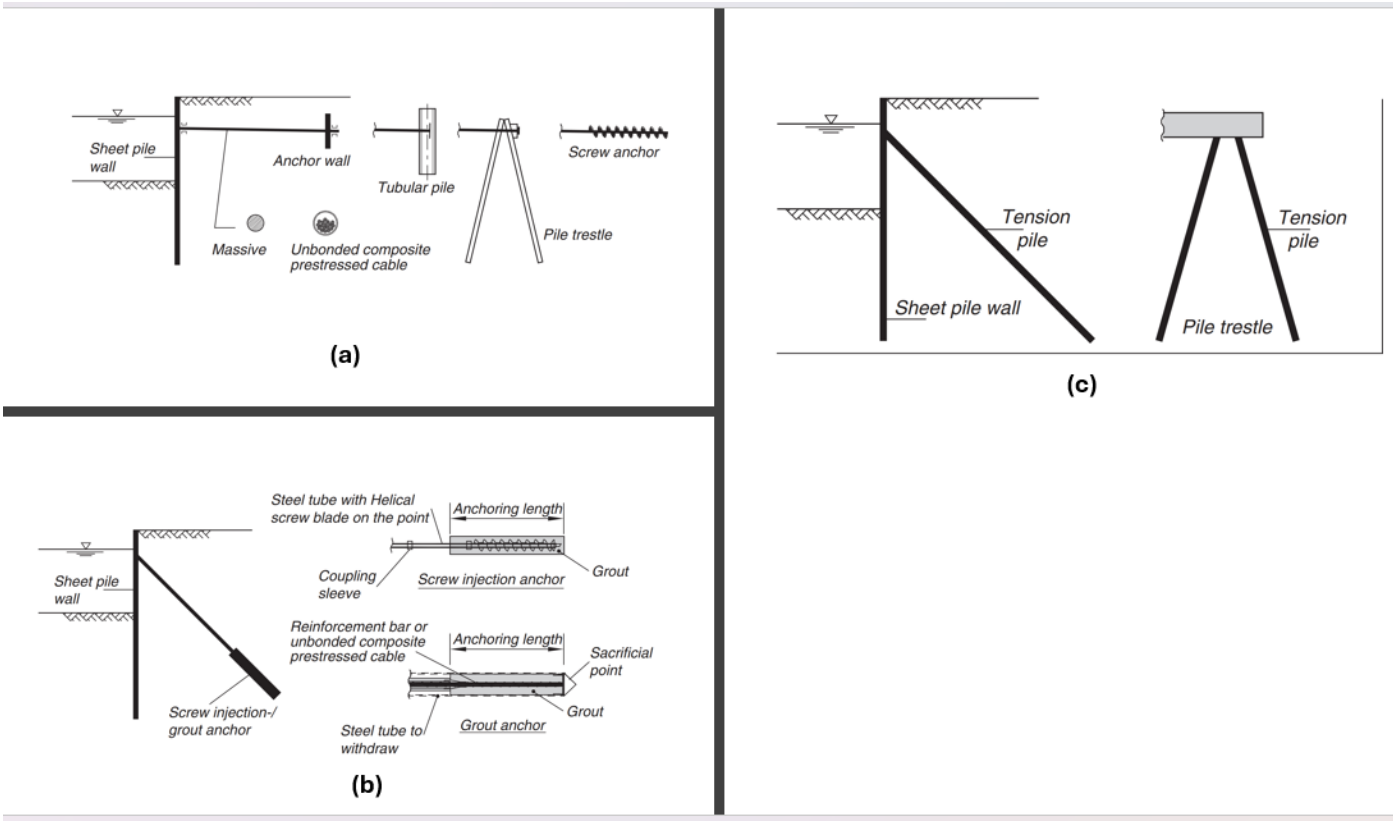

Figure 2.4: Types of Quay walls: (a) Horizontal Anchorage, (b) Anchorage with a Grout Body, (c) Tension Piles [10]

Screw Injection Anchors with Grout Body

This system transfer an applied tensile force (pre-stressing force) to a load-bearing layer of subsoil [24]. This system consists of a hollow stem auger with a perforated tube. During installation, a grout mixture is forced through the tube and injected into the soil thus forming a layer with high strength capabilities. The diameter of the anchor body is more or less the same as that of the hollow stem auger. From design experience, it is recommended that the pre-stressing process must be carried out in phases in order to get an even distribution of the pre-stressing in the anchors, and to prevent overloading of the quay structure, this is due to the apparent relaxation of the soil [24].

2.2.6. Relieving Platform

The use of a relieving platform reduces the active earth pressure on the upper portion of the sheet pile wall. This, in turn, lowers the deformations and the bending moment acting on the wall, allowing for a shallower pile depth and the selection of a smaller steel section, therefore leading to a more cost effective design, (De Gijt and Broeken, 2013)[10]. Relieving platforms are integrated into sheet pile wall systems in cases involving high retaining heights and heavy loads. There are two configurations of relieving platforms, high relieving platforms and low relieving platforms.

High relieving platforms are typically constructed above water level. In this configuration, the horizontal soil load is transferred through a pile trestle system that includes tension and bearing piles located beneath the superstructure [10].

Low relieving platforms are installed at greater depths, below water level, to reduce pile-driving challenges. The platform is supported by foundation elements on the water side through the sheet pile wall; and on the land side, through one or two rows of prefabricated concrete bearing piles and one row of tension piles. A key feature in such configuration is the use of cast iron saddles between the relieving platform and the sheet pile wall, which creates a hinge [10]. Figure 2.5 illustrates quay wall configurations with low and high relieving platforms.

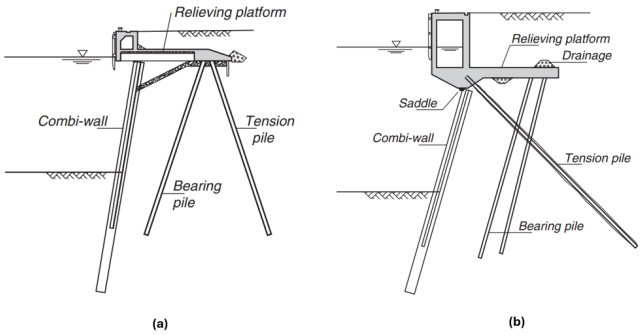

Figure 2.5: Layout of Quay Walls with Reliving Platforms: (a) Low Relieving Platform (b) High Relieving Platform [10]

2.2.7. Connection of superstructure and sheet pile wall

The connection between the relieving platform, the front wall, and the combi-wall can be made in two ways: as a fixed (rigid) connection or as a hinged connection. The fixed connection is designed to resist both bending moments and shear forces, effectively behaving as if the joined structural elements were a single, continuous element. The hinge connection is designed to allow for relative rotation between connected structural elements while restricting translation. They allow for rotation around a specific axis and generally do not transfer bending moments between structural elements.

In a fixed connection the anchor forces are considerably higher than those occurring in a hinged connection [10]. A hinged connection can be achieved with the aid of a cast iron saddle. A hinged connection results in a more statically determinate system. Figure 2.6 illustrates the cast iron saddle.

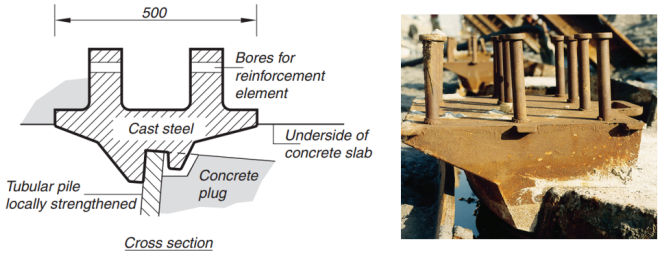

Figure 2.6: Iron cast saddle cross section and real life application [10]

2.3. Structural Deformation Behavior of Quay Walls

Understanding the deformation behavior of quay walls is critical for the safe and effective design of waterfront infrastructure, particularly in ports subjected to complex loading conditions. This section discusses the typical loading mechanisms acting on quay walls, the role of lateral earth pressures, and the deformation characteristics of sheet pile retaining systems.

2.3.1. Loads Acting on Quay Walls

Quay walls are subjected to a combination of horizontal and vertical loads arising from soil and hydrostatic pressures, structural self-weight, and operational activities. These loads can be grouped as follows:

Horizontal Loads:

- Active earth pressures exerted by the retained soil on the landward side.
- Hydrostatic pressures acting on both sides of the wall due to groundwater and surface water levels.
- Operational loads transmitted through the superstructure, including those from cranes, berthing impacts, and platform surcharges.

Vertical Loads:

- Dead loads from the superstructure and permanent surface installations.
- Overburden from backfill and operational surcharges placed atop the relieving platform.

Resisting Mechanisms:

- Passive earth pressure mobilized on the seaward side of the wall or combi wall toe, contributing to lateral resistance.
- Anchor forces developed through tie rods or struts that counteract horizontal displacements.
- Lateral resistance offered by intermediate structural elements (e.g., foundation piles) due to arching or screening effects.

2.3.2. Overview of Lateral Earth Pressure Mechanisms

Lateral earth pressures are key drivers of structural demand in quay walls. As with traditional retaining structures, these pressures are classified into:

- At-rest pressure (K_0), representing the condition where no wall movement occurs;
- Active pressure (K_a), mobilized when the wall moves away from the retained soil;
- Passive pressure (K_p), mobilized when the wall moves toward the soil mass.

The mobilization of passive resistance requires more wall movement than the active condition. During dredging, the reduction in passive pressure due to soil removal in front of the wall critically influences overall stability. In the early stages, pressures are close to at-rest, but as excavation progresses, redistribution toward active and passive states occurs, depending on the deformation mode and support conditions.

In classical Rankine or Coulomb theory, these pressures are typically computed assuming vertical walls, horizontal backfills, and no wall friction. The stress distribution increases linearly with depth and is governed by the soil's effective stress and friction angle ϕ'. However, real field conditions, such as wall-soil friction, sloping backfills, and construction sequence, cause deviations from these idealized models.

2.3.3. Deformation Behavior of Quay Walls

The deformation response of a quay wall system is governed by the interaction between the wall stiffness, soil behavior, and support systems such as anchors. Key influencing factors include:

- The geometry and bending stiffness (EI) of the wall elements;
- The depth of the excavation;
- The stiffness and pre-stressing of anchors;
- Soil stratigraphy, strength, and stiffness;
- Groundwater conditions and changes in pore pressures.

In cantilever walls, the deflection shape generally displays a single curvature, with the maximum lateral displacement occurring just below the excavation level. Anchored or multi-supported walls, by contrast, show more complex deformation shapes with multiple inflection points between anchor levels. The shape and magnitude of displacement evolve with each excavation stage, highlighting the importance of staged construction analysis.

Wall stiffness has a significant influence on deformation behavior. An increase in flexural rigidity (EI) generally leads to reduced lateral deflections. However, this increased stiffness can also result in higher bending moments, depending on the deformation profile, which may in turn lead to increased anchor forces. Conversely, more flexible systems allow for redistribution of loads, often at the cost of greater displacements.

Anchor systems play a vital role in deformation control. Pre-stressed anchors installed at optimal depths reduce wall movement and stabilize bending moments. However, if the anchors are inadequately pre-stressed or mobilize resistance only after large wall movements, the structure may experience excessive deformation before the anchors provide effective support.Anchor stiffness itself also governs how efficiently the loads are transferred and resisted.

Factors Influencing Deformation Behavior

Figure 2.7 illustrates the typical deformation shape of an anchored sheet pile wall. As excavation progresses, deformation modes change due to shifting soil pressures and the staged activation of support systems. The key factors include:

- **Wall stiffness:** Higher stiffness reduces deflections but increases anchor forces.
- **Anchor configuration:** The depth, stiffness, and prestress level of anchors govern when and how they engage to resist lateral movement.
- **Excavation sequence:** Each stage results in a different deflection mode, emphasizing the need for time-dependent or staged analysis.
- **Soil behavior:** The stress–strain response of soils, particularly under unloading and reloading conditions, directly affects deformation patterns.
- **Groundwater:** Elevated pore water pressures reduce effective stress and can exacerbate deformation if not properly drained.

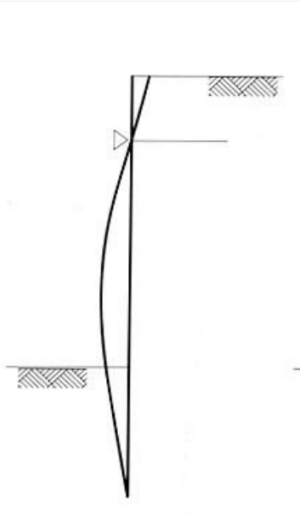

Figure 2.7: Typical Deflection Shape of Anchored Sheet Pile Wall [18]

In conclusion, the deformation behavior of sheet pile walls results from a combination of wall stiffness, excavation sequence, and the interaction between lateral earth pressures and support systems such as anchors. Accurate prediction of deflection and internal forces requires careful consideration of these factors.

2.3.4. Deformation Caused by Dredging in Front of the Quay Walls

Dredging refers to the excavation of soil or sediments located in front of the quay wall down to a predefined elevation. The resulting deformation of the quay wall due to dredging activities is governed by two principal mechanisms:

- **Reduction of vertical effective stress** in the soil mass located in front of the quay wall due to the removal of overburden.
- **Activation of the quay wall's retaining function**, which mobilizes structural resistance against the lateral earth pressures.

The first mechanism is heave, which occurs when the excavation leads to a significant decrease in vertical effective stress. This reduction allows the underlying soil to undergo elastic or plastic expansion, thereby inducing upward movement. Consequently, the sheet pile wall experiences vertical displacement and rotational deformation, typically characterized by a greater upward movement at the front of the quay wall relative to the rear. The magnitude of this heave is closely related to the extent of dredging (i.e., the depth of excavation) and the resulting drop in overburden pressure. This behavior is especially pronounced in quay walls with large retained heights and in construction scenarios involving dry excavation pits.

The second mechanism involves the mobilization of the structural resistance of the quay wall as it begins to retain the lateral pressures from the surrounding soil. This mechanism is predominantly influenced by the effective retaining height and the stiffness of the quay wall system. A stiffer structural system leads to reduced deformations but may increase internal forces, while a more flexible wall may deform more readily but with a different distribution of anchor and bending moments.

Understanding the relative contributions and interplay of these two mechanisms is essential for accurately predicting quay wall performance during dredging operations and for calibrating numerical models that simulate soil-structure interaction.

2.4. Geotechnical Factors that Affect the Quay Wall Behavior

Predicting the behavior of quay walls is inherently complex due to various sources of uncertainty that affect both the design process and the structure's performance. Uncertainty is a fundamental aspect

of geotechnical engineering and can generally be categorized into two types.

The first is epistemic uncertainty, which stems from a lack of knowledge or incomplete understanding of a system or parameter. This may include limitations in measurement techniques, inaccuracies in parameter estimation, or simplifications in modeling assumptions [19].

The second is aleatory uncertainty, which refers to the natural variability or randomness inherent in geotechnical systems, for example the spatial variability of soil properties that cannot be eliminated, only quantified [19]. The sources of uncertainty in geotechnical engineering include:

- Inherent Soil Variability: Soil is a heterogeneous and anisotropic material, meaning its properties differ with location and direction. This natural variability across a site and with depth makes it challenging to accurately characterize subsurface conditions [29].
- Limited Site Investigation Data: Site investigations often involve a limited number of tests, which may not fully capture the subsurface conditions [29].
- Complexity of Geological Processes: Geological processes such as weathering, erosion, and sedimentation result in complex subsurface conditions that are difficult to model accurately. In some cases, human activities like land reclamation further contribute to this complexity [29].
- Measurement Errors and Biases: Errors may arise during laboratory testing or in-situ measurements, introducing uncertainty into the collected data [29].
- Model Simplifications and Assumptions: Geotechnical models often involve simplifications and assumptions regarding soil behavior and loading conditions, which can introduce additional uncertainty [29].

There are several techniques and strategies available to help manage uncertainty in geotechnical engineering. These include:

- Thorough Site Investigation: Conducting comprehensive site investigations, including a variety of in situ and laboratory tests, can help reduce uncertainty, [29].
- Model Calibration and Validation: Calibrating and validating geotechnical models using site-specific data can help reduce model uncertainty, [29].

Uncertainty in geotechnical engineering plays a critical role in the behavior of quay walls, especially in terms of stability and deformation. Variations in soil properties, such as shear strength and stiffness, can lead to unpredictable lateral earth pressure distributions, resulting in lateral displacements, differential settlement, and increased bending moments in quay walls [14]. As noted by Korff (2023) [18], failure mechanisms in quay walls include horizontal and vertical instability, as well as deformation in the surrounding environment, all of which are influenced by the strength, stiffness, and permeability of the subsoil and the site's hydro-geological conditions.

Building on this, Seo et al. (2023) [33] conducted a numerical study using finite element analysis to identify the key factors affecting the performance of anchored earth-retaining walls during excavation. The study found that soil properties,particularly soil stiffness and shear strength, have the most significant impact on wall displacement. In contrast, groundwater level, surcharge loads, and structural stiffness showed relatively minor influence. Sensitivity and coefficient of variation (CV) analysis further highlighted that the friction angle,and the stiffness moduli are the most influential parameters due to their high variability. The results emphasized the importance of accurately characterizing soil conditions to improve the reliability of quay wall performance predictions.

2.5. Finite Element Modeling of Quay Walls

Numerical modeling is a method used to solve the differential equations that describe physical phenomena. These equations are often too complex to solve analytically and therefore require numerical approaches to obtain approximate solutions. Numerical modeling provides a discrete approximation of a continuous function using computational methods.

One of the most widely used numerical techniques in engineering is the Finite Element Method (FEM), which is the focus of this thesis. Any numerical model must include the following components:

- Governing equation: Represents the physical laws (i.e., equilibrium, conservation) relevant to the problem.
- Constitutive model: Describes the material behavior, specifically the stress-strain relationship of the material.
- Defined domain: The physical region over which the equations are solved, requiring specified boundary and initial conditions.

The Finite Element Method is a numerical technique for solving partial differential equations that govern physical systems [34]. In geotechnical engineering, these equations often represent coupled hydro-mechanical processes. The method involves discretizing the problem domain into smaller sub-regions, called elements, typically of simple geometric shapes. This process forms a mesh over which the governing equations are solved [34]. The resulting system of equations relates nodal inputs (forces, displacements) to outputs (stresses, deformations), enabling an approximate solution of the problem.

FEM is particularly useful in modeling complex geometries and capturing soil-structure interaction. It allows for detailed calculations of soil deformations, stress distributions, and anchor forces across various construction stages.FEM has certain limitations: it can be computationally demanding, highly sensitive to input parameters, and requires expert knowledge for effective model setup. Additionally, FEM accuracy is limited by an inherent inaccuracy margin of $\pm 30\%$, [10].

In this thesis, the software package PLAXIS is used to carry out FEM simulations. PLAXIS offers both 2D and 3D environments for geotechnical analysis and includes a range of constitutive soil models to represent different types of soil behavior.

Among the available models in PLAXIS are:

- **Mohr-Coulomb (MC)** – A simple elastic-perfectly plastic model commonly used for preliminary designs.
- **Hardening Soil (HS)** – A more advanced model that accounts for non-linear stiffness and plasticity.
- **Hardening Soil with Small-Strain Stiffness (HSsmall)** – An extension of the HS model, capturing small-strain stiffness effects.
- **Soft Soil Creep (SSC)** – A model designed for long-term consolidation and creep behavior in soft soils.

The MC model transitions from linear elasticity to perfectly plastic behavior, defined by the Mohr-Coulomb failure criterion. This model is commonly used for preliminary analyses and draft designs (De Gijt and Broeken, 2013) [10].

The Hardening Soil Model (HS) builds upon the Mohr-Coulomb failure criterion but offers a more advanced representation of soil behavior. Unlike the basic elasto-perfectly plastic Mohr-Coulomb (MC) model, the HS model accounts for nonlinear, stress-dependent stiffness and progressive plastic strain accumulation through hardening laws [30]. It incorporates three yield mechanisms: deviatoric (shear) hardening, volumetric (cap) hardening, and a tension cut-off. Figure 2.8 illustrates the yield surfaces associated with the model [30]. The deviatoric mechanism follows a hyperbolic stress-strain relationship, similar to the Duncan-Chang model, using stress-dependent stiffness based on Mohr-Coulomb parameters. Figure 2.9 shows this relationship under drained triaxial compression. The volumetric mechanism simulates compaction using an elliptical yield surface in p–q space, while the tension cut-off limits tensile stresses based on material strength [30].

Additionally, the HS model captures more realistic elastic behavior by distinguishing between unloading and reloading stiffness. It supports the modeling of pre-consolidation effects and allows for dilatancy. The stiffness moduli are defined as functions of confinement stress, making the model suitable for simulating a wide range of geotechnical problems.

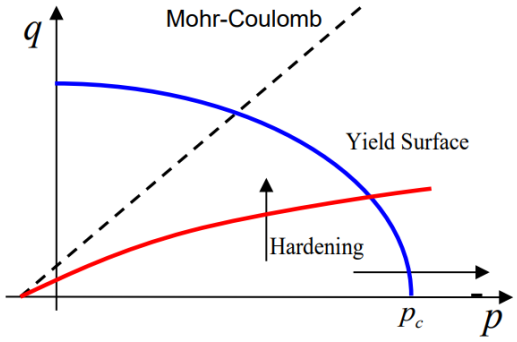

Figure 2.8: The yield surfaces of the Hardening Soil model; Deviatoric yield surface (red) and elliptical cap (blue) [30]

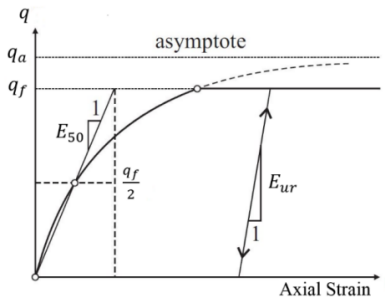

Figure 2.9: Hyperbolic stress-strain curve in a drained compression triaxial test [30]

The HSsmall model is an extension of the Hardening Soil model that incorporates small-strain stiffness, allowing for increased accuracy in predicting deformations at low strain levels [10].

The SSC model focuses on the time-dependent behavior of soils, such as creep, making it ideal for soft soils. It combines the Mohr-Coulomb failure criterion with stress-dependent stiffness and includes pre-consolidation stress effects. This model distinguishes between unloading/reloading behavior (De Gijt and Broeken, 2013) [10].

The HS model, with or without small-strain stiffness, is generally regarded as the most suitable for retaining structures[30]. Table 2.1 shows the general input parameters for the hardening soil model.

Table 2.1: General input parameters for the Hardening Soil (small strain) model

Parameter	Unit	Description
γ_{sat}	kN/m^3	Saturated soil weight
γ_{unsat}	kN/m^3	Unsaturated soil weight
ϕ	°	Soil strength, effective angle of soil friction
c'	kN/m^2	Effective cohesion
ψ	°	Angle of dilatancy
E_{50}^{ref}	kN/m^2	Secant soil stiffness, for a shear stress level that is 50% of the maximum shear stress in triaxial testing; for a reference stress commonly the reference stress is $p_{ref} = 100$ kPa
E_{oed}^{ref}	kN/m^2	Oedometer stiffness for the reference stress
E_{ur}^{ref}	kN/m^2	Unloading-reloading stiffness
$\gamma_{0.7}$	-	Shear strain for which the shear modulus is reduced to its 70% value compared to its small strain value **(HS small-strain only)**
G_0^{ref}	kN/m^2	Shear modulus for very small strains; onset of the shear modulus at the start of shearing **(HS small-strain only)**
$k_{x,y}$	m/sec; m/day	Soil permeability in x respectively y-direction; required if a groundwater flow analysis is needed to establish the pore water distribution field
R_{int}	-	Interface strength ratio; ratio of the interface's shear strength compared to shearing in the soil; indicatively: $R_{int} \approx \frac{\tan(\delta)}{\sin(\phi)}$

2.6. Field Measurements

Field measurements are essential for calibrating and validating finite element models to improve their accuracy and reliability in analyzing quay walls. These measurements provide real-world data that refine model assumptions and adjust input parameters, ensuring the models better reflect actual behavior. The focus in this thesis is on inclinometer readings measured during the dredging phase.

2.6.1. Inclinometer

An inclinometer is an instrument used to measure the angle of tilt, slope movement, or lateral displacement of the ground, structures, or retaining systems over time. Inclinometers are a simple, cost-effective, piece of equipment that usually consists of a hollow PVC tube with two sets of internal grooves which allow measuring wheels to measure deflection in two directions, [11]. The installation of inclinometers helps to determine the following: the nature of deformation patterns, the rate of deformation, or whether the deformations are within relevant limits for the project, [11]. Inclinometers can be installed inside the structure whose deflection is required to be monitored . Figure 2.10 demonstrates how a inclinometer is placed inside the structure and the typical configuration of an inclinometer. Using either manual or automatic measuring equipment, the local 'tilt' and cumulative deflection of the ground or the structure can be determined to a high degree of accuracy, [11]. Inclinometers can be installed vertically or horizontally depending on which direction is required to monitor deflections. A vertical inclinometer will provide information on the horizontal deformation of the ground, whereas a horizontal slope inclinometer will demonstrate characteristics of vertical movement, [11]. Ideally, inclinometers should be installed before any excavation works take place to get an accurate baseline position, [11].

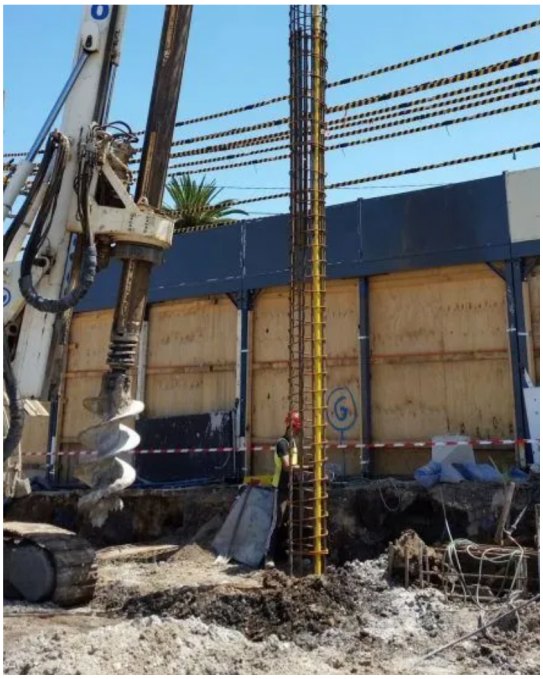

(a) Installation of an inclinometer inside a structure. [11]

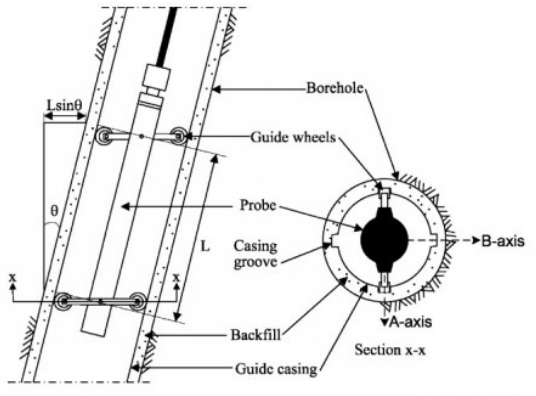

(b) Inclinometer configuration. [15]

Figure 2.10: Inclinometer installation and typical configuration.

Measurements begin at the bottom of the casing (i.e., at the tip of the combi-wall), and readings are taken at regular 0.5-meter intervals as the probe is raised. While the inclinometer does not directly record horizontal displacements, it captures angular tilt, which must be converted to lateral movement. The horizontal deviation at each interval is computed using the following formula:

$$\textit{deviation} = \sin\theta \cdot L_{\textit{interval}} \tag{2.1}$$

The relative horizontal displacement over the height of the combi-wall and the front wall is obtained by summing the deviation of each interval . Figure 2.11 illustrates the incremental horizontal displacement of the measurement. The aim of the inclinometer measurements is to determine the change in horizontal deformations of the combined wall. The measured horizontal deformations are therefore made relative to a reference measurement, which is taken after the concrete relieving platform and the front wall is poured.

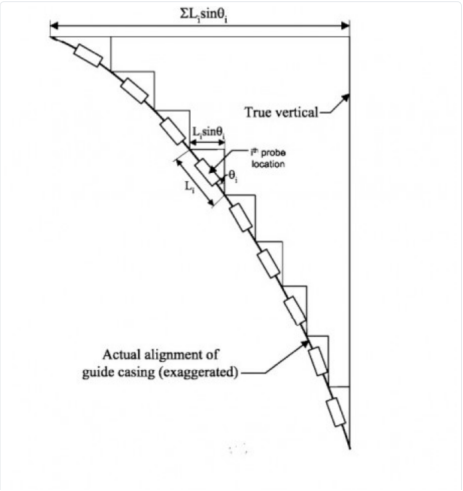

Figure 2.11: Incremental horizontal displacement of inclinometer measurement. [15]

When using inclinometer data to calibrate or validate a finite element model, it is important to recognize that the toe of the combi-wall is not perfectly fixed. Therefore, corrections may be needed to adjust the relative displacement readings and ensure a valid comparison with the FEM output.

2.7. Calibration and Validation Methods

Finite Element Modeling (FEM) has become a core tool in geotechnical engineering, enabling detailed simulation of soil-structure interaction. However, the accuracy and reliability of FEM rely heavily on proper calibration and validation. Stiffness and strength parameters for the Hardening Soil model can be estimated from field investigation data, such as Cone Penetration Tests (CPT) or Standard Penetration Tests (SPT), using established empirical correlations, [6]. Furthermore, typical ratios between different stiffness parameters, such as the secant stiffness in standard drained triaxial loading (E_{50}^{ref}), the tangent stiffness for oedometer loading ($E_{\text{oed}}^{\text{ref}}$), and the unloading/reloading stiffness ($E_{\text{ur}}^{\text{ref}}$), are well-documented for various soil types, [6]. As a result, once one stiffness parameter is determined with confidence, the others can often be reliably inferred using these characteristic relationships.

Model calibration involves adjusting input parameters, such as soil stiffness, and strength to reproduce observed behavior from laboratory or field data. Given the heterogeneous and anisotropic nature of soils, simple deterministic calibration is often insufficient. Instead, inverse analysis is commonly used to systematically update model parameters based on real-world measurements. Once calibrated, the model must be validated to confirm that it can reliably predict behavior under conditions not used in the calibration phase. The validation process involves the comparison of the results of our model with the reference value. Specifically checking the limits and tolerances, How much deviation from the reference value that is acceptable.

Inverse analysis, also known as back-analysis, uses measurement data, such as wall displacements, to refine input parameters and reduce uncertainty. This process improves the alignment between model outputs and observed field behavior. Two main approaches are used in inverse analysis: semi-probabilistic and probabilistic methods.

2.7.1. Semi-probabilistic Method

In a semi-probabilistic approach, parameters are adjusted manually or iteratively until the model results closely match measured data. This process requires a strong understanding of the model's sensitivity to each parameter, especially in layered or complex soil conditions. While this method can yield a single set of improved parameters, it does not consider the full range of possible combinations that might also fit the data. However, it can be used when other methods or techniques are more complex to implement.

2.7.2. Probabilistic Method

Probabilistic methods treat input parameters, such as soil properties and loading conditions, as random variables characterized by statistical distributions. These methods aim to capture the inherent uncertainties in geotechnical systems and provide more realistic assessments of structural performance.

One widely adopted probabilistic framework is Bayesian updating, which enables the refinement of prior parameter distributions based on observed data. Through this process, both the most probable values (e.g., mean friction angle or stiffness modulus) and their associated uncertainties (e.g., standard deviation or confidence intervals) are iteratively updated. This results in a more accurate and reliable representation of soil behavior, incorporating site-specific information into the model in a systematic and statistically consistent manner.

Bayesian methods are particularly effective in geotechnical engineering, where high variability and limited data are common. They allow engineers to incorporate real-world measurements, such as inclinometer readings, anchor loads, and ground settlement, into the modeling process to update model parameters and reduce uncertainty. This leads to a better understanding of the reliability and safety of retaining structures, especially when dealing with complex soil-structure interactions.

For example, Den Adel (2018) [9] demonstrated the successful application of Bayesian updating in improving the reliability assessment of a complex quay wall. By using artificially generated measurements, including horizontal displacements of the combi wall and strains in anchor rods, the study showed that significant reductions in parameter uncertainty could be achieved. The refined model outputs were not only more consistent with observed behavior but also offered increased confidence in the structural reliability of the quay wall.

In another study, Huang et al. (2016) [16] applied Bayesian updating to combine laboratory preconsolidation pressures with shear wave velocity measurements from a seismic dilatometer test. This integration allowed for a statistically rigorous combination of in-situ and laboratory data, significantly reducing the uncertainty of estimated soil parameters. The method demonstrated the potential of Bayesian updating to enhance material characterization even with limited data and has promising applications in multi-dimensional geotechnical modelling.

Despite their advantages, probabilistic methods such as Bayesian updating involve greater computational complexity and demand more advanced data acquisition and statistical modeling techniques.

2.8. Existing Case Studies

Several recent case studies demonstrate the use of Finite Element Modelling (FEM) in conjunction with monitoring data to improve the understanding and reliability of quay wall performance. These studies inform the methodology adopted in this thesis, particularly in the context of model calibration and the integration of field data.

Schouten (2020) [31] investigated the potential of using measurement data from smart quay walls to optimize their functionality. The case study focused on the HES Hartel Tank Terminal (HHTT) quay wall in the Port of Rotterdam, which includes sections with and without a relieving platform. The study set up a PLAXIS FE model using parameters from cone penetration and triaxial tests and validated it with field measurements obtained during the construction process, particularly inclinometer data (horizontal displacements) and anchor forces. A strong agreement between model predictions and measurements was observed when realistic friction angle values were used, accounting for peak behavior and plane strain conditions. Although the model was successfully validated and did not require updating of mean soil parameters, a sensitivity analysis revealed that the friction angle explained 60–70% of the quay wall's behavior during construction, rising to 80% in the Ultimate Limit State. The study concluded that monitoring data collected during construction can provide meaningful insight into key soil parameters, especially the friction angle, and therefore improve the reliability and optimization of quay wall design.

Tolba et al. (2022) [35] analyzed the long-term horizontal displacement of an existing anchored quay wall in the Port of Rotterdam using PLAXIS 3D (version 2013), comparing model outputs to five years of field monitoring data. The study emphasized the importance of time-dependent effects in predicting quay wall deformation. The PLAXIS 3D model produced displacement results within +5.8% of measured values, validating its effectiveness. The study found that realistic predictions required careful

selection of soil parameters and the use of advanced constitutive models; in particular, the Hardening Soil Model (HSM) provided better agreement with measured displacements than the Mohr-Coulomb model. A key observation was the impact of anchor wall displacements, which significantly influenced the movement of the front combi wall. The authors identified a linear relationship, where anchor wall movements contributed to approximately 15% of additional horizontal displacement in the front wall during the operational phase.

Roubos et al. (2020) [28] conducted a finite element-based reliability assessment of real-life quay walls. A key outcome was that the variation in the soils' angle of internal friction greatly influences quay-wall reliability. The authors emphasized that neglecting model uncertainty and correlations between input variables leads to an underestimation of failure probability, thereby compromising the reliability assessment. Furthermore, they showed that local soil stratigraphy and project-specific functional demands, such as operational loads and retaining height, significantly impact reliability outcomes. The study strongly recommended the use of field monitoring, such as measurements of deformations, water levels, and anchor forces, to reduce modelling uncertainties and enable Bayesian updating of reliability over time. This monitoring-based approach, they argued, could improve the understanding of quay wall capacity and support more robust asset management decisions.

Collectively, these studies underscore the critical role of integrating field monitoring data with finite element modelling to enhance the accuracy, reliability, and practical value of quay wall assessments. Across all three investigations, the friction angle emerged as a highly influential parameter, reinforcing the importance of accurate soil characterization. Moreover, the consistent emphasis on time-dependent behavior, construction-phase loading, and anchor wall interaction highlights the complexity of quay wall performance and the limitations of simplified modelling approaches. The findings also point to the value of constitutive models and probabilistic frameworks, particularly when calibrated with high-quality field measurements. These insights support the approach of this thesis, which seeks to develop a calibrated and validated FEM of a quay wall using field data from the Amaliahaven Project in the Port of Rotterdam.

This chapter has provided an in depth review of the key theoretical aspects relevant to modelling the behavior of quay walls during construction, particularly under dredging conditions. It began with a technical overview of quay wall systems, highlighting their structural components, functional requirements, and the specific design context of the Port of Rotterdam. The discussion then explored the deformation behavior of quay walls under various loading conditions and the critical influence of dredging activities on wall performance.

Subsequent sections addressed the impact of geotechnical uncertainty, especially regarding soil strength and stiffness parameters, and its implications on quay wall behavior. Afterwards, the use of finite element method was examined for capturing the complex soil–structure interaction inherent in quay wall systems. Additionally, the field measurement techniques relevant to the thesis were discussed. Additionally, calibration and validation methods were discussed, establishing the importance of accounting for model uncertainty and parameter variability. Finally, existing case studies demonstrated practical applications of FEM and the integration of field measurements.

Many studies either make use of field measurements or recommend their use to calibrate and validate finite element models. There is very limited research that specifically incorporates data from smart quay walls, which are quay walls equipped with integrated sensors and monitoring instruments, into the FEM calibration and validation process. This represents a gap in the literature, especially as smart quay walls becomes more central to practice.

In addition, there are currently no published studies that focus on the quay walls in the Amaliahaven Project in the Port of Rotterdam. A field validated FEM can help evaluate how the quay wall behaves over time, especially during dredging and under various loading conditions. Such a model could also support future decision-making, for example, by predicting how the structure would respond to deeper berthing levels or increased operational loads.

This thesis responds to that gap by developing, calibrating, and validating a finite element model for a quay wall in the Amaliahaven Project using actual field measurements taken during dredging. In doing so, it aims to enhance predictive accuracy, reduce epistemic uncertainty, and establish a foundation for future research and practice in smart quay wall analysis.

3

Methodology

3.1. Introduction

The aim of this chapter is to present the methodology adopted to achieve the research objective of this thesis: developing, calibrating, and validating a finite element model for a quay wall in the Amaliahaven Project, located in the Port of Rotterdam. The chapter introduces the case study, the available field measurements, and the procedures followed to set up and calibrate the finite element model in PLAXIS. It also outlines the approach used for validation and the parametric study. Together, these elements provide the methodological foundation for the analyses carried out in this research.

Table 3.1: Overview of Data Sources

Data	**Source**
Site Investigation – including 154 CPTs and 17 Boreholes	Provided
Laboratory Tests – including Sieve Analysis, Oedometer tests, Triaxial tests, and Atterberg limits tests	Provided
Dredging Details – including Contour Maps and XYZ data files	Provided
Inclinometer Measurement Data (Relative Lateral Displacement)	Provided
Soil Stratigraphy and Soil Profile	Conducted in Research
Parameter Determination	Conducted in Research
Quay Wall Structural Layout, Geometry and Details	Provided
PLAXIS Structural Elements and Model Inputs	Conducted in Research
Construction Stages	Interpreted from Literature

3.1.1. Methodology Workflow

This subsection outlines the sequential workflow adopted in this study to develop, calibrate, and validate a finite element model (FEM) for simulating the behavior of the quay wall during dredging activities. Figure 3.1 presents the workflow of the adopted methodology.

The process begins with the identification of the study area, specifically located within the Amaliahaven development in the Port of Rotterdam.

Following the site selection, the geological and geotechnical conditions in the vicinity are examined to establish a preliminary understanding of the expected subsurface stratigraphy. Based on the structural layout of the selected quay wall section, relevant Cone Penetration Tests (CPTs) and boreholes near the site are identified and analyzed. These investigations are used to define the representative soil stratigraphy necessary for geotechnical modeling.

Subsequently, soil constitutive parameters are derived for the Hardening Soil (HS) model. The parameter estimation primarily relies on CPT data, supplemented by empirical correlations and laboratory test results where available. This stage is critical in defining the input for the soil behavior in the FEM simulations.

The next phase involves the analysis of the structural components of the quay wall system. Detailed geometrical and mechanical properties of the combi-wall, front wall, relieving platform, anchor system, and bearing piles are compiled to construct an accurate FEM representation.

Following the structural definition, field measurements are incorporated. These include the dredging history and inclinometer data, which are essential for model calibration and validation.

Finally, the finite element modeling process is initiated. This includes setting up the FEM in PLAXIS, defining the construction sequence, calibrating the model based on field measurements, and validating its predictive capability. The calibration is carried out using inverse analysis techniques, and the model validation assesses the degree of agreement between FEM results and observed field data.

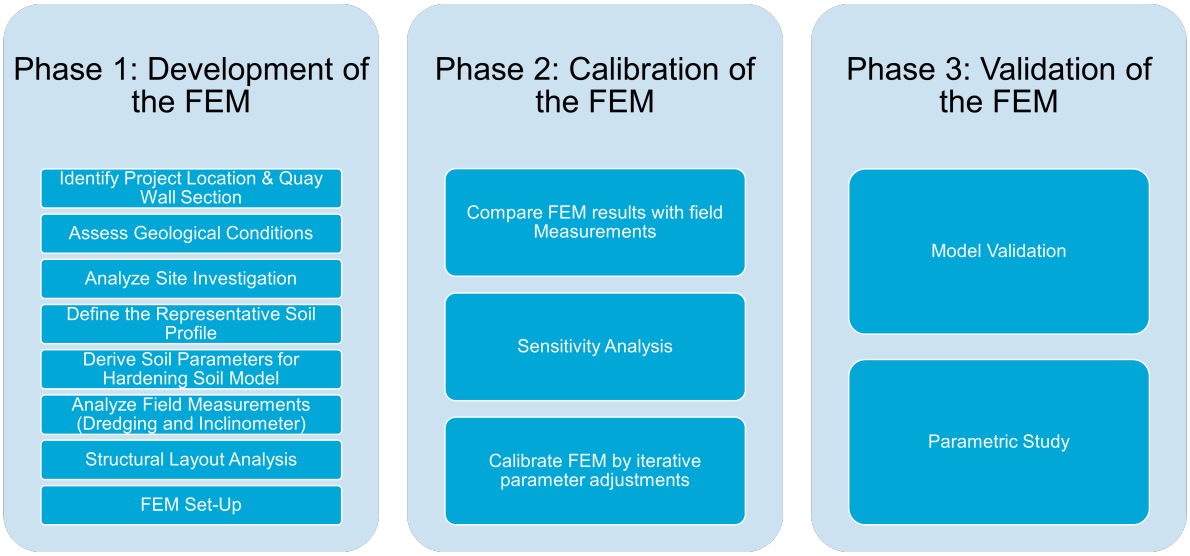

Figure 3.1: Methodology Workflow

3.2. Case Study Description

The case study focuses on the Amaliahaven project, located in Maasvlakte in the Port of Rotterdam. Figure 3.2a shows the location of the project. The new quay walls are constructed on both sides of the approximately 2.5 kilometer long port basin, as illustrated in Figure 3.2b. The project includes 1,825 meters of deep-sea quay wall with a retaining height of 29 meters, along with dredging works reaching depths of more than 20 meters below NAP. The quay wall is equipped with sensors to monitor the behavior of the structure, making it a smart quay wall.

(a) The Project Location Acquired from Google Earth

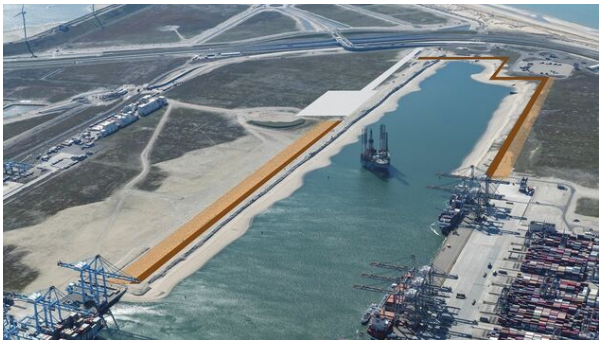

(b) The Amaliahaven Project.[25]

Figure 3.2: The Project Location.

3.2.1. Geological Conditions

To better understand the expected soil conditions, a geological investigation was conducted to identify the subsurface layering and formation at the project site. This is particularly important given that the study area was reclaimed land, which often leads to irregular and unpredictable soil layering.

Geological information was obtained from DINOloket, which is the national database for shallow and deep geology in the Netherlands. Since no direct geological cross-sections were available near the Amaliahaven project, data from a nearby area, the Prinses Margriethaven, was used instead. Due to DINOloket's minimum required spacing of 1 km for cross-sections, the section had to be extended slightly.

Figure 3.3 presents a geological cross-section based on the GeoTOP subsurface model. The analysis primarily focuses on the soil layers located on the right-hand side of the cross-section, which are considered representative of the Amaliahaven area.

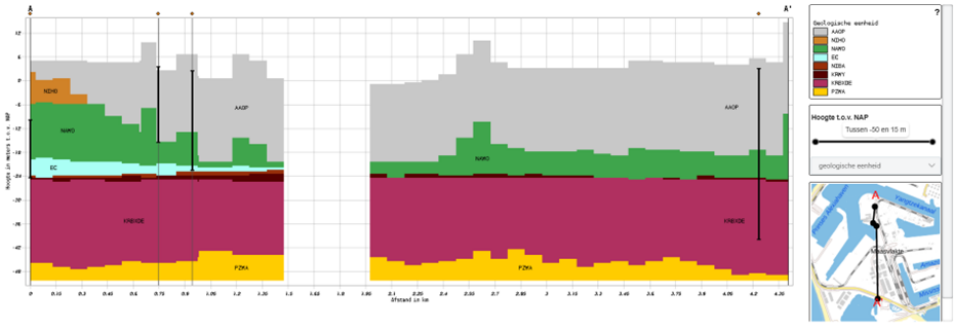

Figure 3.3: Cross-section of the Estimated Subsurface in the Port of Rotterdam using GeoTop Model. Source:DINOloket

There are four distinctive geological layers at the project site. The top layer, AAOP (grey), consists of anthropogenic deposits, mainly reclaimed soil. Beneath it lies the NAWO layer (green), which is highly variable and composed of grey to light yellow sand ranging from very fine to very coarse (105–420 µm). This layer is partially clayey or silty, calcareous, and contains shells, along with grey to blue silt and clay, humus, coarse lags, and thin, discontinuous peat layers. Below that is the KRBXDE layer (purple), which includes light yellow to dark brown sand (105–300 µm), often silty, with grey-brown to dark grey sandy loam. It also features thin peat and gyttja layers, some detrital material, and local zones of coarse sand with fine gravel lags. The deepest layer identified is PZWA (yellow), characterized by stacked fining-upward sequences of grey to grey-white sand ranging from extremely fine to extremely coarse (63–2000 µm). The sand is micaceous and partially variegated with red grains, locally very gravelly, and contains blue-grey to brown-grey clay, silty to sandy, with peat intercalations and siderite.

In a study conducted by Duffy et al. (2024) [12] around the Port of Rotterdam, a discontinuous clay layer was observed at depths ranging from approximately –16.5 m to –25.5 m NAP. It is therefore necessary to investigate whether this clay layer is also present in the vicinity of the quay wall section under study. Identifying the presence or absence of this layer is essential, as it plays a critical role in accurately modelling the soil conditions. This issue will be examined in more detail in the following sections.

3.2.2. Soil Stratigraphy & Representative Profile

In order to determine the soil stratigraphy at the site, Cone Penetration Tests (CPTs) are essential. After identifying the location of the quay wall, only the CPTs and boreholes located in the immediate vicinity were considered for this study. The general layout of all CPTs and boreholes conducted on-site is shown in Figure 3.4.

Based on this selection, three perpendicular and two longitudinal cross sections were extracted. Among these, the perpendicular cross sections are considered most relevant for the analysis. This is because the finite element model in PLAXIS will be conducted in a two-dimensional (2D) framework, making the stratigraphy perpendicular to the wall critical for accurate representation of soil behavior.

The longitudinal cross sections were included to assess the degree of spatial variability along the quay wall. They serve as a check to determine whether any localized soil layers or significant variations exist, and to verify that the stratigraphy observed in the perpendicular sections is consistent along the wall's length. This comparison helps ensure that no major deviations are overlooked and increases confidence in the representativeness of the selected soil profile for the FEM analysis.

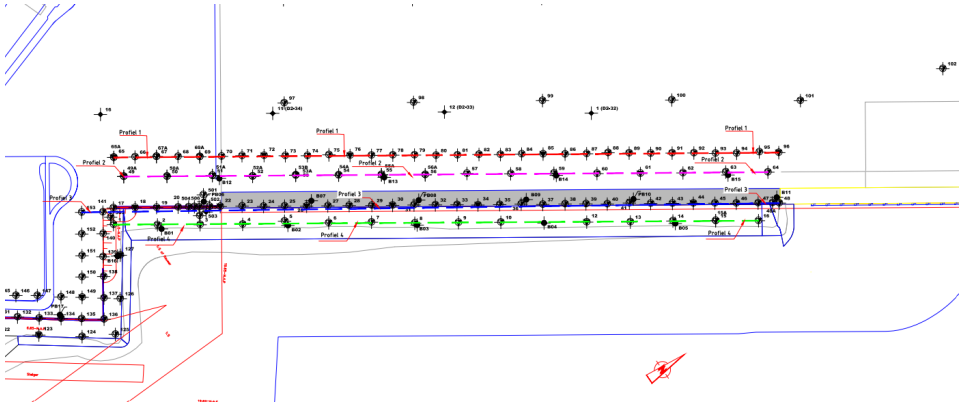

Figure 3.4: Layout of CPTs conducted at the project site.[23]

Soil Stratigraphy

To identify the soil stratigraphy at the project site, Cone Penetration Test (CPT) data is utilized. One of the most effective and widely accepted approaches for classifying soil behavior from CPT results is the Soil Behavior Type Index (I_c), which enables the interpretation of soil types using the cone resistance q_t and the friction ratio R_f , (Mayne, Cargill, & Greig, 2023) [20].

The calculation of I_c is based on the stress-normalized cone resistance Q_{tn} and the normalized friction ratio F_r. In order to compute the effective vertical stress σ'_v, an estimate of the soil unit weight γ is required. The phreatic level is assumed to be at 0 m NAP. This assumption is based on the pore pressure profile obtained from CPT 26 (the only CPT with pore pressure data), as shown in Figure 3.6. Although Boreholes 2 and 7 are located within the study area and report phreatic levels of 0.42 m NAP and –1.66 m NAP respectively, these values were measured during drilling and represents only a snapshot in time. Due to the influence of pore water pressure, soil layering, local conditions, and seasonal factors, the actual groundwater level may vary significantly from the measured value. Therefore, the CPT-derived phreatic level is considered more reliable.

The total unit weight of the soil is estimated using the empirical correlation proposed by Robertson et al. (2010) [26], which relates unit weight to cone resistance and friction ratio:

$$\frac{\gamma}{\gamma_w} = 0.27 \cdot \log R_f + 0.36 \cdot \log\left(\frac{q_t}{p_a}\right) + 1.236 \tag{3.1}$$

where:

- γ is the total unit weight of the soil,
- γ_w is the unit weight of water,
- q_t is the corrected cone tip resistance,
- p_a is the atmospheric pressure (typically 100 kPa),
- R_f is the friction ratio (in percent).

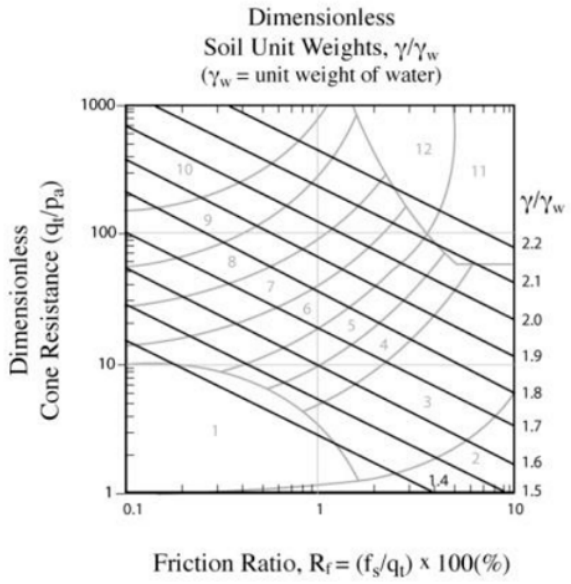

Figure 3.5: Correlation for estimating unit weight from CPT data (Robertson et al., 2010 [26])

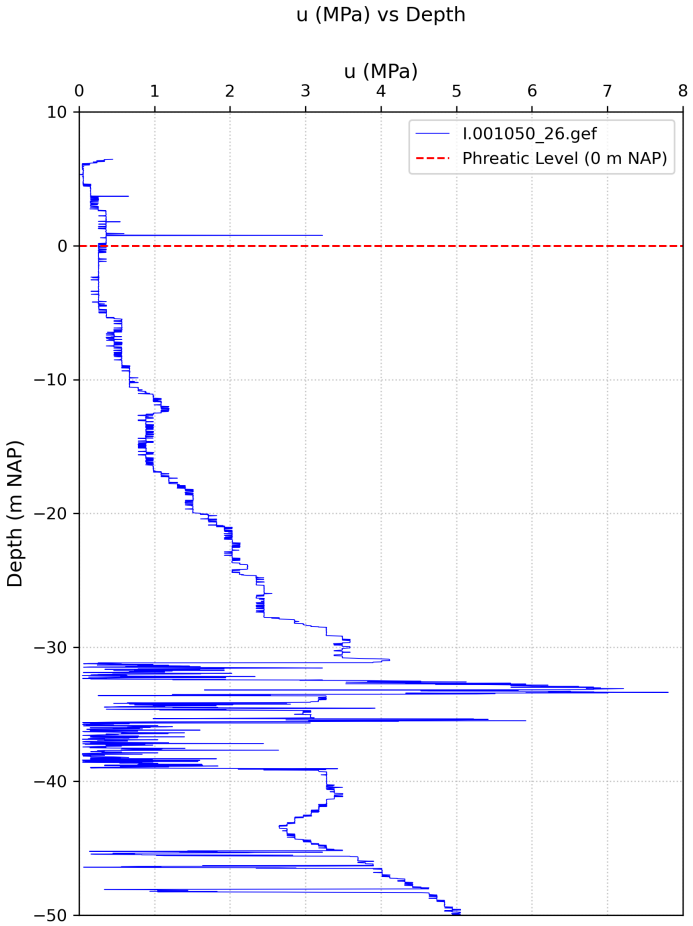

Figure 3.6: u2 profile from CPT 26 indicating the phreatic level at 0 m NAP

The estimated unit weight is then used to compute the effective vertical stress, which is required for calculating the normalized cone resistance Q_{tn} as follows (Mayne, Cargill, & Greig, 2023) [20]:

$$Q_{tn} = \frac{q_{net}}{\sigma'_{atm}} \left(\frac{\sigma'_v}{\sigma'_{atm}} \right)^n \tag{3.2}$$

The normalized parameters are then used to compute I_c as:

$$I_c = \sqrt{(3.47 - \log_{10} Q_{tn})^2 + (1.22 + \log_{10} F_r)^2} \tag{3.3}$$

Since Q_{tn} is dependent on the exponent n, and n itself is calculated from I_c, an iterative process is required. The value of n is updated using (Mayne, Cargill, & Greig, 2023) [20]. :

$$n = 0.381 \cdot I_c + 0.05 \cdot \frac{\sigma_{vo'}}{\sigma_{atm}} - 0.15 \leq 1 \tag{3.4}$$

Typically, 2 to 3 iterations are sufficient for convergence of the I_c value. The resulting I_c value corresponds to one of nine soil behavior types, as shown in the classification chart by Robertson (1990, 2009) in Figure 3.7. The classification is as follows:

- $I_c < 1.31$: Gravelly Sand (Zone 7)
- $1.31 < I_c < 2.05$: Sand (Zone 6)
- $2.05 < I_c < 2.60$: Sandy Mix (Zone 5)
- $2.60 < I_c < 2.95$: Silty Mix (Zone 4)
- $2.95 < I_c < 3.60$: Clay (Zone 3)
- $I_c > 3.60$: Organic or Sensitive Soil (Zone 1, 2)

A value of $I_c = 2.6$ is used as the boundary between drained and undrained soil behavior. Soils with $I_c > 2.6$ are generally considered to behave in an undrained manner, typical of clays and organic soils, while those with $I_c < 2.6$ are more likely to exhibit drained behavior, typical of sands, (Mayne, Cargill, & Greig, 2023) [20]. .

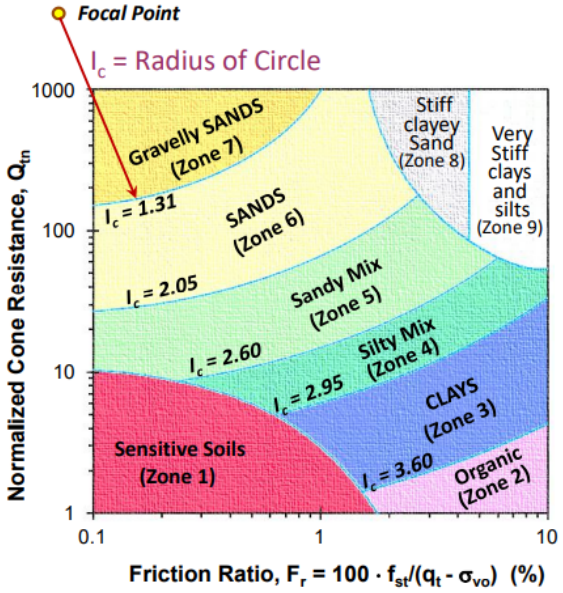

Figure 3.7: CPT Classification Index (Ic) Chart

To define the soil stratigraphy at the site, four plots were generated for each cross section: cone resistance (q_c), sleeve friction (f_s), friction ratio (F_r), and Soil Behavior Type Index (I_c), all plotted against depth (in meters NAP). These plots are presented side by side, allowing for easier interpretation and visualization of the stratified layers.

Additionally, a mean trend line is included in each plot to highlight general trends and support more accurate identification of the soil layers. Figures 3.8 to 3.12 present the resulting plots for the analyzed cross sections.

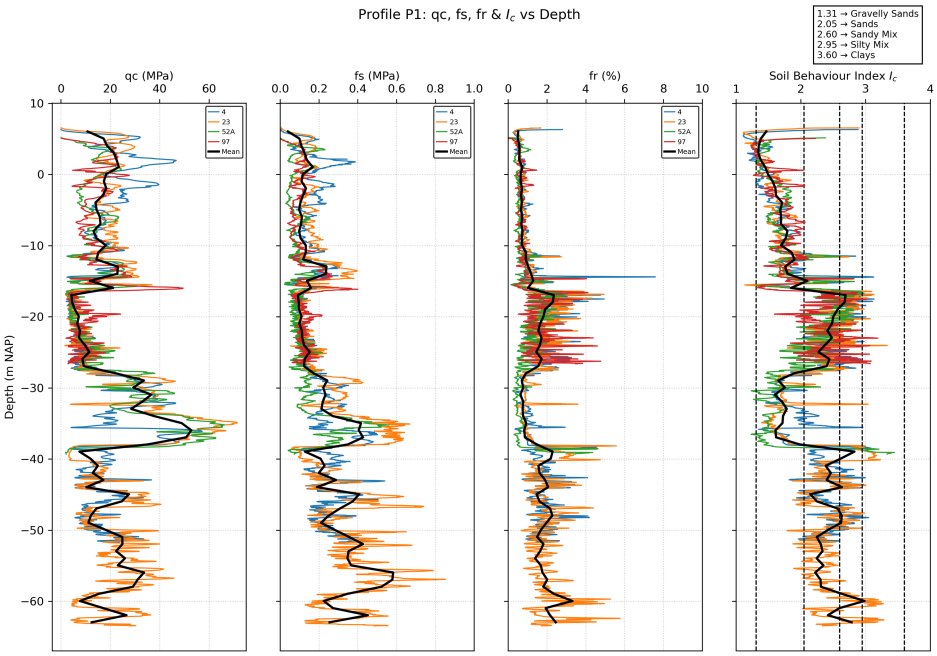

Figure 3.8: Profile P1

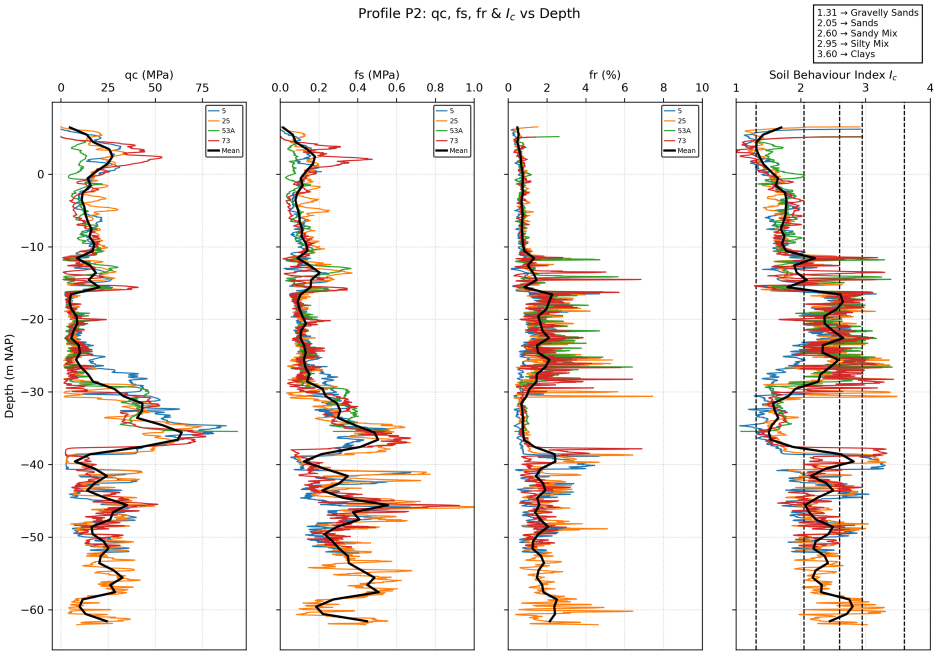

Figure 3.9: Profile P2

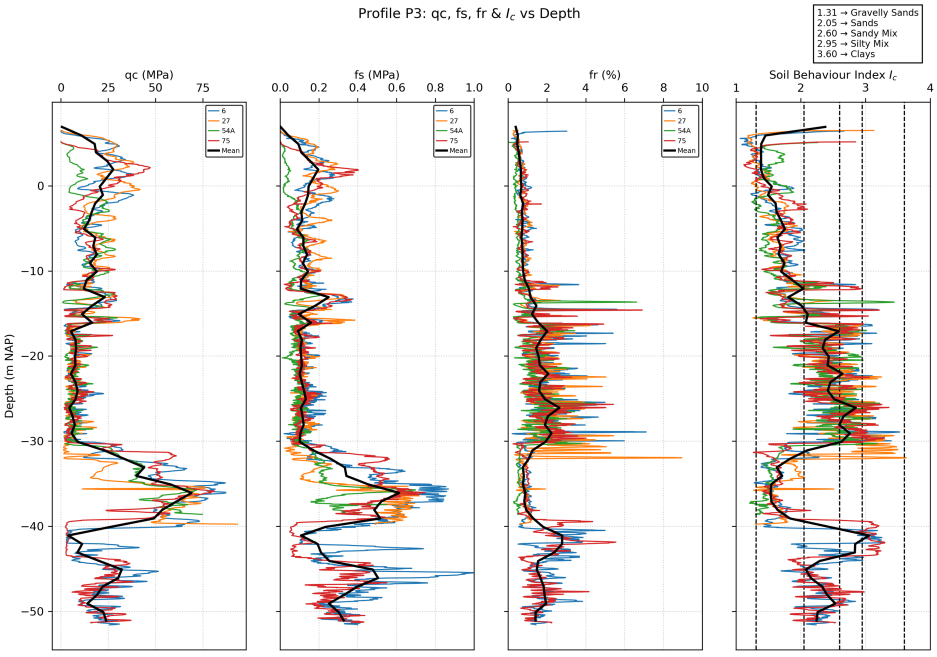

Figure 3.10: Profile P3

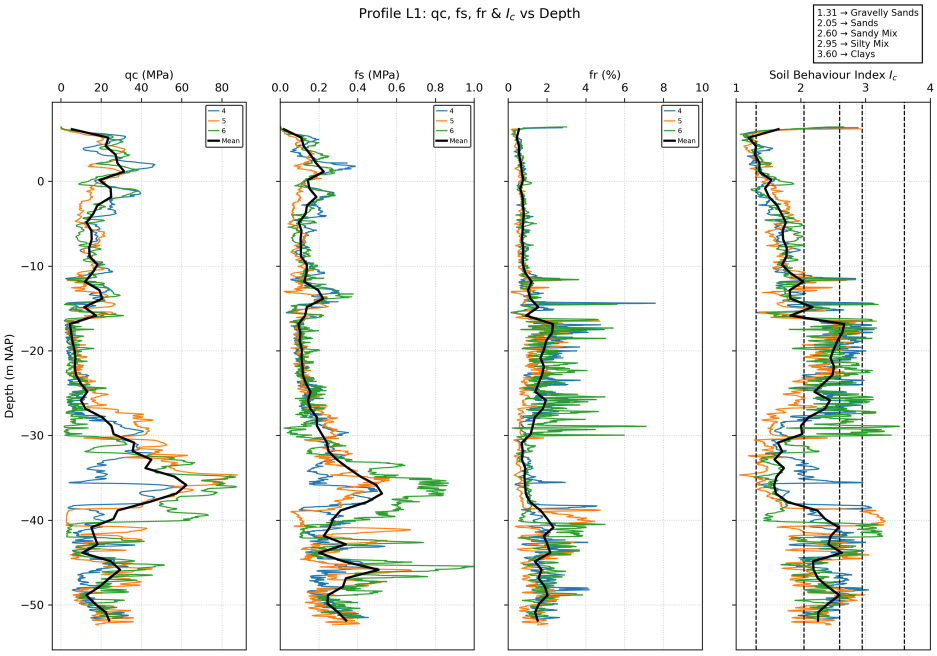

Figure 3.11: Profile L1

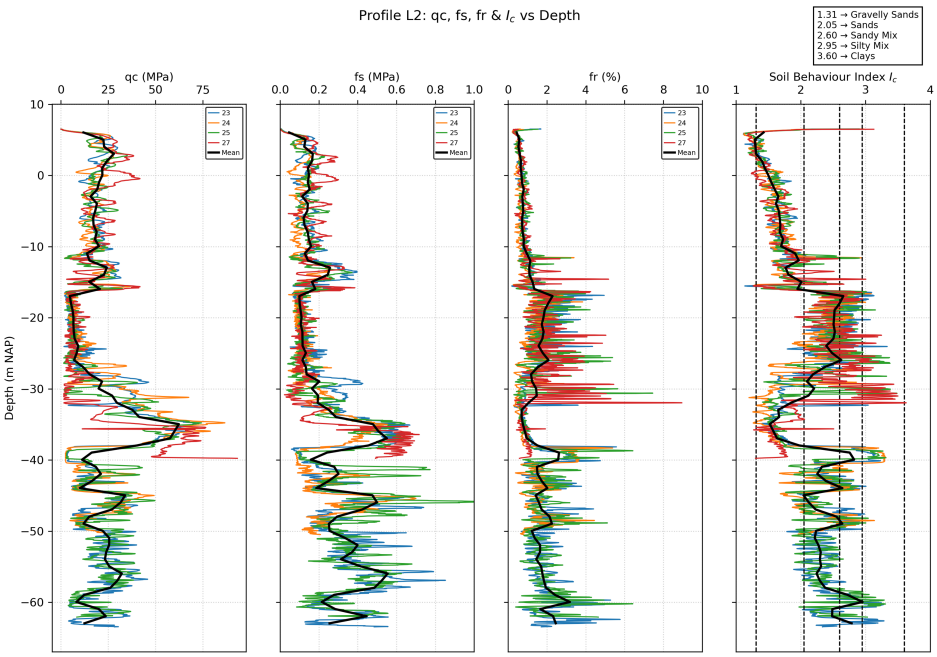

Figure 3.12: Profile L2

It is evident that four distinct soil layers are consistently observed across all profiles. Consequently, Profile P2, which is closest to the quay wall section under study, is selected as the reference for defining the site stratigraphy and determining the parameters.

The layer boundaries are initially identified using the I_c plots and subsequently verified using the corresponding q_c, f_s, and F_r profiles. The I_c plot indicates that:

- **Layer 1** extends from ground level (+ 5 m NAP) to approximately (-16.5 m NAP) and is characterized by I_c values ranging from approximately 1.0 to 1.5, indicating a dense sand, likely of anthropogenic origin.
- **Layer 2** extends from -16.5 m NAP to -25.5 m NAP, with I_c values ranging from about 2.0 to 2.5, indicating a sandy and silty mix.
- **Layer 3** extends from -25.5 m NAP to -40 m NAP, with I_c values between 1.5 and 2.0, indicating a dense sand.
- **Layer 4** extends from -40 m NAP to the end of the CPT test, with I_c values returning to approximately 2.0 to 2.5, indicating another sandy mix layer.

To confirm the accuracy of these layer boundaries, the mean values of I_c, q_c, and f_s for each identified layer were computed. The results were found to align well with the initial visual assessment, supporting the defined stratigraphy. A summary of the computed values is presented in Table 3.2.

Table 3.2: Summary of Mean Soil Parameters for Identified Layers

Layer	**Top Depth** (m NAP)	**Bottom Depth** (m NAP)	**Thickness** (m)	q_c **Mean** (MPa)	f_s **Mean** (MPa)	f_r **Mean** (%)	**Unit Weight** (kN/m^3)	σ_{v0} (kPa)	σ'_v (kPa)	Q_{tn}	I_c **Mean**
Layer 1	5.0	-16.5	21.5	17.4	0.1	0.8	20.0	215.0	132.5	47.2	1.9
Layer 2	-16.5	-25.5	9.0	9.1	0.1	1.7	19.0	386.0	258.5	17.2	2.6
Layer 3	-25.5	-40.0	14.5	40.6	0.3	1.0	21.0	690.5	490.5	57.0	1.9
Layer 4	-40.0	-60.0	20.0	19.8	0.3	1.8	19.0	1070.5	770.5	21.3	2.5

Representative Soil Profile

The soil profile that will be used for analysis is provided in Table 3.3. It consists of four distinct layers identified from CPT data: an anthropogenic sand layer at the top, followed by a silty - clayey sand layer, then a slightly silty dense sand layer, and finally a silty sand layer. The phreatic level is assumed at 0 m NAP based on CPT pore pressure data.

Table 3.3: Representative Soil Profile Adopted for Analysis

Layer Number	Layer Description	Top Depth (m NAP)	Thickness (m)
1	Anthropogenic Fill – Sand	5.0	21.5
2	Silty-Clayey Sand	-16.5	9.0
3	Sand	-25.5	14.5
4	Silty Sand	-40.0	10.0
–	End of Profile	-50.0	–

3.2.3. Parameter Determination

The constitutive model adopted for the analysis is the Hardening Soil (HS) model. This is due to the fact that the Hardening Soil model captures more realistic elastic behavior by distinguishing between unloading and reloading stiffness. It allows for dilatancy. In addition, the HS model takes into account the stress dependency of the soil stiffness that is often observed in general soil behaviour.

Model parameters required for the HS model can be estimated using Cone Penetration Test (CPT) data, as well as through empirical correlations with other known parameters. In addition, parameters, particularly stiffness and strength parameters, can be derived from laboratory tests such as triaxial tests, provided these tests were conducted under appropriate conditions that ensure the reliability of the results.

In this study, the initial estimation of the HS model parameters is primarily based on CPT data and empirical correlations. Laboratory test results are then considered for the calibration of stiffness and strength parameters to enhance the accuracy of the finite element model. However, before incorporating these results, the quality and reliability of the laboratory tests are first critically assessed to determine their suitability for calibration purposes. This includes evaluating the testing procedures, saturation levels, and consistency of the results with site-specific conditions. The laboratory testing program, along with the types of tests conducted, their relevance to parameter estimation, and any limitations, is discussed in detail in the subsequent sections. Table 3.4 presents the model parameters and the corresponding methods used for their computation.

Table 3.4: Hardening Soil Model Parameters and Computation Methods

Parameter	Symbol	Computation Method
Unit Weight	γ	CPT
Relative Density	D_r	CPT
Peak Friction Angle	ϕ'	CPT
Dilation Angle	ψ	Empirical
Reference Secant Stiffness in Standard Drained Triaxial Test	$E_{50,\text{ref}}$	Empirical
Reference Tangent Stiffness for Primary Oedometer Loading	$E_{oed,\text{ref}}$	CPT
Reference Unloading/Reloading Stiffness	$E_{ur,\text{ref}}$	Empirical
Power for the Stress-Level Dependency of Stiffness	m	Empirical
Permeability	k	Empirical

Relative Density

The strength and stiffness of coarse-grained soils, such as sands, are highly dependent on their in-situ density. In geotechnical engineering, it is standard practice to express this density in terms of Relative Density (Dr), which compares the in-situ void ratio to its maximum and minimum possible values. The relative density is given by:

$$Dr = \frac{e_{\text{max}} - e}{e_{\text{max}} - e_{\text{min}}} \tag{3.5}$$

where:

- e is the in-situ void ratio,
- e_{max} is the maximum void ratio,
- e_{min} is the minimum void ratio.

The void ratio e represents the ratio of the volume of voids to the volume of solid particles in a soil mass. Since relative density is closely linked to the mechanical behavior of coarse-grained soils, particularly strength and stiffness, it is often used for parameter estimation. Numerous empirical correlations have been developed between cone resistance (q_c) and relative density (D_r).

The correlation used in this analysis is the one proposed by Kulhawy & Mayne (1990) [17]. This correlation estimates the relative density using the cone resistance (q_c), atmospheric pressure (P_a), and the effective vertical stress (σ'_v). The correlation is given as:

$$D_r^2 = \frac{\frac{q_c}{P_a}}{350\left(\frac{\sigma'_v}{P_a}\right)^{0.5}} \quad [\%] \tag{3.6}$$

where:

- D_r = relative density,
- q_c = cone tip resistance (in kPa),
- σ'_v = effective vertical stress (in kPa),
- P_a = atmospheric pressure (100 kPa).

Peak Friction Angle

Mayne and Kulhawy (2023)[20] defined a correlation between the peak friction angle (ϕ'_p) and the normalized cone resistance Q_{tn} . This correlation was derived from calibration chamber tests conducted on 26 different types of clean sands. In a subsequent study, Mayne and Kulhawy (2023) [20] demonstrated that this correlation also provided a good agreement with triaxial test results for silty sands containing up to 30% fines. Figure 3.13 illustrates the correlation and the fit to experimental data. Therefore, this correlation can be applied for soils with moderate fines content. The correlation is defined below:

$$\phi'_p = 17.6^\circ + 11.0 \cdot \log_{10}(Q_{tn}) \quad [^\circ] \tag{3.7}$$

where:

- ϕ'_p is the peak friction angle in degrees,
- Q_{tn} is the normalized cone resistance
- q_t is the corrected cone resistance,
- σ'_v is the vertical effective stress,
- σ_{atm} is the atmospheric pressure, typically 100 kPa.

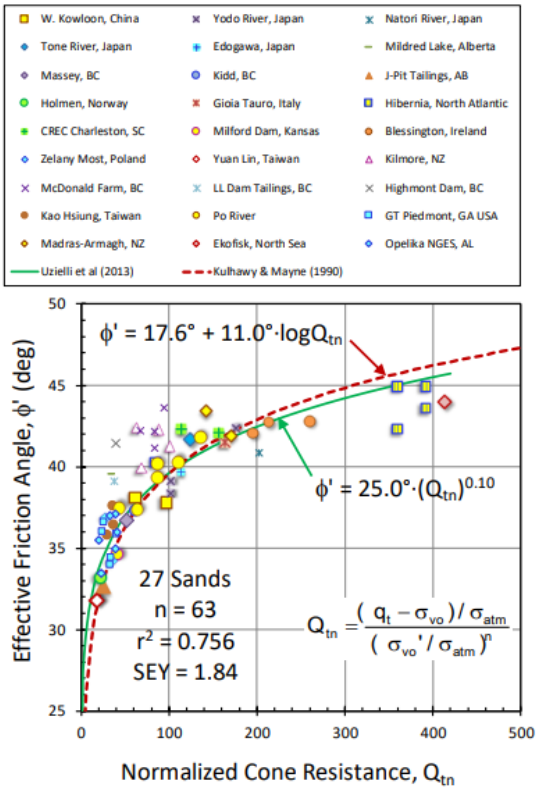

Figure 5.8: Peak friction angle of 27 sands and silty sands versus stress-normalized cone resistance, Q_{tn} (data from Uzielli & Mayne 2019)

Figure 3.13: Correlation for Estimating the Peak Friction Angle [20]

Dilatancy Angle

The dilatancy angle describes the volume change behavior of soil during shearing and indicates whether the soil tends to expand (dilate) or contract (compress) under shear stress. In this analysis, the dilatancy angle is estimated based on the relative density D_r, using the empirical correlation proposed by Brinkgreve et al. (2010) [3], as given by the following equation:

$$\psi = -2 + \frac{12.5 D_r}{100} \quad [^\circ] \tag{3.8}$$

Power Parameter

The power parameter m, which accounts for the stress-dependency of the stiffness moduli in the Hardening Soil model, is correlated with the relative density D_r as proposed by Brinkgreve et al. (2010) [3]. The correlation is given by:

$$m = 0.7 - \frac{D_r}{320} \quad [-] \tag{3.9}$$

Stiffness Moduli

In the Hardening Soil model (HS), stiffness moduli are stress-dependent. To input these into the model, the moduli must be referenced to a standard stress level. The reference stress, denoted as p_{ref}, is typically set to 100 kPa. For normally consolidated coarse-grained soils, the initial estimate of the constrained tangent stiffness modulus, E_{oed}, can be obtained using CPT-based correlations. Mayne and Kulhawy (1990) [17] proposed the following relationship between E_{oed}, the cone resistance q_c, and the relative density RD:

$$E_{oed} = q_c \cdot 10^{1.09 - 0.0075 \cdot RD} \tag{3.10}$$

To convert the stress-dependent modulus to the reference stress level, the following normalization is applied:

$$E_{oed}^{ref} = \frac{E_{oed}}{\left(\frac{\sigma'_v}{p_{ref}}\right)^m} \quad [MPa] \tag{3.11}$$

where σ'_v is the vertical effective stress, and m is the power parameter that defines the stress-level dependency of stiffness.

Based on recommendations by Brinkgreve et al. (2019a), CUR (2003), and Obrzud and Truty (2018) [5], the remaining stiffness moduli used in the HS model are derived as follows:

- $E_{50}^{ref} \approx E_{oed}^{ref}$ for sand layers
- $E_{ur}^{ref} \approx 3 \cdot E_{50}^{ref}$

For different soil types, variation in the multiplier for E_{ur}^{ref} may be used:

- $E_{ur}^{ref} = 3.0 \cdot E_{oed}^{ref}$ for medium to dense sands
- $E_{ur}^{ref} = 4.0 \cdot E_{oed}^{ref}$ for loose sands
- $E_{ur}^{ref} = 5.0 \cdot E_{oed}^{ref}$ for clay layers

Permeability

The permeability (k) of soil layers is estimated using soil behavior type index (I_c) following the correlations proposed by Robertson (2010) [26]. The empirical relationships for different I_c ranges are given as:

$$\text{When } 1.0 < I_c \leq 3.27: \quad k = 10^{(0.952 - 3.04\, I_c)} \quad \text{[m/s]} \tag{3.12}$$

$$\text{When } 3.27 < I_c < 4.0: \quad k = 10^{(-4.52 - 1.37\, I_c)} \quad \text{[m/s]} \tag{3.13}$$

The permeability can also be used to determine the drainage conditions of the layers.

- Soils with permeability $k \geq 10^{-7}$ m/s are typically considered drained.
- Soils with permeability $k \leq 10^{-9}$ m/s are generally considered to behave in an undrained manner.
- Permeability values in the intermediate range $10^{-9} < k < 10^{-7}$ m/s may exhibit partially drained behavior, depending on the loading rate and boundary conditions.

Initial Parameter Values of the Representative Profile

Profile P2 as illustrated in Figure 3.9, which is closest to Quay Wall Section 76, is selected as the reference for defining the site stratigraphy and determining the parameters.

Table 3.5 presents an overview of the initial model parameters adopted for the finite element model (FEM). These parameters are derived based on the average values of cone penetration test (CPT) results, including cone resistance (q_c) and other relevant data, computed per stratigraphic layer.

Cohesion (c') is assumed to be 0 MPa for all layers, given that the soil profile is predominantly coarse-grained.

The unloading-reloading stiffness modulus (E_{ur}) is calculated using a stiffness multiplier of 3, which is deemed appropriate for medium-dense to dense soils, as indicated by the computed relative densities.

The estimated permeability values for all layers fall within the range indicative of drained behavior, as discussed in the preceding section.

No direct information regarding the over-consolidation ratio (OCR) of the soil layers in the Port of Rotterdam area was available in the literature. Therefore, an OCR value of 1.5 is assigned to Layer 3 and 1.2 to Layer 4 to account for possible slight over-consolidation and to better match observed performance.

Table 3.5: Soil Layer Properties

Layer	**Top Depth** (m NAP)	$\mathbf{q_c}$ (MPa)	$\mathbf{k}$ (m/s)	$\mathbf{k}$ (m/day)	**OCR**	D_r (%)	ϕ (°)	ψ (°)	$\mathbf{m}$	E_{oed}	E_{oed}^{ref} (MPa)	E_{50} (MPa)	E_{ur} (MPa)
Layer 1	5.0	17.4	1.18×10^{-5}	1.02	1.0	65	36	6	0.5	69	60	60	180
Layer 2	-16.5	9.1	1.10×10^{-7}	0.0092	1.0	40	31	3	0.6	56	33	33	100
Layer 3	-25.5	40.6	1.35×10^{-5}	1.17	1.5	72	37	7	0.5	143	67	67	202
Layer 4	-40.0	19.8	1.97×10^{-7}	0.017	1.2	45	32	4	0.6	112	36	36	108

Laboratory Test Data

Two boreholes are located within the vicinity of the study area. For triaxial testing, only samples retrieved from one of the two boreholes were available. These triaxial tests may be used to calibrate the strength and stiffness parameters of the soil layers, provided the test data is deemed reliable.

A total of five samples were included in the site investigation report. Among these, four samples fall within the boundaries of Layer 4, while one sample lies between the boundaries of Layer 2 and Layer 3. According to the site investigation report, the sample preparation and testing procedures followed the NEN 5117 standard.

The tests performed were Consolidated Undrained (CU) triaxial tests. This contradicts the initial assumptions made during the preliminary analysis conducted. Therefore, a closer examination of the triaxial test results is essential to evaluate their quality and reliability, ensuring sufficient confidence for the calibration of the initial strength and stiffness parameters used in the FEM analysis.

Triaxial testing remains one of the most essential laboratory techniques for evaluating the stress-strain response and shear strength characteristics of saturated soils. To ensure reliable results, test specimens are typically saturated using back pressure, aiming for a near-complete degree of saturation. Once saturated, isotropic consolidation is usually applied, often by increasing cell pressure, to replicate in-situ conditions, [7].

In Consolidated Undrained (CU) triaxial tests, where no drainage is permitted during shear, it is crucial that the strain rate is low enough to allow uniform distribution of pore pressure throughout the specimen. This is necessary to accurately determine effective stress parameters at failure [7]. Although CU tests are commonly used to estimate undrained strength and stiffness, these values are approximate due to their sensitivity to initial moisture content, sample disturbance, and soil structure [7].

To interpret effective stress parameters from CU tests, precise pore pressure measurements are required. These are typically recorded at the base of the specimen, though mid-height measurements

may be employed to reduce error. If the shear strain is applied too quickly, non-uniform pore pressure distribution may result, particularly due to end restraints. This can lead to inaccurate assessments of effective stresses. Slower strain rates help promote pore pressure equalization, improving the reliability of measurements [7].

It is important to note, however, that even with saturation and proper testing, the soil stiffness values derived from CU tests are typically not reliable for design purposes [7]. This is due to the non-linear response of soil and potential sample disturbance. As emphasized by Atkinson (2000) and Clayton (2011), these limitations must be recognized when interpreting laboratory test data for use in numerical modeling and design [7].

According to the NEN 5117:1991 standard [21], the Consolidated Undrained (CU) triaxial test is a laboratory method used to determine both the undrained shear strength and, depending on the procedure, the effective strength parameters (ϕ' and c′) of saturated soils. The test comprises three main stages: saturation, consolidation, and shearing, with drainage permitted only during the consolidation phase.

The soil specimen is enclosed in a membrane and placed between porous stones within a triaxial cell equipped with pore pressure and cell pressure monitoring systems. Saturation is achieved by applying back pressure until the B-value (Skempton's saturation coefficient) exceeds 0.96, confirming adequate saturation. The specimen is then isotropically consolidated under a predefined effective stress with open drainage lines, allowing volume change measurements until equilibrium is reached.

Following consolidation, axial loading is applied at a constant strain rate with drainage lines closed to maintain undrained conditions. Throughout this shearing phase, axial deformation, load, and pore pressure are continuously recorded. These measurements are used to determine the deviator stress and to calculate the effective stress path. The strain rate must be carefully controlled to prevent significant pore pressure dissipation during loading.

In multi-stage CU testing, the sample undergoes successive consolidation and loading cycles at increasing confining pressures. The standard also outlines requirements for correcting the effects of membrane stiffness and filter reinforcement, and includes protocols for temperature regulation, equipment calibration, dimensional consistency, and thorough sample documentation to ensure test reliability and reproducibility.

Table 3.6 shows the results of the test samples provided in the site investigation report.

Table 3.6: Laboratory Test Results for Clay Samples

Sample no.	Sample Description	Sample Depth (m NAP)	Layer no.	B-Parameter	c' (kPa)	ϕ (°)	$E_{undr;50}$ (MPa)	c_u (kPa)
1	Clay, moderately sandy, medium to fine	-26.2	2	0.97	19.46	35.1	99.56	456.25
2	Clay, strongly humic.	-40.18	4	0.97	36.94	23.5	100.16	471.51
3	Clay, moderately silty	-42.12	4	0.93	75.84	24.6	148.91	705.70
4	Clay, strongly silty	-43.12	4	0.95	7.45	33.9	191.49	1006.28
5	Clay, strongly silty	-44.05	4	0.94	74.81	17.8	90.57	455.89

The reported fitted values of effective friction angle (ϕ'), undrained shear strength (c_u), and secant stiffness modulus (E_{50}) from the triaxial tests appear high when compared to typical expectations for fine-grained soils. Friction angles exceeding 30°, undrained strengths greater than 700 kPa to 1000 kPa, and stiffness values above 50 MPa are uncharacteristic of soft to medium clays and silty clays, and may suggest either overconsolidation, cementation, or issues related to testing quality, such as incomplete saturation.

It is noted that the tested samples contain considerable silt and sand content, which may contribute to enhanced strength and stiffness. However, the $E_{undr;50}$ values ranging from 70,92 MPa to 146,06 MPa significantly exceed the expected range of 10 MPa to 50 MPa typically associated with the described fine-grained soil types. This raises concerns regarding the reliability of the test results.

Furthermore, the Skempton's B-values, used to assess the degree of saturation, were found to be 0,93 for Sample 3, 0,94 for Sample 5, and 0,96 for Sample 4. These values fall just below the recommended minimum threshold of 0,96, indicating that full saturation may not have been achieved. As full saturation is critical for reliable CU test interpretation, particularly for accurate pore pressure measurements, these findings suggest that the tests may not fully capture undrained behavior.

Additionally, the fitted friction angle values reported for Samples 1 and 4 (35,1° and 33,9°, respectively) are unusually high for cohesive soils and indicate a shear strength response more strongly influenced by internal friction rather than cohesion. These high values may reflect the presence of dense sandy or silty inclusions within the clay matrix, or they may be artifacts of test conditions.

Given these inconsistencies, the triaxial test results should be interpreted with caution, as they may not reliably represent the in-situ soil behavior. Contributing factors may include poor test quality, the potentially inappropriate choice of test type, specifically performing Consolidated Undrained (CU) tests instead of Consolidated Drained (CD) tests, and possible miss-classification of the soil.

To verify whether the tested samples are indeed fine-grained, as indicated in the site investigation report, the provided sieve analysis results were reviewed. Sieve analysis is a standard procedure used to determine the particle size distribution (PSD) of granular materials by passing soil through a series of sieves with decreasing mesh sizes. The results are typically presented as a particle size distribution curve, showing the percentage of particles passing through each sieve. According to the site investigation report, the test procedures adhered to NEN 2560 (1980) and NEN 5104 (1989).

Samples corresponding to similar depths as those tested in the triaxial tests were analyzed. Figures 3.14 and 3.15 show the PSD curves for samples 738A and 752, taken at depths of -26.98 m NAP and -44.55 m NAP, respectively. The results indicate that both samples are predominantly sandy soils. Sample 738A exhibits a uniformity coefficient (C_u) of 10.47 and a median grain size (D_{50}) of 275 µm, classifying it as medium, well-graded sand. Sample 752 shows a C_u of 2.99 and D_{50} of 110 µm, indicating a poorly graded fine sand. The percentage of fines (particles < 63 µm) for samples 738A and 752 are 13.4% and 16.6%, respectively, suggesting limited silt or clay content.

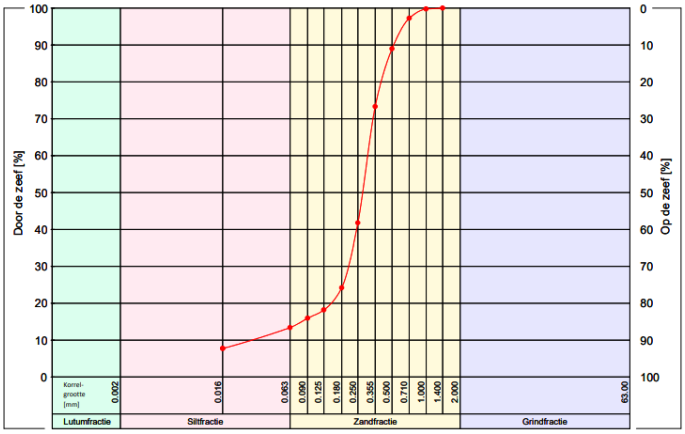

Parameters (alle fracties)								Parameters (zandfractie)						Overige waarden		
	D10 [µm]	D50 [µm]	D60 [µm]	D70 [µm]	D90 [µm]	C_u [-]	C_c [-]	$D10_Z$ [µm]	M_Z [µm]	$D60_Z$ [µm]	$D70_Z$ [µm]	$D90_Z$ [µm]	C_{uZ} [-]	M_g [mm]	<63µm/<2mm [%]	>2mm [%]
●	29	275	305	340	517	10.47	4.84	164	295	322	359	540	1.96	-	13.4	-

C_u = D60 / D10 = Gelijkmatigheidscoëfficient
C_c = $(D30)^2$ / (D60 * D10) = Krommingscoëfficient
M_Z = M_{63} = $D50_Z$ = Zandmediaan
C_{uZ} = $D60_Z$ / $D10_Z$ = Gelijkmatigheidscoëfficient (zandfr.)
M_g = M_{2000} = Grindmediaan

Figure 3.14: Particle size distribution for a sample at a depth corresponding to layer 2

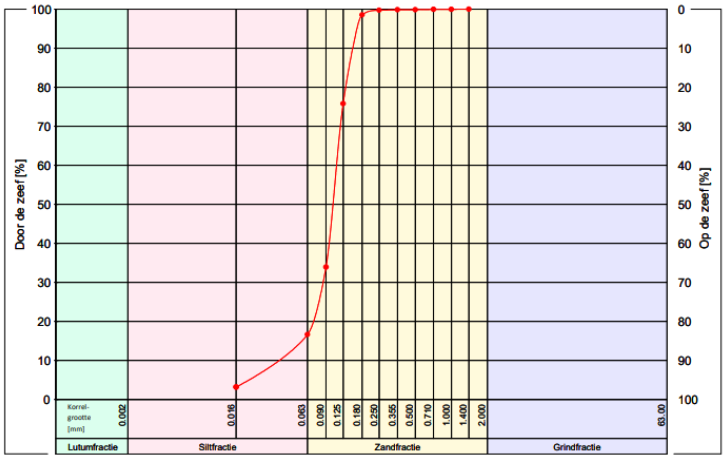

Parameters (alle fracties)								Parameters (zandfractie)						Overige waarden		
	D10 [µm]	D50 [µm]	D60 [µm]	D70 [µm]	D90 [µm]	C_u [-]	C_c [-]	$D10_Z$ [µm]	M_Z [µm]	$D60_Z$ [µm]	$D70_Z$ [µm]	$D90_Z$ [µm]	$C_{u,Z}$ [-]	M_g [mm]	<63µm/<2mm [%]	>2mm [%]
	37	103	110	118	150	2.99	1.79	78	109	115	124	154	1.47	-	16.6	-

C_u = D60 / D10 = Gelijkmatigheidscoëfficient
C_c = (D30)^2 / (D60 * D10) = Krommingscoëfficient
M_Z = M_{63} = $D50_Z$ = Zandmediaan
$C_{u,Z}$ = $D60_Z$ / $D10_Z$ = Gelijkmatigheidscoëfficient (zandfr.)
M_g = M_{2000} = Grindmediaan

Figure 3.15: Particle size distribution for a sample at a depth corresponding to layer 4

This analysis suggests that the tested samples primarily consist of sand, contradicting the initial classification of the materials as fine-grained soils in the triaxial test documentation. Whether the samples contained clay or not, it can be concluded that the site may contain localized pockets of clay. However, these clay inclusions are not extensive and are unlikely to significantly influence the overall soil behavior at the site. Therefore, the soil classification and parameters derived from the CPTs are considered more consistent and representative for defining the stratigraphy.

Nevertheless, the strength parameters from the triaxial tests, particularly the friction angle, can be used to validate the CPT-based estimates. For example, the fitted friction angle for the second layer from the triaxial test was $35.1°$, compared to a computed peak friction angle of $36°$ from CPT correlations. Similarly, for the fourth layer, the fitted value was $33.9°$, while the CPT-derived value was $32°$. This consistency supports the reliability of the CPT-based estimates for defining strength parameters.

3.2.4. Quay Wall Structural Details

The structural layout details discussed in this section are based on the drawings and documentation provided as part of the project resources, unless stated otherwise.

The structural system consists of a combi-wall made up of two primary tubular steel piles connected by intermediate sheet piles. A concrete relieving platform is integrated into the system. This platform is supported by inclined screw injection bearing piles and further stabilized by two rows of screw injection anchors.

Figure 3.16 shows the overall structural configuration of the quay wall system. The system includes a crane rail located 31.75 m away from the front wall, supported by a set of bearing and tensile piles. In this analysis, the crane rail is not taken into consideration, as the focus is primarily on the combi-wall, the relieving platform, and their associated foundation and support systems.

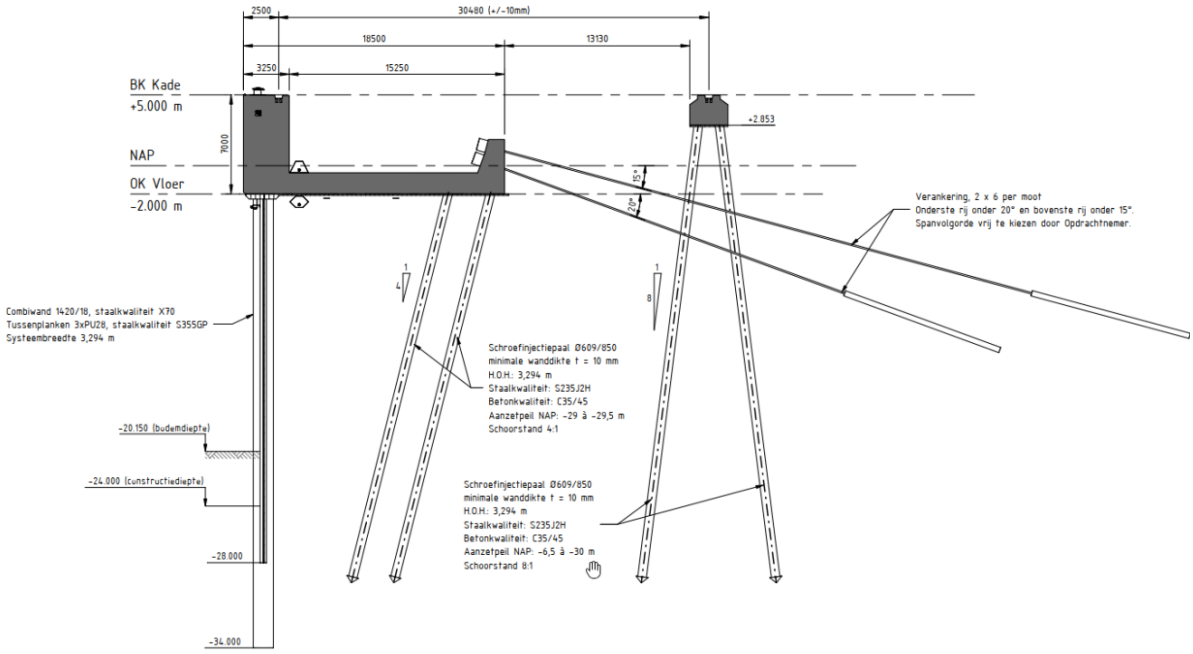

Figure 3.16: Structural layout and key components of the quay wall under study.[23]

This simplification is justified because the crane rails are not structurally connected to the quay wall and are located outside the active zone of lateral earth pressure. Assuming a conservative friction angle of $25°$, and a total wall height (combi-wall and front wall) of 40.5 m, the extent of the active zone can be estimated using Rankine theory as:

$$\theta = 45° - \frac{\phi'}{2} = 32.5°$$

The horizontal width of the active zone is approximately:

$$\text{Width} = 40.5 \cdot \tan(32.5°) \approx 26 \text{ m}$$

Since the crane rail is positioned 31.75 m from the wall, beyond the estimated active zone, it is assumed to have a negligible impact on the structural behavior of the quay wall system. The following sections will present a detailed description of each structural component and its role in the quay wall system. The detailed structural layout for all quay wall structural components together with the summary tables can be found in Appendix C.

Combined Wall System

The system center to center spacing is 3.294 meters. The primary structural elements consist of steel tubular piles with a diameter of 1420 mm and a wall thickness of 20 mm. These piles have a steel grade X70 and extend from -2.0 m NAP to -35.5 m NAP, therefore the primary tubular piles have a total embedded length of 33.5 meters. The tubular piles are equipped with welded interlocks of type C9 (steel grade S355GP) to connect with the intermediate sheet piles. Figure 3.17 shows the structural layout of the Combi-Wall.

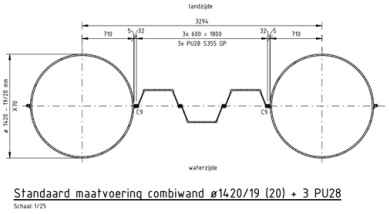

Figure 3.17: Structural Layout of the Combi-Wall

The secondary structural elements consist of 3 PU28 U-profile sheet piles made from S355GP steel. Each sheet is 600 mm wide, forming a combined sheet pile width of 1800 mm between tubular piles. These sheet piles extend from -2.0 m NAP to -28.0 m NAP, providing 26 meters of embedded length. Figure 3.18 shows the layout of the intermediate sheet piles.

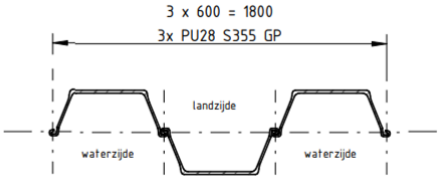

Figure 3.18: Structural Layout of Secondary Sheet Pile

Front Wall and Relieving Platform

The dimensions of the relieving platform and front wall were determined based on the structural layout of the quay wall shown in Figure 3.16. The front wall has a width of 3.25 m and a length of 7 m. The relieving platform measures 1.8 m in thickness and 15 m in total length. Anchors connect to the platform via a concrete plate measuring 1 m in width and 3 m in length.

The concrete is assumed to behave as uncracked, with an elastic modulus of $E = 30{,}000$ N/mm^2, based on recommendations in [10]. As a reference, the stiffness of concrete elements can vary significantly—typically by a factor of three—depending on whether the concrete is assumed to be cracked ($E \approx 10{,}000$ N/mm^2) or uncracked ($E \approx 30{,}000$ N/mm^2).

The relieving platform is supported by two rows of inclined screw injection bearing piles and further stabilized using two rows of screw injection anchors.The front wall and the combi wall are connected by a cast iron saddle, forming a hinged connection between the two structural elements.

Bearing SI Piles

The project includes two screw injection bearing piles with a diameter of 609 mm and a total length of approximately 31 m each, installed at an inclination of 4:1. These piles are constructed using C35/45 concrete with a concrete cover of 40 mm and are reinforced in the upper section (from -2.00 m to -4.00 m NAP). Below -4.00 m NAP, the pile is not reinforced and extends until -35 m NAP. Table 3.7 presents the structural details of the bearing piles used in the quay wall system.

Table 3.7: Bearing Pile Specifications

Type	Wall thickness (mm)	Quantity	Cut off level (m NAP)	Inclination	Length (m)	Concrete grade	Steel grade
SI 609/850	10	2	–32.000	4:1	30.923	C35/45	S235 J2H

Anchor System

The quay wall has a total width of 23 m. The quay wall anchorage system consists of screw injection anchors arranged in two rows of six anchors each, totaling twelve anchors. The lower row is inclined at an angle of 20°, while the upper row is inclined at 15°.Each anchor comprises a steel tube with an outer diameter of 101.6 mm and a wall thickness of 25 mm, resulting in a cross-sectional area of 5755 mm^2.

The total lengths of the anchors are approximately 46.0 m for the lower row and 54.5 m for the upper row. The lengths of the grout bodies are 18.0 m and 16.8 m for the lower and upper rows, respectively. The grout body begins at approximately –9.0 m NAP.

All anchors are pre-stressed with an initial load of 220 kN and are designed for a maximum working load of 2200 kN. The steel used in the anchors has an elastic modulus of 185 GPa. The horizontal center-to-center spacing between adjacent anchors is 3.294 m. Table 3.8 presents the structural details of the anchor used in the quay wall system.

Table 3.8: Anchor Specifications

Anchor Angle	Quantity	Insertion Level (m NAP)	Start Grout (m NAP)	Pmax (kN/anchor)	Prestress (kN/anchor)
20.00°	72	0.350	–9.000	2200	220
15.00°	72	1.350	–9.000	2200	220

3.3. Field Measurement During the Dredging Phase

In this section, the field measurements conducted at the site during the dredging phase are discussed. First, the dredging activities are described, including their extent and sequence. Following this, the inclinometer measurement data corresponding to the dredging activities are presented. These measurements are essential for the calibration and validation of the Finite Element Model (FEM). Moreover, the dredging phases are also critical for modelling the construction stages.

3.3.1. Dredging Details

The dredging data provided included XYZ files, along with contour maps showing ground elevations before and after dredging. There are a total of six dredging phases. Table 3.9 provides a summary of the dredging details, including the date and the approximate ground elevation after each phase.

To evaluate the change in ground level relative to the quay wall, the horizontal distance of each XYZ measurement point from the wall was calculated using the X and Y coordinates. The corresponding Z-value (elevation) from the XYZ data was then plotted against this horizontal distance for each dredging phase. This enables a clear visualization of the dredging progression.

Figure 3.19 shows the plot of dredging depth (m NAP) against horizontal distance from the wall, covering all six dredging phases.

Table 3.9: Dredging Activity Details

Phase	Week	Date	Ground Level After Dredging (m NAP)
1	25	23/06/2024	-8.5
2	26	30/06/2024	-12.5
3	27	07/07/2024	-16.5
4	33	18/08/2024	-21
5	34	25/08/2024	-22
6	35	01/09/2024	-21

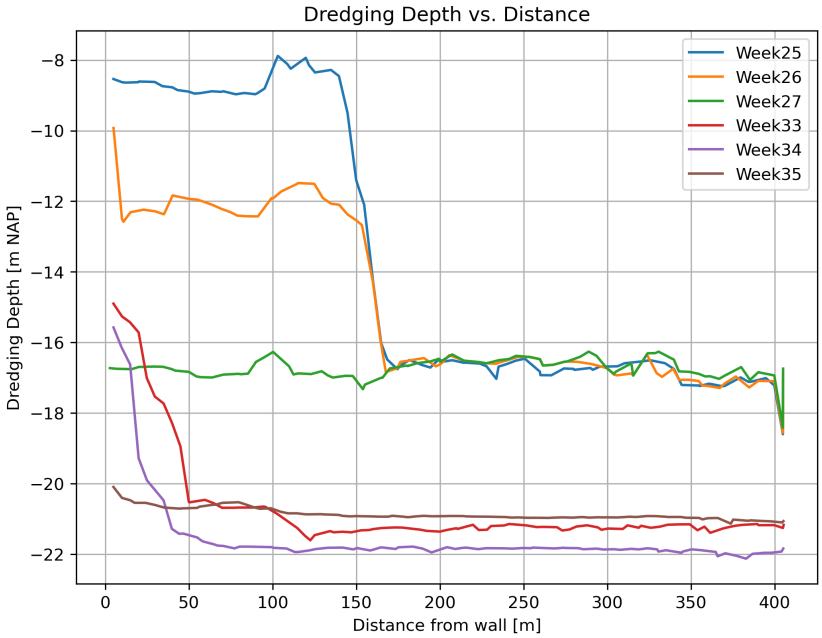

Figure 3.19: Dredging depth (m NAP) vs. Distance from the Wall for all Dredging Phases

3.3.2. Inclinometer Data

The inclinometer data were provided to monitor the lateral displacement of the wall. Table 3.10 summarizes the measurement numbers and corresponding dates. The inclinometers were installed to monitor the lateral displacements of the quay wall. They extend from the top of the front wall through to the toe of the combi wall, with tubes positioned inside both structural elements. This configuration ensures that the measured data captures the full depth of the wall behavior.

To ensure accurate modelling of the construction stages and reliable calibration and validation of the Finite Element Model (FEM), the inclinometer readings should be taken after the dredging phases. Table 3.11 summarizes the inclinometer measurements selected for FEM calibration and validation, together with the corresponding dredging phase details.

Figures 3.20 and 3.21 present the inclinometer measurement data plot given in the documentation as lateral displacement (mm) versus depth (m), alongside the profile of the final dredging depth used in analysis. The top of the front wall is located at 40 m depth, while the toe of the combi wall is positioned at 0 m depth. In these plots, negative lateral displacements indicate movement towards the landside, whereas positive values represent displacements towards the waterside.

During Dredging Phase 1, the maximum measured lateral displacement is approximately –15 mm, occurring primarily in the front wall. This restrained movement toward the landside can be attributed to three key factors: (1) the anchors were already pre stressed, mobilizing sufficient tension and generating a counter-moment that holds the wall landward; (2) the wall's flexural rigidity resists rotation; and (3) the residual soil wedge on the passive side continues to provide substantial earth resistance. Consequently, any initial tendency for the wall to shift waterside is effectively arrested by the combined action of anchor pretension, structural stiffness, and passive soil support. For Dredging Phase 3, the displacement increases to around $+16$ mm, while Phase 6, representing the final and deepest dredging stage, shows a maximum lateral displacement of approximately $+30$ mm.

It is important to note that inclinometer readings are recorded relative to the toe, which is assumed to remain fixed. However, in reality, the toe of the combi wall is not entirely restrained and may undergo minor lateral deformation, especially as dredging progresses and passive resistance reduces at greater depths. This assumption may result in a slight underestimation of absolute wall displacements in the deeper sections.

Table 3.10: Inclinometer Measurement Dates

Inclinometer Measurement No.	Date
Reference	04/07/2023
1	14/06/2024
2	24/06/2024
3	15/07/2024
4	17/09/2024
5	17/10/2024
6	16/12/2024
7	20/01/2025
8	17/02/2025
9	18/03/2025

Table 3.11: Inclinometer Measurements and Corresponding Dredging Phases

Inclinometer Measurement no.	Date	Dredging Phase	Week	Dredging Date	Ground Level After Dredging (m NAP)
2	24/06/2024	1	25	23/06/2024	-8.5
3	15/07/2024	3	27	07/07/2024	-16.5
4	17/09/2024	6	35	01/09/2024	-21.0

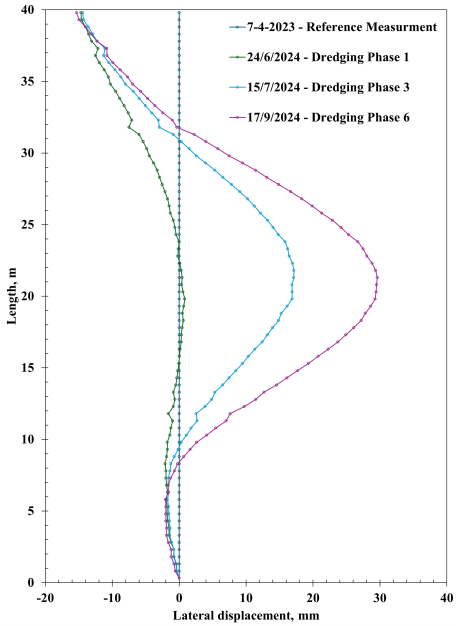

Figure 3.20: Inclinometer Data (Displacement vs. Length).

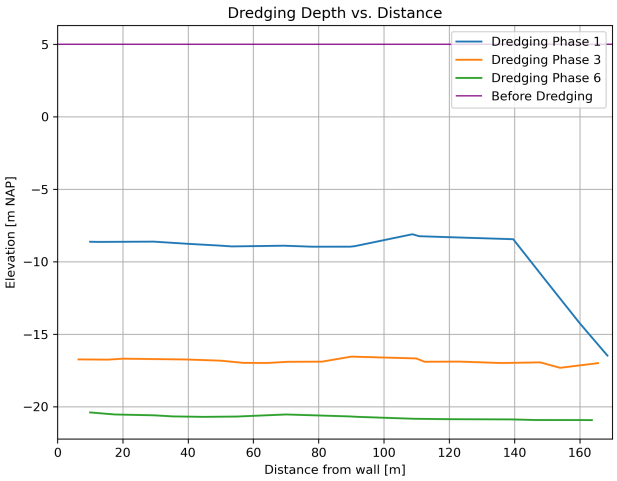

Figure 3.21: Final Dredging Profile along Horizontal Distance from wall.

3.4. FEM Setup

In this section, the setup of the Finite Element Model (FEM) is described. The model was developed and analyzed using PLAXIS 2D software. The section includes a detailed explanation of the model domain dimensions and the rationale behind the selected size, the modeling assumptions made, the mesh size, and the definition of material properties for both structural and geotechnical elements. Additionally, the sequence of construction stages implemented in the model is presented.

3.4.1. Model Assumptions

The analysis is performed under the assumption of plane strain conditions, which is appropriate given the constant cross-sectional geometry of the quay wall and its significant extension in the out-of-plane (z) direction. Under these conditions, the stress and deformation are assumed to occur only in the x

and y directions, while variations in the z-direction are considered negligible.

Following the estimation of soil permeability based on CPT data and the identification of the stratigraphy, a drained analysis is adopted. This assumption is justified by the relatively high permeability values of the soil layers, which suggest that pore water pressures are able to dissipate sufficiently during construction.

At the point between the front wall and the combi wall, a rotational connection is introduced to represent the cast iron saddle, which is designed to function as a hinge. However, in practice such connections may not behave as perfectly free hinges and can exhibit some degree of rotational stiffness. To evaluate the potential impact of this behavior, an additional analysis is carried out in which the hinge is replaced with a fully fixed connection, enabling a comparative assessment of the structural response. This will be further elaborated in the next chapter.

3.4.2. Model Domain

The dimensions of the model domain were defined to ensure sufficient space for accurate stress distribution and to encompass both the active and passive earth pressure zones. The model extends from 0 m to 250 m in the horizontal (x) direction and from 5 m to −60 m in the vertical (y) direction. The quay wall is positioned at x = 100 m, with the top of the front wall aligned at ground level (5 m). This configuration provides 100 m of passive zone and 150 m of active zone relative to the wall. The domain was deliberately chosen to be large enough in both directions to avoid boundary effects influencing the results. This was verified through the model output, which showed no significant stress concentrations or displacement anomalies near the domain boundaries, confirming that the selected model size was sufficient and did not compromise the accuracy of the simulation results.

3.4.3. Model Inputs

Soil Parameters

The first step in setting up the PLAXIS model is defining the soil profile, which is achieved by creating a borehole within the software. The representative soil stratigraphy, as determined in the previous section, is input into the model accordingly. As previously stated, the constitutive model adopted for the analysis is the Hardening Soil Model (HS). In addition, a supplementary analysis will be carried out using the Hardening Soil Small-Strain model (HS-small model) to evaluate the influence of small-strain stiffness on the overall response of the quay wall system, this will be further elaborated in the next chapter.

Table 3.12 provides a summary of the input soil properties, including layer boundaries and the corresponding constitutive model parameters used in the FEM simulations. The phreatic level is defined at an elevation of 0 m.

Table 3.12: Soil Layer Properties for FEM

Layer	Top Depth (m)	Bottom Depth (m)	Saturated γ (kN/m^3)	Unsaturated γ (kN/m^3)	$E_{oed\,ref}$ (MPa)	$E_{50\,ref}$ (MPa)	$E_{ur\,ref}$ (MPa)	ϕ (°)	ψ (°)	m
Layer 1	5	-16.5	20.0	18	60	60	180	36	6	0.5
Layer 2	-16.5	-25.5	19.0	16	33	33	98	31	3	0.6
Layer 3	-25.5	-40	21.0	18	67	67	202	37	7	0.5
Layer 4	-40	-60	19.0	16	36	36	107	32	4	0.6

Additional model parameters are summarized in Table 3.13. These include Poisson's ratio (ν), a material constant that defines the ratio of lateral strain to axial strain under uniaxial loading, set to 0.2 for all soil layers. The coefficient of earth pressure at rest (K_0) for normally consolidated soils is automatically calculated by PLAXIS using the expression:

$$K_0 = 1 - \sin(\phi')$$

where ϕ' is the effective friction angle of the soil.

The interface strength reduction factor (R_{int}), representing the ratio of interface shear strength relative to the adjacent soil, is set to 0.8 based on the recommendations of De Gijt and Broeken (2013) [10].

Finally, the failure ratio (R_f), which governs the failure surface in the hardening soil model, is set to 0.9. These parameters are consistent across all layers in the model.

Table 3.13: Additional Soil Model Parameters Used in FEM

Parameter	Symbol	Value	Unit
Poisson's Ratio	ν	0.2	–
Coefficient of Earth Pressure (NC)	K_0	$1 - \sin(\phi')$	–
Interface Stiffness Ratio	R_{int}	0.8	–
Failure Ratio	R_f	0.9	–

Structural Parameters

Now that the soil layers and their parameters have been inputted, the next step involves defining the structural elements in the model. The structural system of the quay wall consists of the combi-wall, front wall, relieving platform, screw injection (SI) bearing piles, anchor plate, anchors, and grout body.

The combi-wall, front wall, relieving platform, and anchor plate are modeled using plate elements. A plate element in PLAXIS is used to represent thin, linear structures capable of resisting axial forces, shear forces, and bending moments. They are typically applied to model walls, slabs, sheet piles, and similar slender structural components. In PLAXIS, these plate elements are drawn along the centerline of the real-life structural member.

Closer examination of the structural layout shows that the centerlines of the relieving platform, front wall, and combi-wall do not align perfectly. The relieving platform is positioned higher, while the front wall extends slightly below it. Additionally, a small eccentricity of approximately 2 cm exists between the front wall and the combi-wall. This misalignment is considered negligible and is ignored in the model, as it is not expected to significantly affect the results. Figure 3.22 illustrates the relative positions of the structural centerlines.

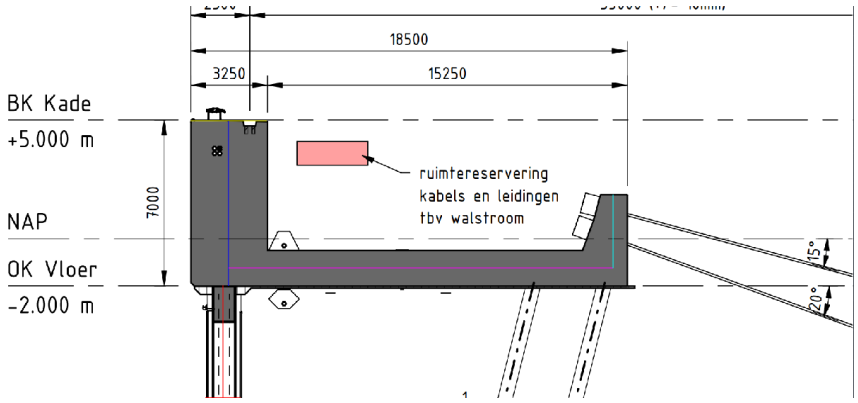

Figure 3.22: Centerline alignment showing minor eccentricity between structural components.

It is important to note that plate elements in PLAXIS have no cross-sectional area, and thus no end-bearing capacity. Without additional treatment, a vertically loaded plate may unrealistically punch through underlying soil layers. To prevent this, PLAXIS offers the option to "prevent punching," which restricts the soil zone directly beneath the plate from undergoing plastic deformation. This is a numerical safeguard to ensure realistic vertical behavior and does not simulate actual end-bearing resistance.

Table 3.14 summarizes the input parameters for the plate elements, including mechanical properties and geometric dimensions. Key input parameters include the self-weight, axial stiffness (EA), bending stiffness (EI), and Poisson's ratio. For the combi-wall, only the contribution of the tubular piles is considered; the intermediate sheet piles are excluded, assuming their effect on global stiffness is negligible.

The self-weight of the combi-wall is also ignored due to its minor influence compared to surrounding soil.

In contrast, for concrete components like the relieving platform and front wall, self-weight is included, as it significantly influences structural response.

The bending stiffness is calculated as:

$$EI = E \cdot I$$

where E is the modulus of elasticity and I is the second moment of inertia. For the combi-wall (tubular sections), I is computed using:

$$I = \frac{\pi(D^4 - d^4)}{64}$$

where D is the outer diameter of the tubular pile and d is the inner diameter (i.e., $D - 2t$, where t is the wall thickness).

For rectangular sections (e.g., front wall, relieving platform, anchor plate), I is calculated using:

$$I = \frac{bh^3}{12}$$

where b is the width (in the out-of-plane direction) and h is the height (in the direction of bending) of the rectangular section.

As the relieving platform and the front wall are continuous elements in the out-of-plane direction, a Poisson's ratio is implemented to account for the out-of-plane stiffness.

Table 3.14: Structural Properties of Wall Elements

Element	Parameter	Value	Unit
Combi-wall	Modulus of Elasticity (E)	210	GPa
	Diameter of Tubular Piles	1.42	m
	Wall Thickness	0.02	m
	Spacing	3.294	m
	Axial Stiffness (EA)	1.12×10^7	kN/m
	Bending Stiffness (EI)	2.69×10^6	kNm^2/m
Front Wall	Modulus of Elasticity (E)	30	GPa
	Width	3.25	m
	Out-of-Plane Thickness	1	m
	Axial Stiffness (EA)	9.75×10^6	kN/m
	Bending Stiffness (EI)	8.58×10^7	kNm^2/m
Relieving Platform	Modulus of Elasticity (E)	30	GPa
	Width	1.82	m
	Out-of-Plane Thickness	1	m
	Axial Stiffness (EA)	5.46×10^7	kN/m
	Bending Stiffness (EI)	1.51×10^7	kNm^2/m
Anchor Plate	Modulus of Elasticity (E)	30	GPa
	Width	1	m
	Out-of-Plane Thickness	1	m
	Axial Stiffness (EA)	3.00×10^7	kN/m
	Bending Stiffness (EI)	2.50×10^6	kNm^2/m

At the point between the front wall and the combi-wall, a rotational connection is introduced to simulate a hinge. This configuration is intended to replicate the behavior of a cast iron saddle, which is assumed to be present based on typical design practices. The hinge connection allows relative rotation between the two wall elements without transferring bending moments, thereby enabling a more realistic representation of their structural interaction in the model. The analysis also includes when the connection between the front wall and the combi wall is fixed.

The SI bearing piles and the grout body are both modelled as embedded beams. Embedded beams are structural elements used to model slender structures, such as piles or ground anchors, that interact with the surrounding soil. Unlike standard beam elements, embedded beams are not physically connected to soil nodes; instead, they are “embedded” in the soil continuum using coupling springs that simulate the interaction between the beam and the soil.

The input parameters of the embedded beams include the modulus of elasticity, unit weight, diameter (or circumference), spacing, skin resistance, and base resistance. The skin resistance and the base resistance are computed using the following equations:

$$F_{\text{max}} = \alpha_p \cdot q_b \cdot A_{\text{tip}} \tag{3.14}$$

$$T_{\text{max}} = \alpha_s \cdot q_s \cdot A_{\text{circumference}} \tag{3.15}$$

In these equations, α_s and α_p are pile factors that depend on the material and installation method of the pile. The values used in this model are $\alpha_s = 0.63$ and $\alpha_p = 0.009$.

For the SI piles, both q_s and q_b are conservatively taken as 15 MPa, which represents the upper limit of cone resistance (q_c). This is justified by the fact that the piles extend through the first three soil layers. The computed maximum skin resistance is 260 kN/m and the maximum base resistance is 2750 kN. Table 3.15 summarizes the input parameters for the SI bearing piles.

Table 3.15: SI Bearing Piles – Embedded Beam Parameters

Parameter	**Value**	**Unit**
Modulus of Elasticity (E)	30	GPa
Unit Weight	25	kN/m^3
Diameter	0.609	m
Spacing (L_{spacing})	3.294	m
qs and qb	15	MPa
Skin Resistance T_{max}	260	kN/m
Base Resistance F_{max}	2750	kN

For the grout body, it is assumed that only the skin friction contributes to the load transfer, with no base resistance ($F_{\text{max}} = 0$). The q_s value is taken from the anchor report as 11 MPa, and the circumference is given as 1.257 m. The same pile factor $\alpha_s = 0.63$ is used. The resulting skin resistance is 130 kN/m. The grout body input parameters are summarized in Table 3.16.

Table 3.16: Grout Body – Embedded Beam Parameters

Parameter	Value	Unit
Modulus of Elasticity (E)	20	GPa
Unit Weight	20	kN/m^3
Circumference	1.257	m
Spacing (L_{spacing})	3.294	m
Skin Resistance T_{max}	130	kN/m
Base Resistance F_{max}	0	kN

Lastly, the anchors are modelled as node-to-node anchors. Node-to-node anchors are a type of structural element that model an elastic connection between two non-adjacent nodes. This is particularly useful for representing the free (unbonded) length of anchors. Since the anchors are pre-stressed in reality, this approach allows pre-stress to be introduced during staged construction, thereby modelling the site conditions more accurately.

The input parameters for the node-to-node anchors include the spacing and the axial stiffness EA. The anchor spacing is provided in the anchor report as 3.294 m, the modulus of elasticity E is given as 185 GPa, and the cross-sectional area is 5755 mm^2. The resulting axial stiffness and the pre-stress force applied are calculated accordingly. Table 3.17 summarizes the input parameters.

Table 3.17: Node-to-Node Anchor Input Parameters

Parameter	Value	Unit
Modulus of Elasticity (E)	185	GPa
Cross-Sectional Area	5755	mm^2
Spacing (L_{spacing})	3.294	m
Axial Stiffness (EA)	1.064E6	kN
Pre-Stress Force	220	kN

Figure 3.23 illustrates the developed FEM configuration, displaying both the defined soil stratigraphy and the modelled structural elements of the quay wall system, including the combi wall, front wall, relieving platform, anchor system, and SI bearing piles.

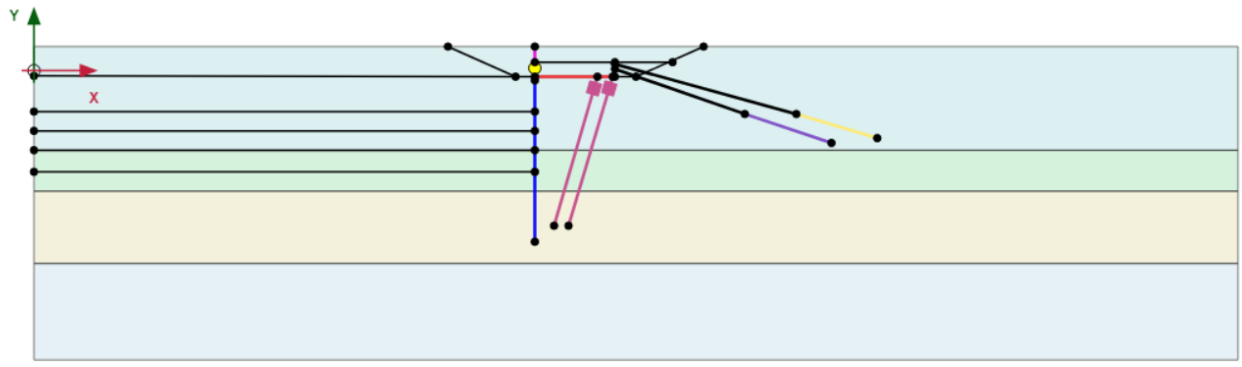

Figure 3.23: FEM model with structural layout and soil layers

3.4.4. Mesh Size

The mesh size used in the analysis is a medium mesh with local mesh refinement near the combi wall, piles, and anchors. This choice ensures a good balance between computational efficiency and numerical accuracy. Medium mesh density across the general domain allows for reasonable run times, while the localized refinement near critical structural components is essential to accurately capture stress concentrations, interaction effects, and deformation behavior. In particular, the interface between structural elements and the surrounding soil requires finer discretizations to model stress transfer mechanisms effectively. Additionally, mesh refinement near anchors and piles improves the resolution of axial and shear force distributions along embedded beams, contributing to a more reliable simulation of structural performance. This approach follows established FEM modelling practices where mesh density is increased in zones of high gradient response, ensuring numerical convergence and reducing the risk of underestimating localized effects. Figure 3.24 presents the finite element mesh of the model.

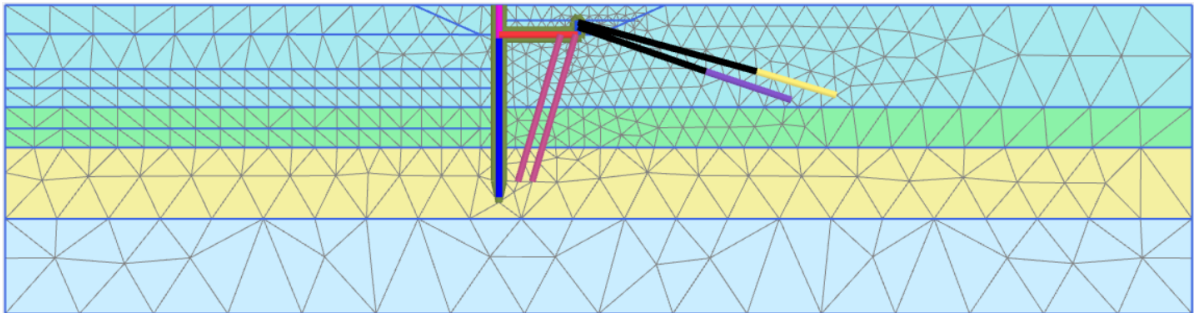

Figure 3.24: FEM Mesh Plot

3.4.5. Construction Stages

The construction sequence was inferred from relevant literature and similar case studies in the Port of Rotterdam. The stages were modelled to reflect the installation of structural elements and the associated ground modifications as realistically as possible.

- **Initial Phase (K_0 Procedure):** The initial stress state is generated using the K_0-procedure in PLAXIS. To satisfy the method's assumptions, the soil profile is first assumed to be horizontal, which justifies application of the K_0-procedure. The coefficient of earth pressure at rest (K_0) is then derived from the soil parameters as described earlier.
- **Excavation and Dewatering:** A shallow sloped excavation is performed down to -2 m (the top level of the combi wall). Simultaneously, the phreatic level is lowered from 0 m to -2.2 m to allow for dry working conditions during structural installation.
- **Installation of Combi-Wall and SI bearing piles:** The combi wall and screw injection (SI) bearing piles are installed.
- **Installation of Concrete Structural Elements:** This phase includes the installation of the front wall, relieving platform, and anchor plate. The hinge connection between the combi wall and front wall is also activated.
- **Sand Fill and Groundwater Restoration:** Sand fill is placed on top of the relieving platform up to the level of the anchor plate to allow anchor installation. The groundwater table is then restored to its original level at 0 m NAP.
- **Anchor Installation and Pre-stressing:** Anchors are installed and pre-stressed based on the design load requirements.
- **Sand Fill to Top of Front Wall:** The area is filled with sand up to the top level of the front wall.
- **Dredging Phases:**
  - **Phase 1:** Dredging from +5 m to -8.5 m.
  - **Phase 3:** Continued dredging from -8.5 m to -16.5 m.
  - **Final Phase:** Final dredging from -16.5 m to -21 m.

Figures 3.25a to 3.25j illustrate the construction sequence as implemented in the PLAXIS model. All subsequent dredging phases after the initial step were modelled in PLAXIS using plastic deformation analysis. This type of analysis enables the simulation of irreversible soil deformations by accounting for material yielding beyond the elastic limit.

Plastic deformation analysis in PLAXIS is conducted using elasto-plastic constitutive models, such as the Hardening Soil model, which distinguish between elastic and plastic strains. Plastic strains represent permanent deformations that occur once the stress state exceeds the yield surface defined by the material model. As plastic straining progresses, the yield surface evolves according to predefined hardening laws, capturing changes in stiffness and strength due to loading history. The output includes not only total deformation, but also the distribution of plastic strain zones highlighting where yielding occurs in the mesh.

It is important to note that in the PLAXIS model, the dredging construction phases are simulated by removing the entire soil block down to the target depth of each respective phase. This represents a simplified approach in which each dredging stage is modeled as a single-step excavation. In real-world projects, however, dredging is not carried out as a single-step excavation. Instead, the actual construction process includes staged depth increases, and the use of temporary slopes or support structures to ensure stability during excavation. Real-life dredging operations are far more iterative and detailed than what is represented in the simplified FEM approach in this model. Consequently, this modeling approximation may influence the predicted wall behavior, particularly in terms of the magnitude and distribution of lateral displacements.

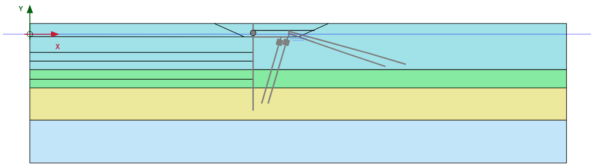

(a) Initial Phase

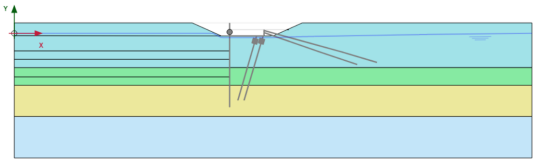

(b) Excavation and Dewatering

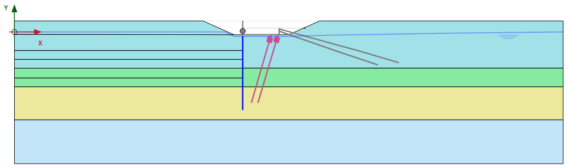

(c) Installation of Combi-Wall and SI bearing piles

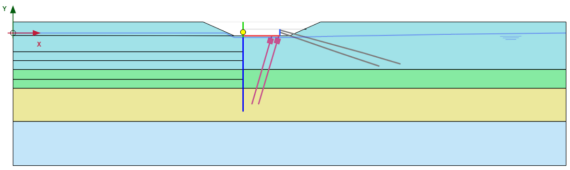

(d) Installation of Concrete Structural Elements

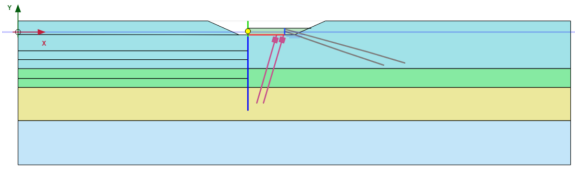

(e) Sand Fill and Groundwater Restoration

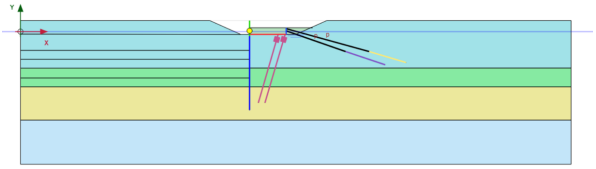

(f) Anchor Installation and Pre-stressing

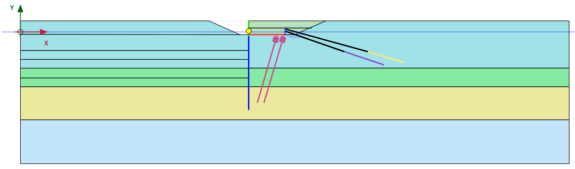

(g) Sand Fill to Top of Front Wall

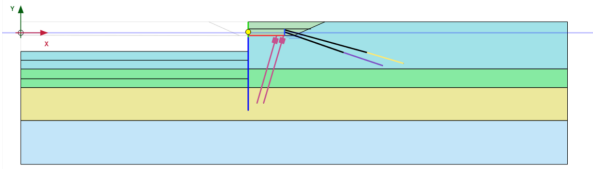

(h) Dredging Phase 1

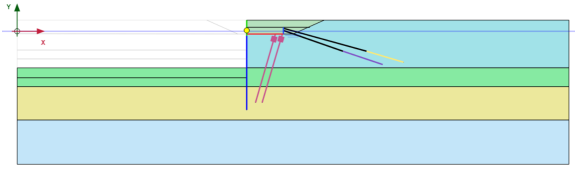

(i) Dredging Phase 3

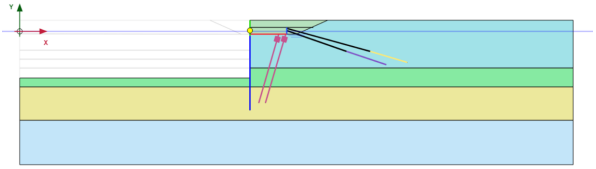

(j) Final Dredging Phase

Figure 3.25: Construction Sequence

3.5. FEM Calibration, Sensitivity Analysis, and Validation

3.5.1. FEM Calibration Method

Calibration of the FEM was performed using inclinometer measurements of wall displacements. Key input parameters, primarily soil stiffness (oedometer, secant, and unloading-reloading moduli) and strength parameters such as friction angle, were iteratively adjusted until the model reproduced observed behavior.

Initial soil properties were derived deterministically from cone penetration test (CPT) data, using mean values of cone resistance, sleeve friction, and friction ratio for each layer. To identify the most influential parameters, a sensitivity analysis was carried out with coefficients of variation from NEN 9997-1.

The calibration aimed to refine stiffness and strength values so that finite element predictions matched inclinometer profiles within an accepted error margin of $\pm 30\%$. Each iteration involved stepwise changes followed by comparison against the full displacement profile, not just maximum values. A model was accepted only if the profile shape was consistent with measurements and errors remained within tolerance. At every step, parameter values were checked for geotechnical plausibility.

It is important to acknowledge that the laboratory triaxial CU tests could not be used directly due to poor quality and incorrect drainage assumptions. A fully probabilistic calibration framework was also excluded, given the limited number of CPTs and the high computational demand of probabilistic simulations.

For these reasons, the calibration strategy adopted in this thesis occupied an intermediate position between deterministic and semi-probabilistic approaches.

3.5.2. Sensitivity Analysis

The sensitivity analysis was conducted to identify the soil parameters that have the most significant impact on lateral displacement during dredging phases 1 (-8.5 m NAP), 3 (-16.5 m NAP), and 6 (-21 m NAP). The analysis focused on a single criterion: the lateral displacement of both the front wall and the combi wall. The soil parameters considered are the friction angle and stiffness moduli, as they are the dominant variables influencing the wall behavior.

To enable a fair comparison between the selected parameters, both were varied by ±1 standard deviation. The coefficients of variation were taken from NEN 9997-1 are: 25% for the stiffness moduli and 10% for the friction angle. During the analysis, the ratio between the stiffness parameters, oedometric stiffness and unloading-reloading stiffness, was held constant.

The impact of each parameter was quantified using the sensitivity score method introduced by Brinkgreve (2019b) [4]. This method evaluates the degree to which variations in a parameter affect the model output. The sensitivity analysis was performed in the following steps:

1. **Parameter Variation**
   For each parameter considered in the sensitivity analysis, the minimum and maximum values were determined by applying ± 1 standard deviation to the base value.
2. **Finite Element Calculations**
   A total of $2n$ calculations were performed, where n is the number of parameters included in the analysis. In each calculation, only one parameter was set to either its maximum or minimum value, while all other parameters remained fixed at their base values. This isolates the influence of each parameter on the model output.
3. **Global Score Calculation**
   The global score quantifies the influence of each parameter on the selected output criterion (lateral displacement). For a given parameter x_i, the global score is calculated as:

$$x_{i,\text{globalscore}} = |f(x_{i,\text{max}}) - f(x_{i,\text{min}})| \tag{3.16}$$

   where $f(x_{i,\text{max}})$ and $f(x_{i,\text{min}})$ represent the model results (e.g., lateral displacement) when the parameter x_i is set to its maximum and minimum values, respectively.

4. **Sensitivity Score Calculation**
   To enable comparison between parameters, the global scores are normalized to obtain a sensitivity score:

$$x_{i,\text{sensitivity}} = 100 \cdot \frac{x_{i,\text{globalscore}}}{\sum_{i=1}^{n} x_{i,\text{globalscore}}} \tag{3.17}$$

   This sensitivity score expresses the percentage contribution of each parameter to the total variation in the model response, allowing for a clear ranking of parameter influence.

3.5.3. FEM Validation

Following the calibration, the FEM must be validated to ensure it reliably captures the behavior of the quay wall. Validation is performed by comparing the model's predicted lateral displacements after each dredging phase with field measurements obtained from inclinometer data. A model is considered valid if the predicted results fall within an accepted margin of error of ±30%, as recommended by De Gijt and Broeken (2013) [10].

3.6. Parametric Study

Once the finite element model (FEM) was validated, a parametric study was conducted to evaluate the influence of varying conditions on the quay wall's response. The study focused on three key factors: variation in soil parameters (stiffness moduli and friction angle), dredging depth, and surcharge loading.

Dredging Level Variation

The design dredging depth reaches a maximum of -24 m NAP, while the final implemented dredging phase (Phase 6) reached -21 m NAP. To assess the potential impact of further deepening, two additional construction stages were analyzed, one at -22.5 m NAP and another at -24 m NAP. This investigation aimed to determine how increased dredging depth may influence lateral wall displacements, in case future deepening is required.

Surcharge Load Variation

The design surcharge load for the project is 40 kN/m². To evaluate its influence, the load was varied between 10 kN/m² and 60 kN/m² in increments of 10 kN/m². The surcharge was applied at the edge of the relieving platform to avoid direct loading on the platform itself. This variation allowed for an assessment of how increased operational loads may affect wall behavior.

Soil Parameter Variation

The variation in soil parameters focused primarily on dredging phases 6. The study concentrated on the stiffness moduli and friction angle of those layers.

A total of 101 FEM simulations were performed. Soil parameters were varied across their mean, upper bound, and lower bound values, calculated using the coefficients of variation recommended in NEN 9997-1. In addition to these discrete values, intermediate values between the bounds and the mean were included to capture a broader range of behavior. This comprehensive approach enabled analysis of how changes in soil properties influence both the maximum lateral displacement and the overall displacement profile of the wall.

Conclusion

This chapter outlined the step-by-step methodology followed to develop a reliable numerical model of the quay wall system. The process began with the interpretation of geotechnical data, including cone penetration tests (CPTs), triaxial tests, and sieve analyses, to establish a representative soil profile and derive input parameters for the Hardening Soil model. Structural elements were modeled using appropriate PLAXIS 2D components, with geometry and mechanical properties derived from site drawings and validated engineering assumptions.

The construction sequence, though not documented, was established using relevant literature and similar case studies. Mesh generation and model boundaries were carefully defined to ensure numerical stability and minimize boundary effects.

A key component of the methodology was the calibration of the model using inverse analysis. Initial soil parameters were derived from CPT data, and then iteratively adjusted based on inclinometer measurements to improve agreement between the model and field observations. To support this process, a sensitivity analysis was conducted using coefficients of variation from NEN 9997-1 to identify the most influential parameters and critical soil layers. This helped focus the calibration on the variables that most significantly affect lateral wall displacements.

Following calibration, the parametric study was explained. The study was carried out to evaluate the effect of varying dredging depths, surcharge loads, and key soil parameters on wall behavior. This included systematic variation of stiffness moduli and friction angles based on their statistical bounds, as well as staged changes in dredging levels and surface loading.

4

Results and Discussion

4.1. Introduction

This chapter presents and discusses the results obtained from the finite element method (FEM) analysis. The primary focus is on the lateral displacements of both the combi wall and the front wall after each dredging phase, as well as the development of anchor forces throughout the construction sequence.

Section 4.2 begins with the results and discussion of four FEA scenarios:

1. The initial base model,
2. The calibrated model,
3. A model variation with a fixed connection between the combi wall and the front wall, and
4. A model incorporating the Hardening Soil model with small-strain stiffness (HSsmall), as introduced in the previous chapter.

This section also includes the model validation, which is performed by comparing the predicted displacements from the calibrated model against field measurements from the inclinometer data. The level of agreement is assessed to evaluate the accuracy and limitations of the modeling approach and to understand the influence of key modeling assumptions on the performance of the quay wall system.

Also, the chapter presents the outcomes of the sensitivity analysis, which was carried out to identify the most influential soil parameters and to guide the calibration process.

Lastly, the results of the parametric study are discussed. This study investigates the influence of varying soil parameters, dredging depths, and surcharge loads on wall behavior.

4.2. FEA Results and Discussion

4.2.1. Field Measurements

This section presents the results of the initial FEM analysis. The base model is developed using the estimated soil parameters prior to any calibration, as listed in Table 3.12. The objective is to evaluate the model's performance by comparing its predictions with field measurements from inclinometer readings.

First, the inclinometer measurements for each dredging phase are plotted to establish the basis for validating the FEM predicted displacements. Inclinometer readings are recorded relative to the wall toe, which is assumed to be fixed, hence the displacement is zero at an elevation of –35 m in all phases. In reality, the toe of the combi wall is not completely restrained, and some lateral movement is expected, especially as dredging progresses and passive soil resistance decreases.

To address this, each results figure includes a Corrected field measurement curve. This curve is generated by adding the FEM-predicted toe displacement to the entire inclinometer profile, thereby aligning the FEM and field measurement baselines. This correction allows for a fair comparison and validation of the FEM results, as demonstrated in the results presentation and subsequent FEM discussion.

The inclinometer plots shown in Figures 4.1, 4.2, and 4.3 illustrate the raw, uncorrected field measurement data. Negative lateral displacements indicate movement towards the landside, whereas positive lateral displacements correspond to movement towards the waterside.

- **Dredging Phase 1** (dredging to approximately -8.5 m NAP): The maximum lateral displacement measured by the inclinometer is approximately -15 mm, occurring predominantly in the front wall.
- **Dredging Phase 3** (dredging to approximately -16.5 m NAP): The maximum lateral displacement is approximately 16 mm. For the front wall, the inclinometer data indicates a maximum displacement of about -15 mm towards the landside.
- **Dredging Phase 6** (dredging to approximately -21 m NAP): The maximum lateral displacement is approximately 30 mm. For the front wall, the inclinometer data indicates a maximum displacement of about -12 mm towards the landside.

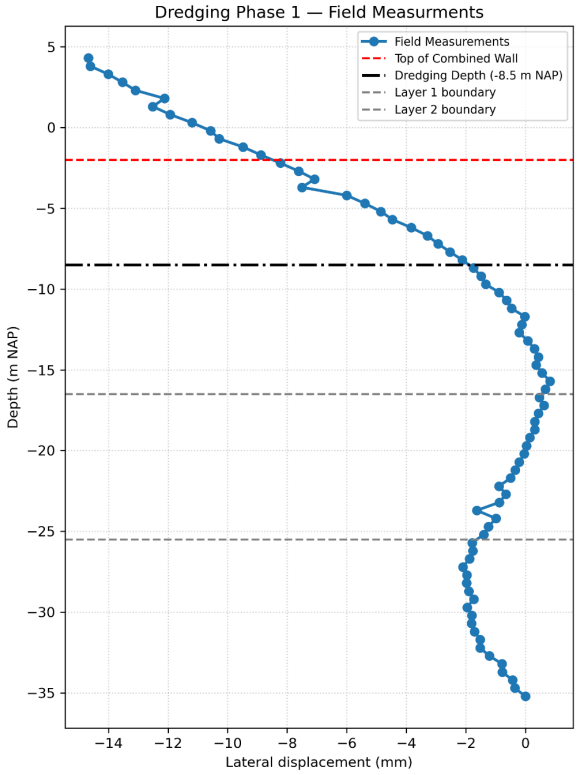

Figure 4.1: Field Measurements Dredging Phase 1

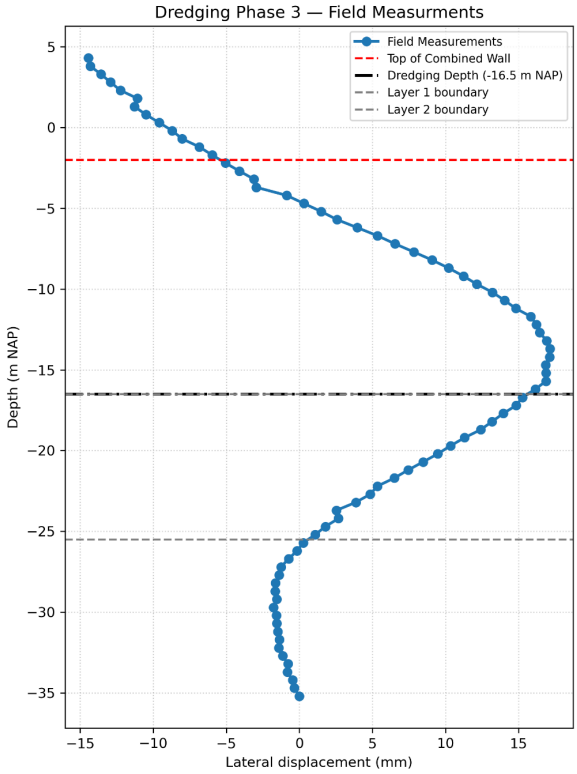

Figure 4.2: Field Measurements Dredging Phase 3

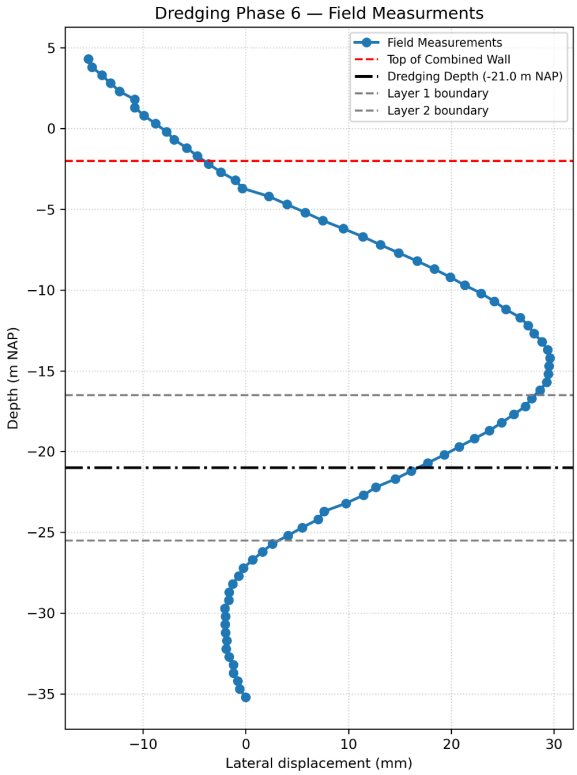

Figure 4.3: Field Measurements Dredging Phase 6

4.2.2. Initial FEA Results

Figures 4.4, 4.5, and 4.6 present the lateral displacement profiles for Dredging Phases 1, 3, and 6, respectively. In each plot, the orange squares represent the FEA predicted displacements, while the green dots correspond to the corrected field measurements. For reference, the red dashed line marks the top of the combi wall, with the dredging level and soil layer boundaries also indicated.

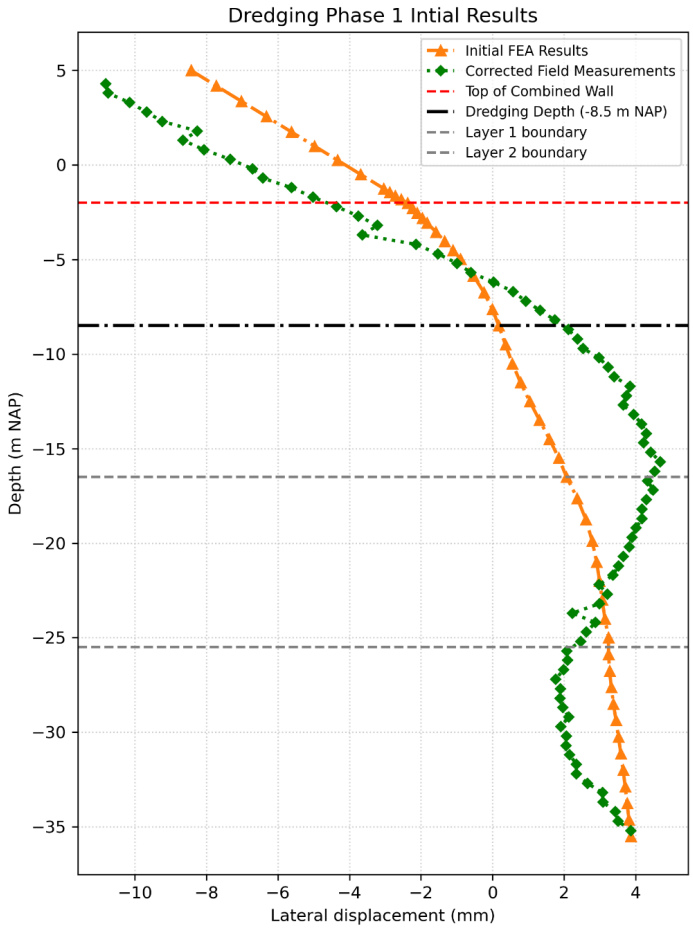

Figure 4.4: Initial FEM results for Dredging Phase 1 compared to inclinometer data.

In Figure 4.4, for Phase 1 (dredging to approximately -8.5 m NAP), the maximum corrected field lateral displacement is approximately -11 mm, while the FEM model predicts a maximum displacement of about -8.5 mm. This corresponds to a discrepancy of roughly 22%. The FE analysis indicates a toe displacement of 4 mm, which was applied to correct the field measurements. The shape of the FEM displacement curve does not align well with the measured data, indicating discrepancies in the model's representation of the wall's deformation profile at this early stage.

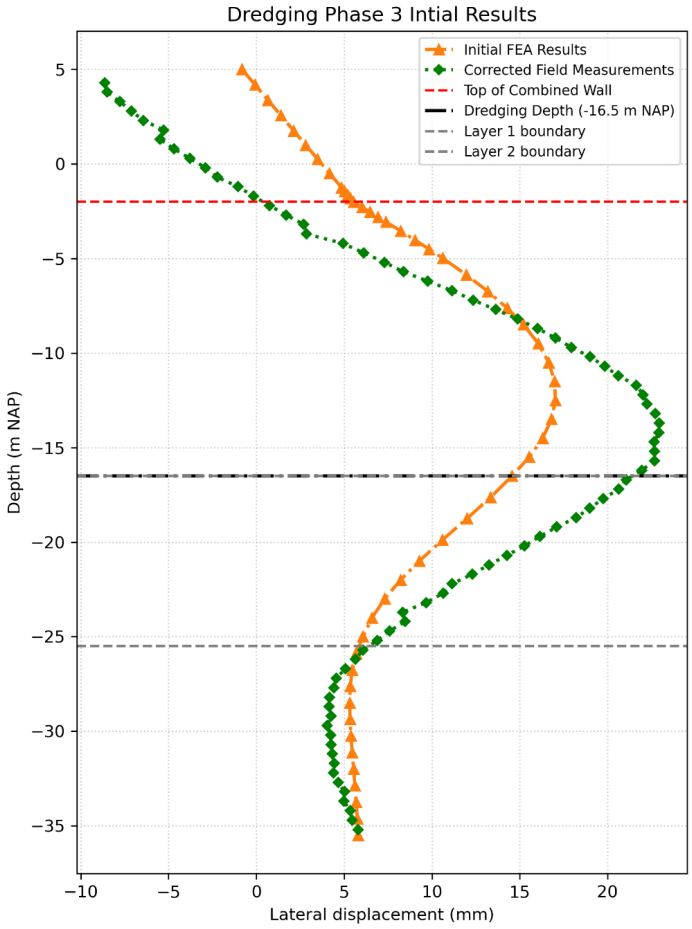

Figure 4.5: Initial FEM results for Dredging Phase 3 compared to inclinometer data.

In Figure 4.5, corresponding to Phase 3 (dredging to approximately -16.5 m NAP), the front wall, the model predicts only a minor movement towards the landside, whereas the corrected field measurements indicates a landside displacement of approximately -9 mm.

Between roughly -5 m and -20 m NAP, the model response appears overly stiff, with a predicted peak displacement of about 17 mm occurring approximately two metres higher than the actual maximum observed in the field data. In contrast, the corrected field measurements show a peak displacement of 22 mm, yielding a difference of approximately 22%. The toe displacement predicted by the FEA is about 6 mm. Furthermore, the deformation curve generated by the FEA does not correspond well with the shape of the measured profile, suggesting that the current parameter set does not adequately represent the wall's deformation behaviour at this stage of construction.

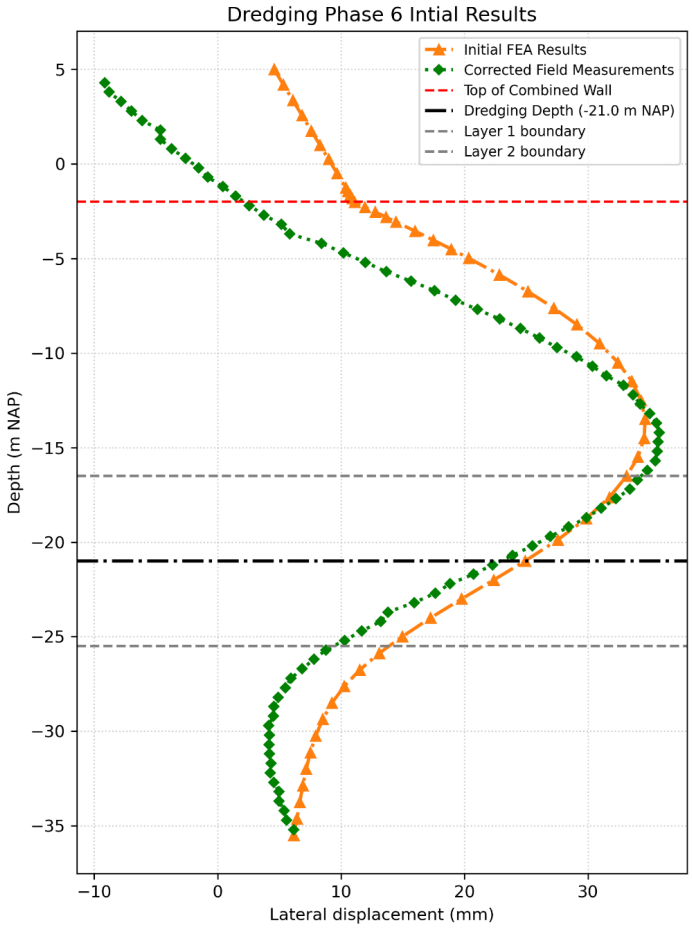

Figure 4.6: Initial FEM results for Dredging Phase 6 compared to inclinometer data.

Finally, Figure 4.6 shows the results for Dredging Phase 6 (final dredging to -21 m NAP). Compared to the earlier phases, the model more accurately captures the overall shape of the displacement profile. The toe displacement predicted by the FEM is approximately 6 mm. For the front wall, the model predicts movement towards the waterside with a magnitude of about -6 mm, whereas the field data indicates a landside displacement of approximately -9 mm. The maximum predicted FEM displacement is approximately 34 mm, while the corrected field measurements indicate a maximum of 35 mm, which is almost identical. The overall profile shape shows good agreement in the upper part of the wall; however, discrepancies remain in the lower section near the dredge level, where the model predicts a slightly stiffer response than observed in the field measurements.

Initial FEA Anchor Forces

Table 4.1 provides a summary of the development of anchor forces throughout the dredging phases for both the upper and lower anchors. This evaluation is essential to verify whether the anchor forces remain within the safe working limits. The anchors are designed for a maximum allowable load, P_{max}, of 2200 kN, and were prestressed to an initial force of 220 kN.

From the results, it can be observed that the forces in both the upper and lower anchors increase progressively with each dredging phase. For the upper anchor, the force rises from approximately 170 kN in Phase 1 to 381 kN in Phase 6. Similarly, the lower anchor increases from 165 kN to 399 kN. These forces remain significantly below the design maximum of 2200 kN, indicating that the anchors are not overstressed and have sufficient capacity to accommodate further loading if necessary. It is also noted that the FEA calculated forces slightly exceed the initial prestressing value of 220 kN, which is expected due to the redistribution of loads during excavation and wall deformation.

Table 4.1: Anchor Forces from Initial FEM Model

Anchor	Dredging Phase	N (kN)	N_{max} (kN)
Upper	1	170.325	220
	3	297.514	297.514
	6	380.9	380.9
Lower	1	164.66	220
	3	314.63	314.63
	6	399.47	399.47

4.2.3. Initial FEA Discussion

For the initial FEA results of Phase 1, the shape of the FEA predicted displacement curve shows poor alignment with the corrected field measurements, suggesting inconsistencies in how the model simulates the wall's deformation behaviour during the early stage of dredging. The front wall shows a lateral movement towards the landside of approximately -8.5 mm, while the corrected field measurements indicate a movement of about -11 mm. This discrepancy may stem from oversimplified assumptions in the model, particularly the idealized hinge connection and its assumed location. It is evident not only in Phase 1 but also in Phases 3 and 6 that the top of the combi wall, representing the hinge location in the model, does not coincide with that implied by the corrected field data. The assumed stiffness of the front wall may also contribute to these differences.

For Phase 3, The FEM again under predicts displacements compared to the inclinometer data. The deformation profile remains too stiff, and the location of maximum displacement is shifted upwards by about 2 meters. This is particularly evident in the layers between -5 m and -20 m NAP, where the model underestimates the deformation. A reduction in stiffness for these layers may be required before the model can fully predict the observed displacements.

For Phase 6, although the earlier phases did not perform well, the final phase demonstrates noticeable improvement in matching the displacement profile's shape and magnitude. However, the shape of lateral movement at the base implies that the base fixation is still misrepresented in the model. This suggests that the stiffness at the base is underestimated.

The comparison across all phases reveals a mixed representation of soil stiffness: the upper two layers appear to be too stiff, while the third layer the stiffness may be underestimated.

With respect to the front wall, the inclinometer data indicates a constant landside displacement throughout the dredging phases. However, this behaviour is unlikely in reality. In the FEA, the front wall rotates progressively: approximately -8 mm landside in Phase 1, approaching zero in Phase 3, and about +6 mm waterside in Phase 6. This behavior implies rotation, which is not captured in the inclinometer data. Moreover, the slope of deformation predicted by the FEA differs from that in the field data. The observed waterside movement in the model is not reflected in the measurements. This behaviour in the model could also lead to an underestimation of anchor forces. As the model predicts waterside movement in later phases, the mobilised anchor load is reduced, whereas the constant landside displacement observed in the field would maintain higher anchor engagement.

This could be attributed to several factors. Firstly, the assumed hinge connection between the combi wall and front wall in PLAXIS may not accurately replicate site conditions. While real-world hinges may permit rotation, they often exhibit frictional resistance. In contrast, the PLAXIS hinge is modelled as frictionless, which may alter the rotation pattern of the front wall. Additionally, the precise location of the hinge in the model may not match the actual detail on site. To investigate this further, a model variation with a fixed connection was developed and is discussed in the following sections.

Another plausible explanation involves the pre-stressing procedure. Literature suggests that anchor pre-stressing is sometimes applied in stages, whereas in the current model, it is implemented in a single step. This simplification could contribute to discrepancies between the model and field data, particularly in the response of the combi wall and front wall.

The results of the initial FEA run indicate that, while the model captures the general trends, discrepancies in both displacement magnitudes and deformation shapes highlight the need to refine the soil

parameters. The following section presents the sensitivity analysis conducted to guide the calibration process and improve the model's fidelity.

4.2.4. Results and Discussion of the Sensitivity Analysis

The sensitivity analysis results presented in this section build upon the procedure outlined in the methodology chapter. The analysis evaluates how variations in the selected soil parameters, namely the friction angle and stiffness moduli, affect the predicted lateral displacements of both the front wall and the combi wall during Dredging Phases 1, 3, and 6. These parameters were varied by ± 1 standard deviation, using the coefficients of variation defined in NEN 9997-1 (5% for the stiffness moduli and 10% for the friction angle), while maintaining a constant ratio between the oedometeric stiffness and the unloading–reloading stiffness. Table 4.2 summarises the baseline (initial) parameter values used for the analysis.

The influence of each parameter was quantified using the sensitivity score method proposed by Brinkgreve [4], enabling a direct comparison of their relative impact on the model output. The following paragraphs present the computed sensitivity scores for the three dredging phases and discusses their implications for model calibration.

Table 4.2: Baseline (Initial) Soil Parameters

Layer	**Top Depth (m NAP)**	ϕ (°)	E_{oed}^{ref} (MPa)	E_{50}^{ref} (MPa)	E_{ur}^{ref} (MPa)
Layer 1	5	36	60	60	180
Layer 2	-16.5	31	33	33	98
Layer 3	-25.5	37	67	67	202
Layer 4	-40	32	36	36	107

For Phase 1, the results of the sensitivity analysis are provided in Table 4.3, with the corresponding graphical representation shown in Figure 4.7. For Dredging Phase 1 (–8.5 m NAP), the sensitivity analysis indicates that the friction angle of Layer 1 (ϕ_1) is the most influential parameter, contributing 37.4 % to the total variation in predicted lateral displacement. This is followed by the stiffness modulus of Layer 4 ($E_{50,4}^{ref}$) and Layer 1 ($E_{50,1}^{ref}$), contributing 24.9 % and 24.7 % respectively. Together, these three parameters account for over 87 % of the total model response variation, underscoring their dominant role in controlling wall displacement during the initial dredging stage.

In contrast, the friction angles of Layers 2, 3, and 4, as well as the stiffness moduli of Layers 2 and 3, exhibit relatively low sensitivity scores, each contributing less than 6 % to the total variation. The lowest influence is observed for ϕ_2 (0.6 %), indicating that uncertainty in this parameter has minimal impact on model predictions for this phase.

The tornado plot visually confirms the strong influence of ϕ_1 and the stiffness of Layers 1 and 4, with notably larger global scores compared to the other parameters. The significance of $E_{50,4}^{ref}$ at this early stage may be linked to heave effects in the lower layers, which can influence the wall's base support and, consequently, its displacement profile, even when dredging is well above the layer. This suggests that calibration efforts for Phase 1 should prioritise refining ϕ_1, $E_{50,1}^{ref}$, and $E_{50,4}^{ref}$ to achieve the most significant improvements in model accuracy.

Table 4.3: Sensitivity Analysis Results – Dredging Phase 1 (-8.5 m NAP)

Parameter	Value (–)	Value (+)	U^- [mm]	U^+ [mm]	Global score	Sensitivity %
ϕ_1	32.4	39.6	7.277	9.603	2.326	37.4
ϕ_2	27.9	34.1	8.403	8.442	0.039	0.6
ϕ_3	33.3	40.7	8.449	8.392	0.057	0.9
ϕ_4	30.0	34.0	8.246	8.613	0.367	5.9
E_1	45.0	75.0	9.322	7.785	1.537	24.7
E_2	30.0	36.0	8.534	8.355	0.179	2.9
E_3	50.25	83.75	8.491	8.329	0.162	2.6
E_4	27.0	45.0	9.361	7.817	1.544	24.9
				Total	**6.211**	**100.0**

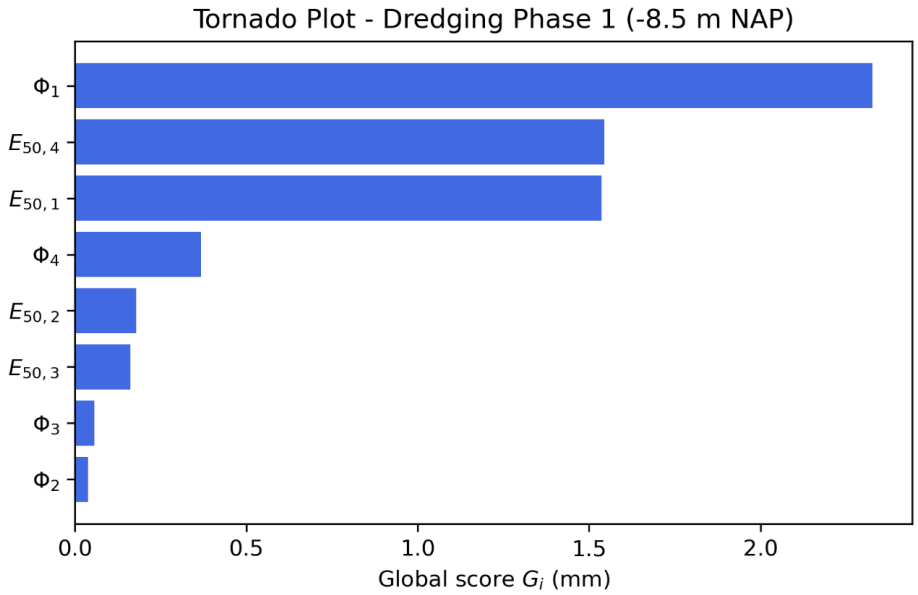

Figure 4.7: Tornado Plot of Dredging Phase 1

For Dredging Phase 3 (–16.5 m NAP), the results of the sensitivity analysis are provided in Table 4.4, with the corresponding graphical representation shown in Figure 4.8. The sensitivity analysis indicates that the friction angle of Layer 1 (ϕ_1) is the most influential parameter, contributing 36.8 % to the total variation in predicted lateral displacement. This is followed by the friction angle of Layer 2 (ϕ_2) at 26.6 %, and the stiffness modulus of Layer 3 ($E^{ref}_{50,3}$) at 14.4 %. Together, these three parameters account for almost 78 % of the total variation, highlighting the importance of both upper-layer strength parameters and the stiffness of deeper strata at this dredge depth.

The remaining parameters, ϕ_4, $E^{ref}_{50,2}$, ϕ_3, $E^{ref}_{50,1}$, and $E^{ref}_{50,4}$, have sensitivity scores below 10 %, indicating a more limited influence on wall displacement for this phase.

The tornado plot for Phase 3 clearly illustrates the dominance of ϕ_1, ϕ_2, and $E^{ref}_{50,3}$, with substantially higher global scores than the other parameters. The notable contribution of the stiffness of Layer 3 may be linked to increasing base heave effects as dredging approaches deeper strata, where reduced confining stresses at the base can alter load transfer and displacement behaviour. This suggests that for Phase 3, calibration efforts should focus on refining the friction angles of the upper layers and the stiffness of Layer 3, while ensuring that deeper layer effects are not underestimated in the model.

Table 4.4: Sensitivity Analysis Results – Dredging Phase 3 (-16.5 m NAP)

Parameter	Value (–)	Value (+)	U^- [mm]	U^+ [mm]	Global score	Sensitivity %
ϕ_1	32.4	39.6	19.71	14.58	5.13	36.8
ϕ_2	27.9	34.1	19.29	15.58	3.71	26.6
ϕ_3	33.3	40.7	16.71	17.67	0.96	6.9
ϕ_4	30.0	34.0	17.04	17.08	0.04	0.3
E_1	45.0	75.0	17.43	16.88	0.55	3.9
E_2	30.0	36.0	18.21	16.71	1.50	10.8
E_3	50.25	83.75	18.06	16.05	2.01	14.4
E_4	27.0	45.0	17.10	17.15	0.05	0.4
				Total	**13.95**	**100.0**

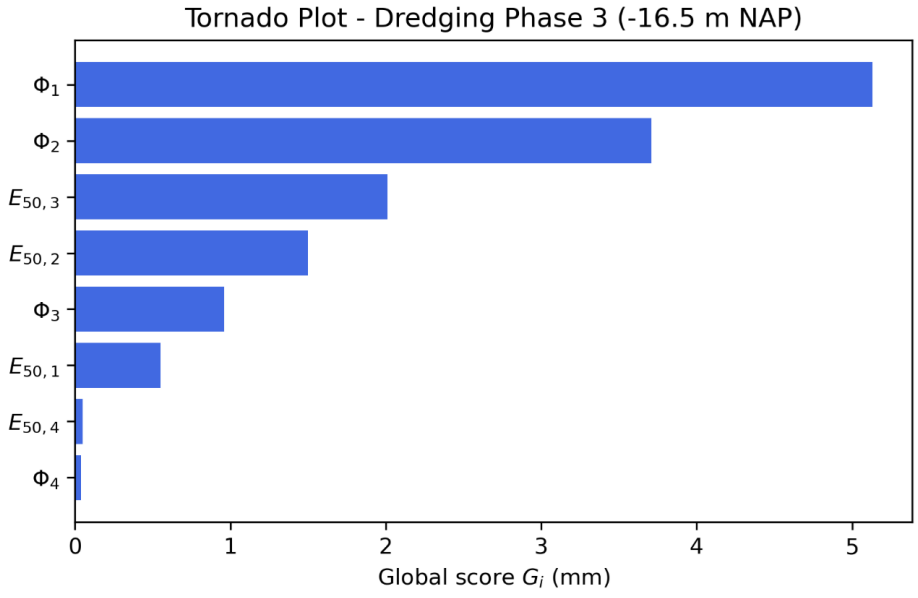

Figure 4.8: Tornado Plot of Dredging Phase 3

For Dredging Phase 6 (–21 m NAP), the sensitivity analysis shows that the friction angle of Layer 2 (ϕ_2) is the most influential parameter, contributing 29.5% to the total variation in predicted lateral displacement. This is followed by the friction angle of Layer 1 (ϕ_1) at 25.7%, and the stiffness modulus of Layer 3 ($E^{ref}_{50,3}$) at 23.9%. Together, these three parameters account for over 79% of the total variation, indicating that both the upper active zone (Layers 1 and 2) and the deeper Layer 3 play key roles in governing wall behaviour at the final dredge depth.

The remaining parameters each have a smaller impact, with sensitivity scores below 10%. These include $E^{ref}_{50,1}$ (7.4%), $E^{ref}_{50,2}$ (9.8%), ϕ_4 (1.5%), $E^{ref}_{50,4}$ (1.4%), and ϕ_3 (0.7%).

The tornado plot for Phase 6 confirms the strong influence of ϕ_2, ϕ_1, and $E^{ref}_{50,3}$, with noticeably higher global scores compared to other parameters. The relatively high influence of deeper Layer 3 stiffness may be associated with base heave effects and reduced passive resistance in the lower strata as dredging approaches the final depth, amplifying the structural interaction between the wall and the lower soil layers. This suggests that calibration at this stage should focus on refining ϕ_2, ϕ_1, and $E^{ref}_{50,3}$, while also ensuring the deeper soil response is accurately represented to capture end-of-excavation behaviour.

Table 4.5: Sensitivity Analysis Results – Dredging Phase 6 (-21 m NAP)

Parameter	Value (–)	Value (+)	U^- [mm]	U^+ [mm]	Global score	Sensitivity %
ϕ_1	32.4	39.6	37.91	31.73	6.18	25.7
ϕ_2	27.9	34.1	38.51	31.43	7.08	29.5
ϕ_3	33.3	40.7	35.40	35.22	0.18	0.7
ϕ_4	30.0	34.0	34.52	34.89	0.37	1.5
E_1	45.0	75.0	35.71	33.93	1.78	7.4
E_2	30.0	36.0	36.04	33.69	2.35	9.8
E_3	50.25	83.75	38.14	32.02	5.74	23.9
E_4	27.0	45.0	34.88	34.54	0.34	1.4
				Total	**24.02**	**100.0**

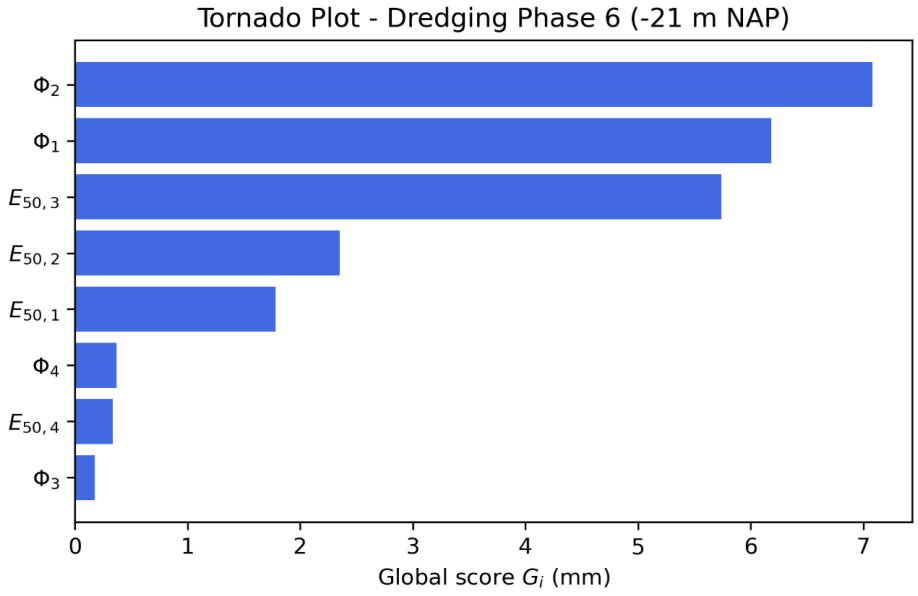

Figure 4.9: Tornado Plot of Dredging Phase 6

Figure 4.10 presents the grouped sensitivity results across all dredging phases, allowing a direct comparison of parameter influence at different excavation depths.

For the friction angle of Layer 1 (ϕ_1), sensitivity remains high across all phases, exceeding 25% in Phases 1 and 3, and remaining significant in Phase 6. This reflects its primary role in controlling the near-surface strength that governs wall rotation and displacement in the early and mid-dredging stages. The friction angle of Layer 2 (ϕ_2) shows a clear trend of increasing influence with depth, becoming the dominant parameter in Phase 6 (29.5%), where deeper passive resistance plays a larger role in system behavior.

The stiffness modulus of Layer 1 ($E^{ref}_{50,1}$) is most relevant in Phase 1, where it contributes notably to displacement control, but its influence diminishes in later phases as deeper layers become more mobilised. The stiffness modulus of Layer 3 ($E^{ref}_{50,3}$) displays the opposite trend, with a modest contribution in early phases but a marked increase in Phase 6 (23.9%), likely due to greater deformation influence from deeper strata as the dredging depth approaches their elevation. The stiffness modulus of Layer 2 ($E^{ref}_{50,2}$) shows moderate sensitivity in Phases 3 and 6 but remains secondary to other parameters.

In contrast, the friction angles of Layers 3 and 4, as well as the stiffness modulus of Layer 4 ($E^{ref}_{50,4}$), maintain consistently low sensitivity scores across all phases, suggesting a limited role in governing wall displacement for the studied conditions.

In summary, the sensitivity analysis highlights ϕ_1, ϕ_2, $E^{ref}_{50,2}$ and $E^{ref}_{50,3}$ as the key parameters influencing displacement behaviour across phases, with $E^{ref}_{50,1}$ also being important in the early stages. Although ϕ_1, ϕ_2, and $E^{ref}_{50,3}$ show the highest overall influence, the remaining parameters will also be adjusted during calibration to account for their secondary but non-negligible effects observed in certain phases. These findings provide a clear basis for targeted calibration efforts, ensuring that adjustments focus on the parameters most capable of improving model fidelity. Using the lower bound for all parameters always yielded higher lateral displacements than the upper bound values across all phases, confirming the direct relationship between reduced soil strength/stiffness and increased wall movement.

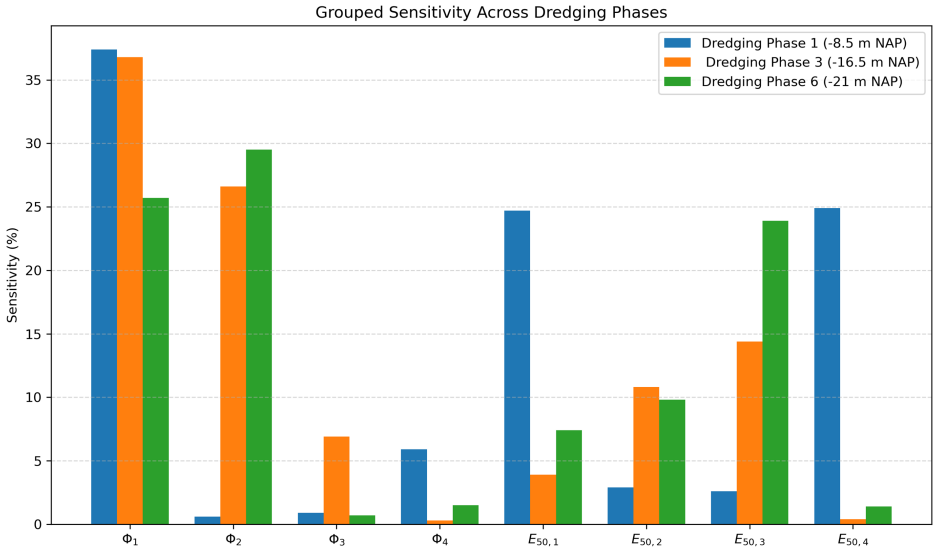

Figure 4.10: Grouped Sensitivity across all Dredging Phases

4.2.5. Calibrated Model Results

The calibration process focused on refining stiffness moduli and friction angles so that the FEA-predicted displacements matched inclinometer measurements within an accepted error margin of $\pm 30\%$. Initial checks showed stiffness was too high in some layers and too low in others, while strength parameters also needed adjustment. Calibration was carried out in small steps, with each model run compared to the full displacement profile rather than only the maximum value. A model was accepted when the overall shape of the profile matched the measurements and errors were within tolerance. At every step, parameter values were checked against geotechnical plausibility, and any unrealistic changes were rejected. Table 4.6 summarises the final calibrated parameters alongside the initial estimates.

The grouped sensitivity results provided a clear basis for these adjustments, identifying the friction angles of Layers 1 and 2 and the stiffness modulus of Layer 3 as the most influential parameters across all dredging phases, with $E_{50,1}^{ref}$ also showing notable influence in the early stages. The ϕ_1 and $E_{50,3}^{ref}$ were increased to better match observed displacements, while ϕ_2 and $E_{50,1}^{ref}$ were reduced to correct overestimated stiffness in the initial model. Less sensitive parameters, such as ϕ_3, ϕ_4, and $E_{50,4}^{ref}$, were modified only moderately to maintain overall model stability.

The stiffness modulus $E_{50,1}^{ref}$ was reduced because the initial model underpredicted near-surface lateral displacements (i.e., it was too stiff in the upper zone during the early dredging stages). Conversely, the friction angle ϕ_1 was increased to correct the lateral earth pressures and the shape of the deformation profile: a higher ϕ_1 lowers the active earth pressure coefficient ($K_a = \tan^2(45° - \phi/2)$), limits unrealistic shallow plasticity, and improves the depth of the neutral point and curvature of the wall. In combination, the lower $E_{50,1}^{ref}$ provides the required compliance to match displacement magnitudes, while the higher ϕ_1 maintains adequate shear resistance and yields a displacement shape and internal force distribution that better agree with the inclinometer data.

This approach ensured that calibration efforts concentrated on parameters with the greatest potential to improve model fidelity.Figures 4.11, 4.12, and 4.13 present the lateral displacement profiles for Dredging Phases 1, 3, and 6, respectively.

Table 4.6: Comparison of Initial and Calibrated Soil Parameters

Layer	Top Depth (m NAP)	Initial Model Parameters				Calibrated Model Parameters			
		ϕ (°)	E_{oed}^{ref} (MPa)	E_{50}^{ref} (MPa)	E_{ur}^{ref} (MPa)	ϕ (°)	E_{oed}^{ref} (MPa)	E_{50}^{ref} (MPa)	E_{ur}^{ref} (MPa)
Layer 1	5	36	60	60	180	38	38	38	114
Layer 2	-16.5	31	33	33	98	30	10	10	30
Layer 3	-25.5	37	67	67	202	40	85	85	255
Layer 4	-40	32	36	36	107	33	38	38	114

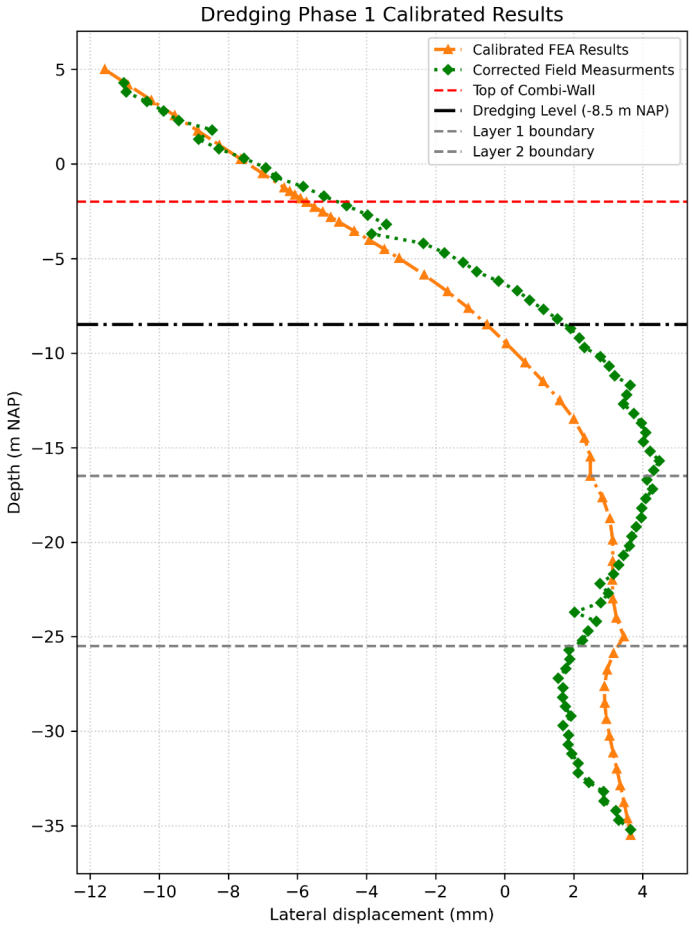

Figure 4.11: Calibrated FEA results for Dredging Phase 1 compared to inclinometer data.

Figure 4.11 shows the results for Phase 1 (dredging to approximately -8.5 m NAP). The maximum lateral displacement of the corrected field measurement is approximately -11 mm, while the calibrated FEA model predicts a maximum displacement of about -12 mm. This yields a discrepancy of approximately 8%.In this phase, the primary structural movement is in the front wall.

The general deformation shape of the FEA results aligns well with the inclinometer measurements. A toe displacement of around 3.5 mm is observed in the FEA model, which is consistent with expectations due to the non-fixed nature of the combi wall toe. The FEA calibrated results curve illustrates that there is a slight underestimation in the displacement in the region from -5 m to -20 m.

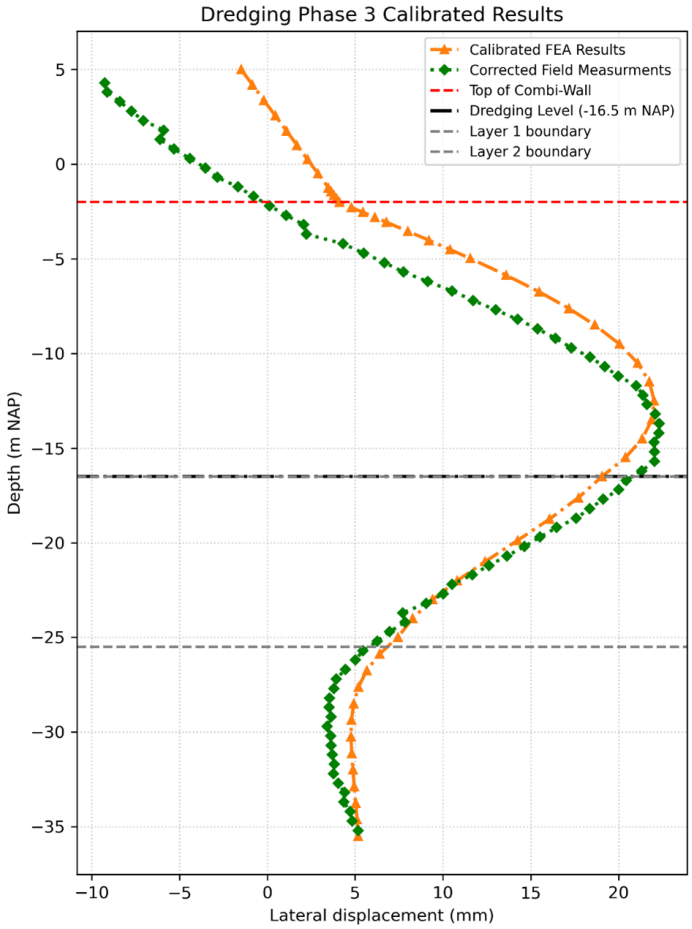

Figure 4.12: Calibrated FEA results for Dredging Phase 3 compared to inclinometer data.

Figure 4.12 shows the results for Phase 3 (dredging to approximately -16.5 m NAP). The maximum lateral displacement of the corrected field data is approximately 22 mm, while the calibrated FE model predicts a maximum displacement of about 21 mm. This yields a discrepancy of approximately 5%. For the front wall, the inclinometer data indicates a maximum lateral displacement of -9 mm towards the landside, whereas the FEA results predict a displacement of only -1.5 mm in the same direction. This discrepancy will be further discussed in the results discussion section.

The general deformation shape of the FEA results aligns well with the inclinometer measurements. A toe displacement of around 5 mm is observed in the FE model. A key observation is the early onset of the maximum lateral displacement predicted by the FEA. There appears to be a horizontal shift of approximately 2 m between the FEM results and the inclinometer data. The initiation point of the combi wall's lateral displacement in the FEA output does not fully align with the inclinometer measurements. This discrepancy may explain the premature occurrence of the maximum lateral displacement in the FEA profile; however, a more detailed discussion on this issue is provided in in the discussion.

When examining the FEA results, the agreement with the corrected field data is more evident near the toe of the combi wall. The shape and magnitude of displacements at the lower boundary are consistent between the two datasets. Nevertheless, despite the alignment at the toe, a noticeable offset remains at the location of the maximum lateral displacement near -15 m, indicating that the calibrated FE model may still under predict the displacement in that region.

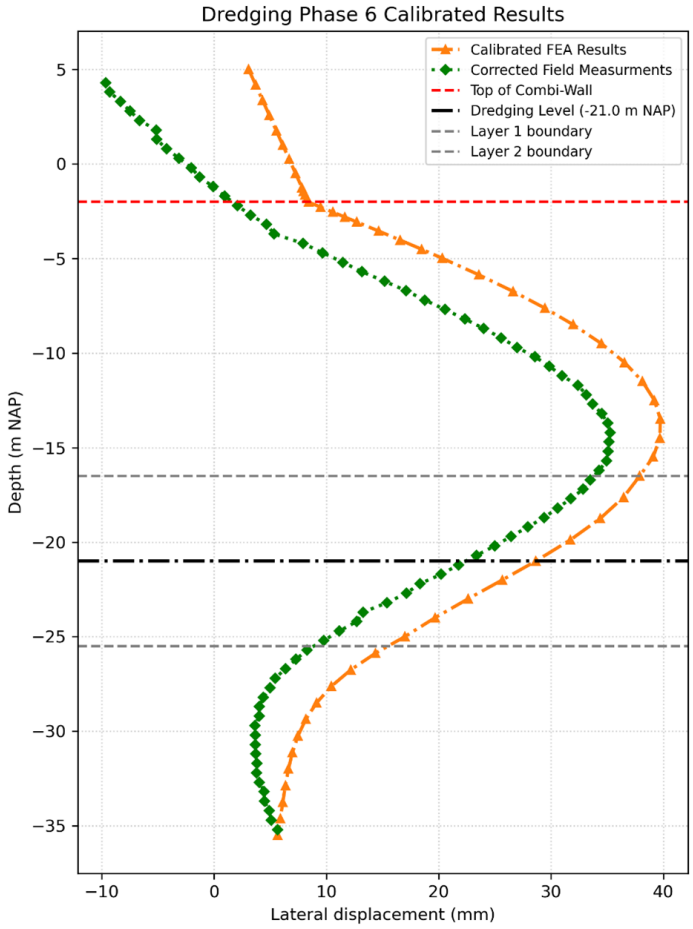

Figure 4.13: Calibrated FEM results for Dredging Phase 6 compared to inclinometer data.

Figure 4.13 shows the results for Phase 6 (dredging to approximately -21 m NAP. The maximum lateral displacement of the corrected field data is approximately 35 mm, while the calibrated FE model predicts a maximum displacement of about 39 mm. This yields a discrepancy of approximately 11%. For the front wall, the corrected field data indicates a maximum lateral displacement of -9.5 mm towards the landside, whereas the FEA results predict a displacement of only 3 mm towards the waterside. This discrepancy will be further discussed in the results discussion section.

The general deformation shape of the FEA results aligns well with the inclinometer measurements. A toe displacement of around 5 mm is observed in the FE model. The maximum lateral displacement is observed at approximately -15 mm for both the inclinometer measurements and the FEM predictions, indicating good agreement in the location of peak displacement.Examining the corrected lateral displacement profile, the shape closely aligns with the corrected field data throughout the wall depth.

Calibrated FEM Anchor Forces

Table 4.7 presents the anchor forces obtained from the calibrated FEM model. The assessment of these forces is essential to ensure that the anchor loads remain within the allowable working limits throughout the construction stages. As previously stated, the maximum allowable anchor load, P_{max}, is 2200 kN, with an initial prestressing force of 220 kN.

For the upper anchor, the force develops from 155 kN in Phase 1 to 357 kN in Phase 6. Similarly, the lower anchor increases from 151 kN in Phase 1 to approximately 391 kN in Phase 6. Both anchors experience a noticeable increase in load with the progress of dredging activities, which is expected due to increased wall deflection and soil unloading. Despite the increases, the forces remain well below the maximum design load, indicating adequate safety margins.

Compared to the initial FEM results, the calibrated model shows slightly lower anchor forces in Phase 1, which is consistent with the refined stiffness and strength properties of the soil. However, the forces in later phases (especially Phase 6) are marginally higher, reflecting a more accurate response to increased wall deformation in deeper dredging stages.

Table 4.7: Anchor Forces from Calibrated FEM Model

Anchor	Dredging Phase	N (kN)	N_{max} (kN)
Upper	1	155	220
	3	298.232	298.232
	6	357.358	357.358
Lower	1	151.36	220
	3	329.138	329.138
	6	390.854	390.854

4.2.6. Calibrated Model Discussion

The calibrated FEM model demonstrates a marked improvement over the initial predictions, both in the magnitude and shape of the lateral displacement profiles. Iterative refinement of the stiffness and strength parameters led to closer agreement with inclinometer measurements, particularly in the deeper dredging phases, while maintaining acceptable anchor force levels.

In Phase 1 (Figure 4.11), the calibrated model predicts a maximum lateral displacement of approximately $-12\ \mathrm{mm}$, compared to a corrected field measurement of $-11\ \mathrm{mm}$, yielding a discrepancy of about 8%, well within the $\pm 30\%$ acceptance range. The deformation profile from the FEM results closely matches the inclinometer data, especially after correcting for toe movement. A toe displacement of approximately $3.5\ \mathrm{mm}$ was observed, consistent with the expected non-fixed toe behaviour of the combi wall. Minor underestimation of displacement is evident between elevations $-5\ \mathrm{m}$ and $-20\ \mathrm{m}$, suggesting that further refinement of stiffness in these zones could improve the match.

For Phase 3 (Figure 4.12), the calibrated model predicts a maximum lateral displacement of about $21\ \mathrm{mm}$, compared to $22\ \mathrm{mm}$ from the corrected field data, corresponding to a 5% discrepancy. The general profile shape is well captured however, for the front wall, the FEM predicts only $-1.5\ \mathrm{mm}$ landside movement versus the $-9\ \mathrm{mm}$ measured. Additionally, the peak displacement in the FEM occurs about $2\ \mathrm{m}$ shallower than in the field data. This offset may be due to the representation of stiffness in Layer 3, or simplifications in modelling the dredging progression. The underestimation around $-15\ \mathrm{m}$ depth suggests that localised stiffness adjustments could further improve accuracy.

In Phase 6 (Figure 4.13), the calibrated model predicts a maximum displacement of approximately $39\ \mathrm{mm}$ compared to $35\ \mathrm{mm}$ measured, an 11% discrepancy. The location of the maximum displacement aligns well with the field data at around $-15\ \mathrm{m}$ elevation, and the overall profile matches closely. The toe displacement remains about $5\ \mathrm{mm}$ in the FEM results. However, for the front wall, the FEM predicts a $3\ \mathrm{mm}$ waterside movement, while the corrected field measurements show a $-9.5\ \mathrm{mm}$ landside movement consistent with earlier phases.

Across all phases, the front wall in the FEM model exhibits progressive rotation, transitioning from landside movement in early stages to waterside movement in later stages, whereas the inclinometer data indicates near consistent landside displacement. This discrepancy could result from several factors:

1. The assumed frictionless hinge connection between the combi wall and front wall in PLAXIS, which does not capture the frictional resistance often present in real hinges.
2. Potential mismatch between the modelled and actual hinge location, which can alter rotation behaviour.
3. Simplifications in the staged dredging depth simulation, which may influence displacement patterns.

Anchor force development further supports the improved calibration. The forces remain well below the maximum allowable capacity of 2200 kN, with the calibrated model reflecting realistic load increases in

both upper and lower anchors as dredging progresses. The slightly higher forces in later stages reflect the improved representation of wall deflection and resulting tensile demand on the anchors.

Overall, the calibrated model captures the essential behavior of the quay wall during staged dredging, with acceptable error margins in displacement predictions and safe anchor force levels. The model is considered sufficiently accurate for further parametric studies. However, minor discrepancies in the front wall displacements and local stiffness representation remain areas for potential refinement or further investigation, particularly concerning hinge behavior and real-world boundary conditions.

4.2.7. FEM with Fixed Connection Results

This section presents the results of the model variation in which a fixed connection is assumed between the combi wall and the front wall. The fixed connection is implemented by simply removing the rotational (hinge) connection point between the two elements. No further configuration is necessary, as PLAXIS automatically interprets directly connected structural elements as fully fixed.

Figures 4.14, 4.15, and 4.16 illustrate the resulting lateral displacement profiles for Dredging Phases 1, 3, and 6, respectively, allowing for a comparison with the previously calibrated hinged model.

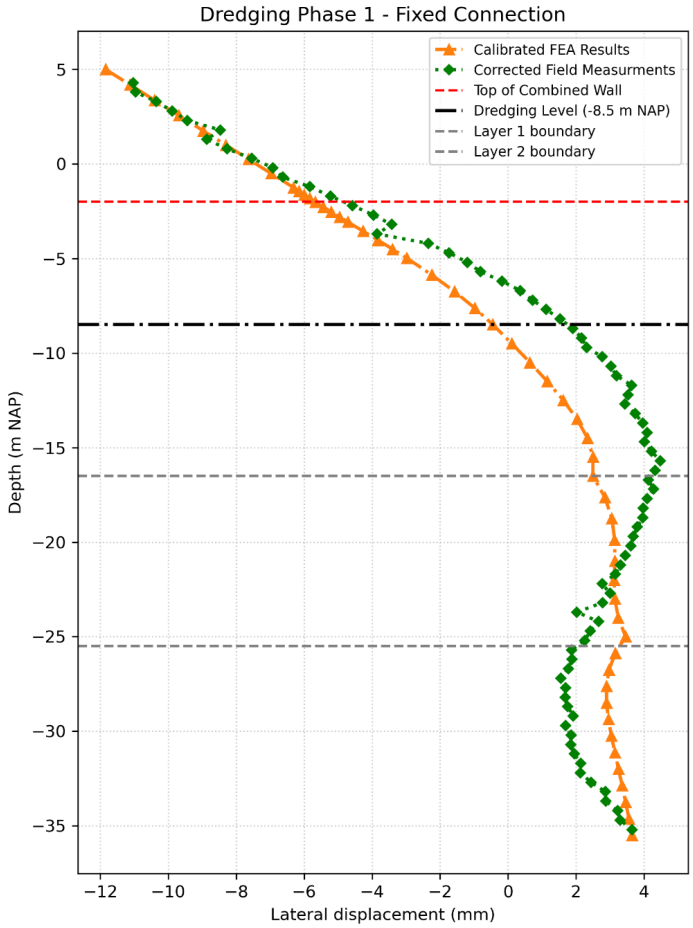

Figure 4.14: Calibrated FEM results with fixed connection for Dredging Phase 1 compared to inclinometer data.

Figure 4.14 shows the results for Phase 1 (dredging to approximately -8.5 m NAP). The maximum lateral displacement of the corrected field measurements is approximately -11 mm, while the calibrated FEM model with a fixed connection predicts a maximum displacement of about -12 mm. This results in a discrepancy of approximately 8%. The general deformation shape of the FEM results aligns well with the inclinometer measurements. A toe displacement of around 3.5 mm is observed in the FEM model, which is consistent with expectations due to the non-fixed nature of the combi wall toe. The

FEM calibrated results curve illustrates that there is a slight underestimation in the displacement in the region from -5 m to -20 m. The results overall is similar to the results obtained in the model variant with a hinge connection.

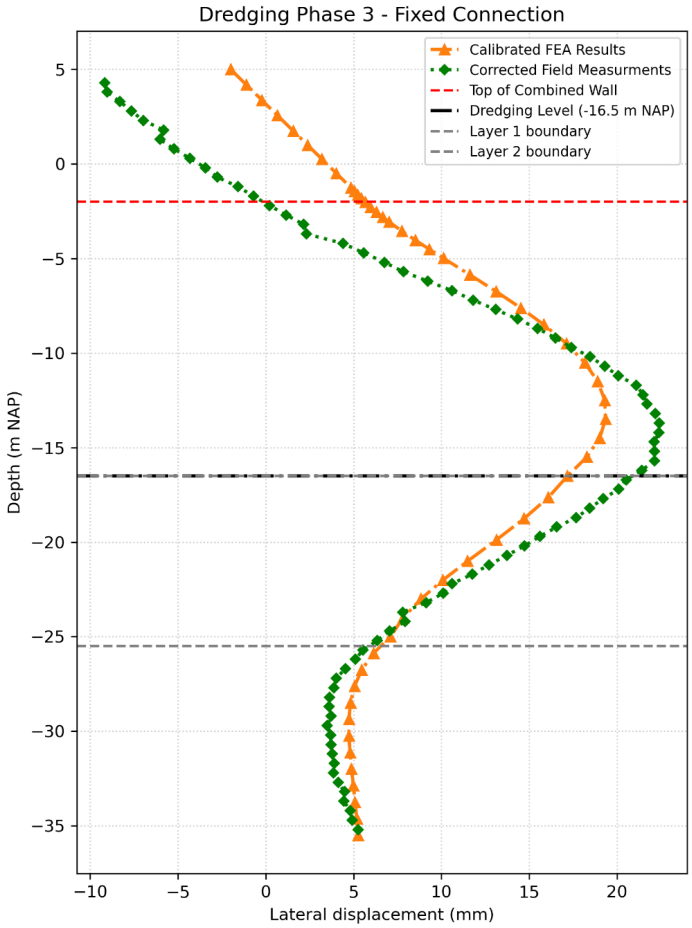

Figure 4.15: Calibrated FEM results with fixed connection for Dredging Phase 3 compared to inclinometer data.

Figure 4.15 shows the results for Phase 3 (dredging to approximately -16.5 m NAP). The maximum lateral displacement of the corrected field measurement is approximately 22 mm, while the calibrated FEM model with a fixed connection predicts a maximum displacement of about 19 mm. This results in a discrepancy of approximately 14%. A toe displacement of around 5 mm is observed in the FEM model. For the front wall, the corrected field data indicates a maximum lateral displacement of -9 mm towards the landside, whereas the FEM results predict a displacement of only -2 in the same direction.

The fixed connection configuration yields a notable improvement in matching the front wall behaviour, particularly in the upper part of the wall, where the frictionless hinge model had previously underpredicted the landside movement. The predicted displacement profile shows reduced rotation at the top and a closer match to the measured displacements between the surface and the dredging level (-16.5 m NAP). A slight underestimation of displacements is observed in the vicinity of the dredging level, although the overall agreement remains good. Below the dredge level, the agreement between the FEM results and field data remains high, with both the magnitude and shape of displacements aligning closely. The fixed connection also eliminates the unrealistic over-rotation observed in the hinge model, suggesting that some degree of rotational restraint exists in the actual structure, even if not fully rigid.

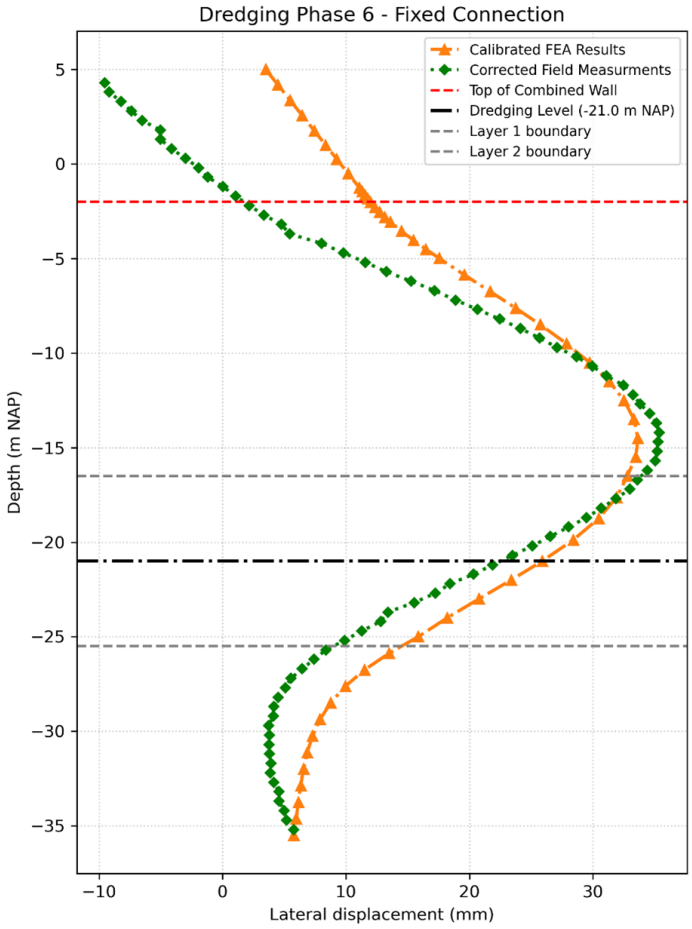

Figure 4.16: Calibrated FEM results with fixed connection for Dredging Phase 6 compared to inclinometer data.

Figure 4.16 shows the results for Phase 6 (dredging to approximately -21 m NAP). The maximum lateral displacement of the corrected field measurement is approximately 35 mm, while the calibrated FEM model with a fixed connection predicts a maximum displacement of about 33 mm. This results in a discrepancy of approximately 6%. A toe displacement of around 5 mm is observed in the FEM model. For the front wall, the corrected field data indicates a maximum lateral displacement of -9.5 mm towards the landside, whereas the FEM results predict a displacement of only 3.5 mm towards the waterside.

The overall deformation profile matches the inclinometer measurements closely. A slight underestimation of displacements is observed at depth -15 m NAP. Notably, the slope of the front wall profile in the fixed-connection model more closely follows the inclinometer data, reducing the mismatch seen in the hinge-connection results.The improved match indicates that incorporating rotational restraint at the wall connection more effectively replicates the actual structural behaviour during deep dredging stages

FEM with Fixed Connection Anchor Forces

Table 4.8 summarizes the anchor forces for both the upper and lower anchor levels during the dredging phases, based on the FEM analysis with a fixed connection between the combi wall and front wall.

As in the previous models, the results are compared to the maximum allowable anchor load, which is governed by the anchor system's capacity. The pre-stressing force is 220 kN, and the anchor's ultimate capacity (P_{max}) is 2200 kN. However, due to the limitations of the anchor elements in PLAXIS, the forces shown reflect the mobilized working loads during the staged construction.

Table 4.8: Anchor Forces – FEM with Fixed Connection

Anchor	Dredging Phase	N (kN)	N_{max} (kN)
Upper	1	150.507	220
	3	318.672	318.672
	6	412.667	412.667
Lower	1	145.736	220
	3	355.638	355.638
	6	461.970	461.970

From the results, we observe that:

- In **Phase 1**, both the upper and lower anchors remain under the limit (150.5 kN and 145.7 kN respectively), showing safe mobilization.
- In **Phase 3**, anchor forces increase significantly as dredging progresses, reaching 318.7 kN (upper) and 355.6 kN (lower), both exceeding the pre-stressing value and reflecting higher mobilization.
- In **Phase 6**, the highest anchor loads are observed: 412.7 kN (upper) and 462.0 kN (lower). These are the largest values among all connection scenarios analyzed (initial, calibrated, and fixed), indicating that a fully rigid connection leads to greater anchor force development.

The increased anchor loads in the fixed connection model are expected, as the rigid connection prevents relative rotation between the front and combi wall, altering the distribution of internal forces. This leads to higher anchor mobilization, especially in the final dredging phase.

Despite this, the values remain below the design capacity of the anchors, and the results demonstrate the structural adequacy of the anchoring system even under more conservative assumptions.

4.2.8. FEM with Fixed Connection Discussion

The results of the fixed connection model demonstrate a notable improvement in the agreement between FEM predictions and inclinometer measurements when compared to the hinged connection model. By removing the rotational freedom at the interface between the combi wall and the front wall, the predicted wall behaviour more closely matches field observations, particularly in terms of displacement magnitudes and the location of maximum deflections.

In Phase 1, the maximum lateral displacement predicted by the fixed connection model is approximately -12 mm, compared to the corrected field measurement of -11 mm, giving a discrepancy of about 8%. The overall deformation shape matches well with inclinometer data, including the observed toe displacement of about 3.5 mm. A slight underestimation of displacements is noted between depths of -5 m and -20 m, but the results remain broadly consistent with those from the hinged model, indicating that connection stiffness plays a limited role in shallow dredging stages.

In Phase 3, the profile more accurately captures the measured behaviour in the upper part of the wall, reducing the underprediction of landside movement observed in the hinged configuration. A slight underestimation remains near the dredging level (-16.5 m NAP), but below this depth, both the shape and magnitude of displacements align closely with the inclinometer data. The elimination of unrealistic over-rotation at the top of the wall indicates that some degree of rotational restraint is likely present in the actual structure.

In Phase 6, the fixed connection model predicts a maximum displacement of 33 mm, compared to 35 mm measured, resulting in a 6% discrepancy. The agreement is strong throughout the depth, with only a slight underestimation observed near -15 m NAP. Importantly, the slope of the front wall profile in the fixed-connection model more closely follows the inclinometer data, resolving much of the mismatch seen in the hinged model. This suggests that incorporating rotational restraint is particularly important for accurately reproducing the structural response during deep dredging stages.

The increased realism in wall movement, however, comes at the cost of higher internal forces. Anchor loads in the fixed model are consistently greater than those seen in the calibrated model with a hinged connection. For instance, in Phase 6, the upper and lower anchors reach 412.7 kN and 462.0 kN, respectively, the highest values recorded across all modeled scenarios. This is attributed to the elimination of the rotational flexibility, which shifts greater bending resistance into the anchor system. Despite this increase, all anchor forces remain well below the design capacity of 2200 kN, confirming the structural adequacy of the system.

In addition to the anchor force comparison, it is instructive to examine the bending moment distributions for the two connection configurations. Figure 4.17 show the bending moments for the hinged and fixed connection models.

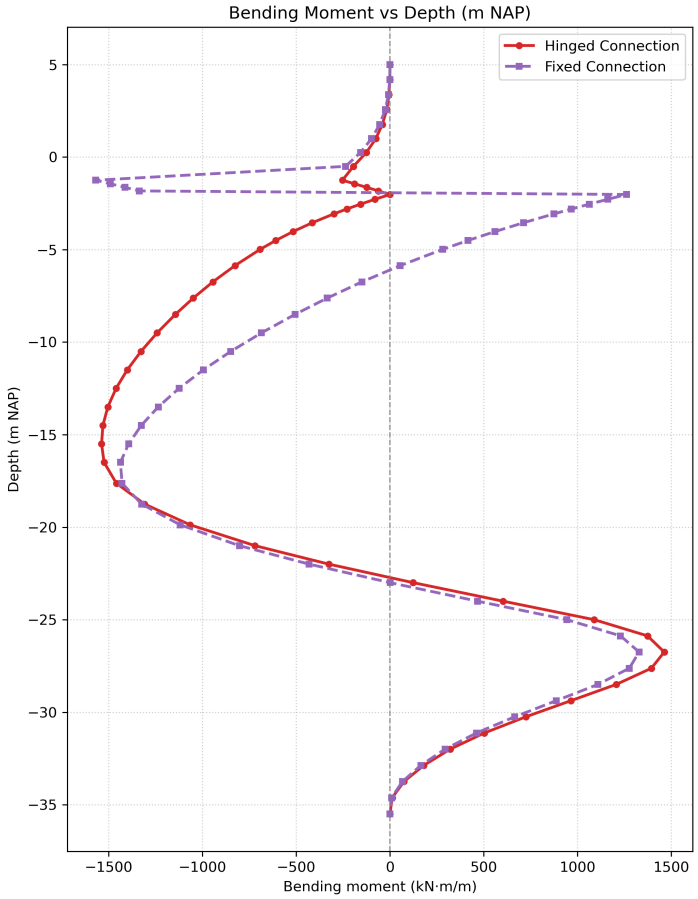

Figure 4.17: Comparison of bending moment distribution for the Combi-Wall and Front Wall under hinged and fixed connection conditions.

When comparing the two cases, the overall shape of the bending moment profile remains broadly similar, with peak positive moments occurring in the upper part of the wall and negative moments concentrated below the dredging level. However, the magnitudes differ:

1. In the hinged model , the maximum positive bending moment reaches 1463 kNm/m and the maximum negative moment reaches -1538 kNm/m.
2. In the fixed connection model, the maximum positive moment is slightly lower at 1328 kNm/m, whereas the maximum negative moment increases in magnitude to -1569 kNm/m.

This shift indicates that eliminating the hinge redistributes bending demand along the wall, slightly reducing the positive peak near the top but increasing the hogging moments in the embedded section. The increased negative bending moments in the fixed connection model suggests greater fixity at the interface, leading to higher bending resistance mobilized in the lower portion of the wall.

If the fixed connection model more closely represents field conditions, it implies that a purely hinged assumption could underestimate hogging moments and stresses during design, particularly in deeper dredging stages. This highlights the importance of selecting an appropriate connection model to avoid conservative bending moment predictions.

Overall, the FEM results with a fixed connection offer a more accurate representation of both the lateral displacement profile and the interaction between wall and soil. The improved agreement with inclinometer data across all phases suggests that the actual structural behavior on site may more closely resemble a semi-rigid or fixed condition, rather than a perfectly hinged interface. These insights are valuable for both future modeling efforts and the refinement of structural assumptions in quay wall design practice.

4.2.9. HSsmall Model Results

The Hardening Soil (HS) model incorporates the stress-dependency of soil stiffness but does not account for changes in stiffness with strain. To address this, the Hardening Soil model with small-strain stiffness (HSsmall) is applied. This enhanced model considers the strain-dependency of stiffness, which could lead to lower predicted horizontal deformations of the retaining structure and reduced heave, Brinkgreve (2019a) [5].

The HSsmall model introduces two additional parameters:

- The small-strain shear modulus, G_0^{ref}
- The threshold shear strain, $\gamma_{0.7}$

The threshold shear strain, $\gamma_{0.7}$, represents the strain at which the shear modulus is reduced to 70% of its initial small-strain value. The small-strain shear modulus is defined as:

$$G_0^{\text{ref}} = \frac{E_0^{\text{ref}}}{2(1+\nu_{ur})} \tag{4.1}$$

where E_0^{ref} is the initial reference stiffness modulus and ν_{ur} is the Poisson's ratio under unloading/reloading conditions. The reference stiffness modulus is related to the secant stiffness E_{50}^{ref} by:

$$E_0^{\text{ref}} = 5 \cdot E_{50}^{\text{ref}} \tag{4.2}$$

as described by Obrzud and Truty (2018) [5].

For sandy soils, the typical range of threshold shear strain $\gamma_{0.7}$ lies between 1×10^{-4} and 2×10^{-4}, where the lower value is associated with dense sands and the upper value with looser sand layers [5]. Based on the CPT data analysis, the relative density of the layers varies between 40% and 70%, indicating that the sands are of medium to high density. Therefore, a representative threshold shear strain value of 1.3×10^{-4} is adopted for the sand layers in this study. Table 4.9 provides a summary of the small-strain stiffness parameters used in the HSsmall model. Figure 4.18 presents a comparison of the FEM results obtained using both the HS and HSsmall constitutive models. The differences in lateral displacements between the two models are minor, approximately 1 to 3 mm during Dredging Phases 1 and 3, and virtually nonexistent during the final dredging phase.

Table 4.9: Small-Strain Parameters for Each Soil Layer

Layer Number	E_0^{ref} (MPa)	G_0^{ref} (MPa)
1	190	63.33
2	50	16.67
3	425	141.67
4	190	63.33

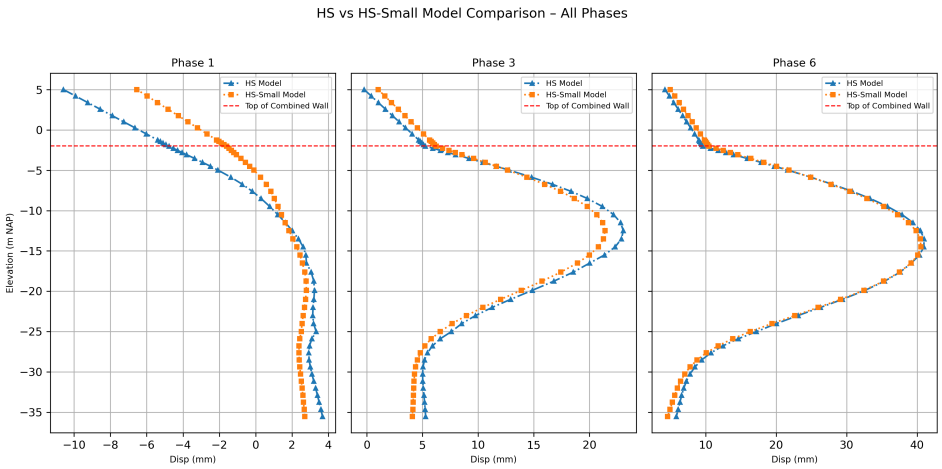

Figure 4.18: HS vs HS-small strain model results

4.2.10. HSsmall Model Discussion

The comparison between the standard Hardening Soil (HS) model and the Hardening Soil model with small-strain stiffness (HSsmall) reveals that incorporating strain-dependent stiffness does not significantly alter the predicted wall displacements in this specific case. As shown in Figure 4.18, the difference in lateral displacements between the two models is minimal, ranging from 1 to 3 mm in Dredging Phases 1 and 3, and becomes negligible in the final phase of excavation.

This limited difference is likely due to the relatively high stiffness moduli of the soil layers derived from CPT interpretation. High initial stiffness results in small shear strains during excavation, which in turn minimizes the influence of the small-strain stiffness enhancement offered by the HSsmall model. In essence, the stress–strain path does not reach strain levels low enough for the nonlinear small-strain stiffness behavior to substantially affect the response.

The parameters used for the HSsmall model, including the threshold shear strain $\gamma_{0.7}$ set at 1.3×10^{-4}, are representative of the medium to dense sand layers present in the site. This choice is supported by CPT-based assessments of relative density. While this small-strain threshold helps ensure realistic stiffness degradation behavior, the high base stiffness values used across layers dominate the overall soil response.

Given the minor differences in model predictions and the substantial increase in computational time associated with HSsmall simulations, it is both efficient and justifiable to continue using the standard HS model for the remainder of the analysis. The HS model adequately captures the deformation behavior of the wall system under the unloading conditions induced by dredging.

In conclusion, while the HSsmall model offers a more advanced representation of soil behavior at very small strains, its impact is not pronounced for the present case study. The HS model strikes a suitable balance between computational efficiency and predictive accuracy for modeling wall displacements.

4.2.11. Results and Discussion of the Parametric Study

Following the successful calibration and validation of the finite element model (FEM), a series of parametric analyses were carried out to investigate the quay wall's performance to variations in key factors.

Three main factors were examined: dredging depth, surcharge loading, and soil properties. The dredging depth analysis explores the effects of deepening beyond the final implemented dredging level of -21 m NAP, considering scenarios down to the design depth of -24 m NAP. The surcharge variation assesses the structural response under operational loads ranging from 10 kN/m^2 to 60 kN/m^2. Finally, the soil parameter variation focuses on stiffness moduli and friction angles for the most influential soil layers identified in the sensitivity analysis, with properties varied across statistically defined bounds in accordance with NEN 9997-1.

In total, 101 FEM simulations were performed, covering the full combination of parameter variations. The results presented in the following subsections provide a detailed assessment of the wall's response under each variation, highlighting trends, critical thresholds, and potential design implications.

Dredging Level Variation

Figure 4.19 presents the displacement profiles for the calibrated model (Phase 6, dredging to -21.0 m NAP) alongside the two extended dredging scenarios: Case A at –22.5 m NAP and Case B at -24.0 m NAP. A clear trend emerges, showing that increasing the dredging depth results in greater lateral displacements along the combi wall.

For the reference Phase 6 case, the maximum lateral displacement is approximately 39.5 mm, occurring at a depth of around -14.0 m NAP. Extending the dredging to -22.5 m NAP (Case A) increases the maximum displacement to about 46.5 mm, while dredging to -24.0 m NAP (Case B) results in the highest displacement of approximately 53.7 mm. These values are summarised in Figure 4.20, which illustrates the direct relationship between dredging depth and maximum displacement.

The increase in displacement with dredging depth can be attributed to the progressive reduction in passive resistance. As the dredging depth increases, a greater portion of the wall is exposed, allowing larger deflections to develop under the same conditions.

In addition to the magnitude changes, the displacement profiles indicate that the location of maximum displacement shifts slightly downward with deeper dredging. This is consistent with the reduction in soil passive support near the dredge level and the redistribution of bending moments along the wall.

From a design perspective, the results highlight the sensitivity of the wall performance to dredging depth. While the wall system remains within allowable displacement limits for the depths investigated, the trend suggests that further deepening would require re-evaluation of wall stiffness, anchor forces, and serviceability criteria to ensure structural and operational safety.

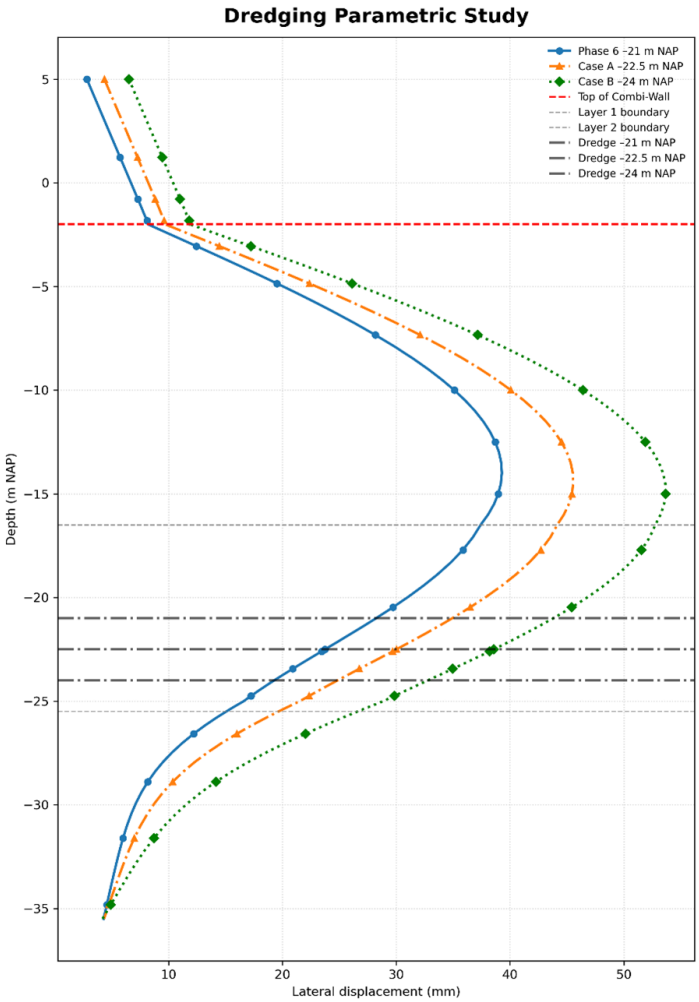

Figure 4.19: Dredging level variation.

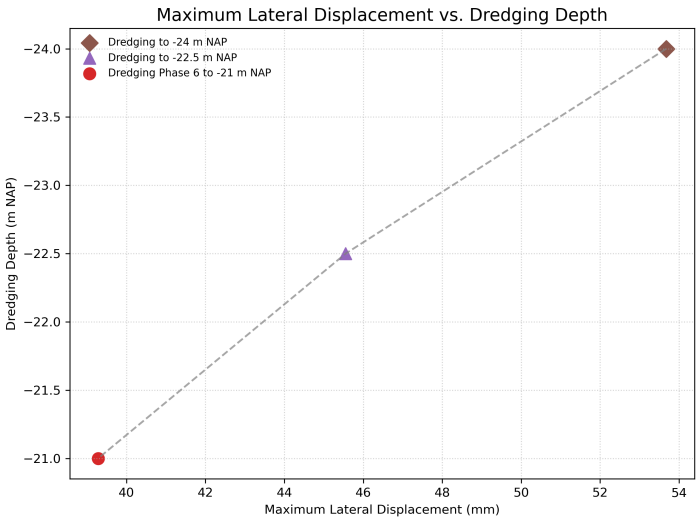

Figure 4.20: Maximum lateral displacement vs. dredging depth.

Surcharge Load Variation

Figure 4.21 shows the lateral displacement profiles for Phase 6 under surcharge levels from 0 kPa (baseline, no surcharge) to 60 kPa, including the design surcharge of 40 kPa. The results exhibit a clear, monotonic trend: increasing surcharge leads to larger lateral displacements, with the strongest amplification in the upper and mid-depth portions of the wall. The curve shapes remain similar across cases, indicating that surcharge primarily scales the displacement magnitude rather than altering the deformation mode.

Relative to the baseline (0 kPa), the 10–60 kPa cases show progressively larger deflections, and the 40 kPa design load lies mid-range within this family of responses.

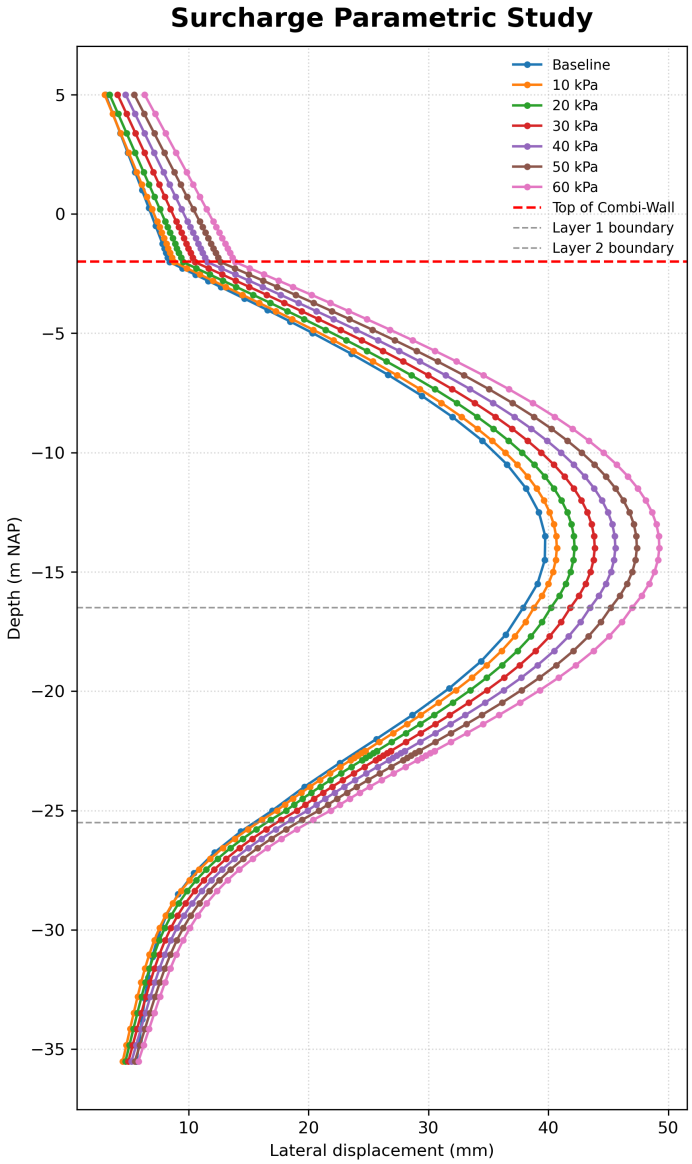

Figure 4.21: Surcharge Load Parametric Study

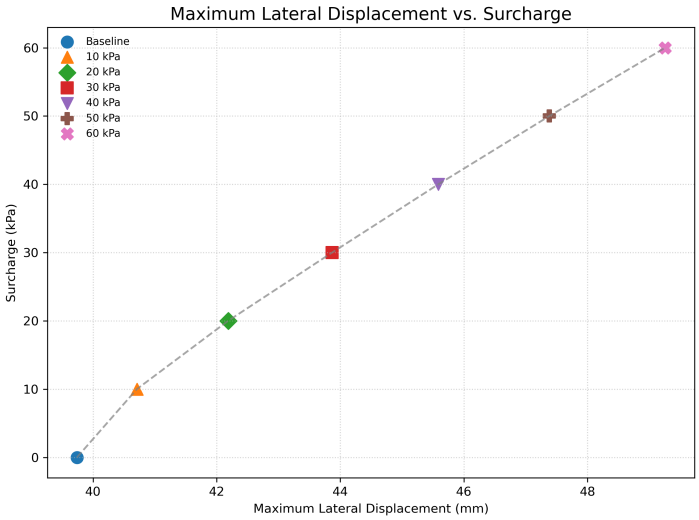

Figure 4.22: Maximum lateral displacement vs. Surcharge Load.

Soil Parameter Variation

+Based on the findings from the sensitivity analysis, the most influential parameters affecting the wall's response were identified as the friction angles of Layer 1 and Layer 2 (ϕ_1, ϕ_2) and the stiffness moduli of Layer 2 and Layer 3 (E_2, E_3). These parameters were systematically varied across their lower bound, mean, and upper bound values, with additional intermediate values to provide a continuous response spectrum. Specifically, six intermediate values were considered for each friction angle and four for each stiffness modulus, resulting in a total of 101 finite element model (FEM) simulations, the complete list of simulation runs and their associated parameter values is provided in Appendix E.

For Phase 6, the computed lateral displacement profiles from the FEM were corrected for toe displacement by adding the inclinometer-measured toe movement. This ensured that both FEM and field measurements shared a common reference point. The corrected displacement profiles were then compared directly with the inclinometer measurements to assess model performance. In addition, the results were compared to the inclinometer measurement in a normalized plot.

An envelope was constructed by identifying, at each depth, the minimum and maximum corrected displacements across all simulations (see Figure 4.23). This shaded region represents the full range of possible wall displacements given the soil property variability. The baseline case, corresponding to mean soil parameters, was plotted as a dashed black line within this envelope to evaluate its position relative to the extremes.

The results clearly demonstrate that ϕ_2 (Layer 2 friction angle) exerts the greatest influence on the maximum lateral displacement in Phase 6 (Figure 4.25b). Reducing ϕ_2 to its lower bound produced the largest displacement increases, with a shift in the displacement profile towards deeper wall movements, particularly near the dredge level. This behaviour reflects the reduced shear strength in Layer 2, allowing greater mobilization of soil deformation. Conversely, increasing ϕ_2 to the upper bound resulted in noticeably stiffer system behaviour, with reduced maximum displacements.

The influence of ϕ_1 (Layer 1 friction angle) is also significant but more pronounced in the upper portion of the wall above the dredge level (Figure 4.25a). Variations in ϕ_1 altered the upper wall curvature and slightly shifted the location of maximum displacement but had a smaller effect on overall displacement magnitude compared to ϕ_2.

Stiffness modulus variations exhibited more localized effects. For E_2 (Layer 2 modulus), lower bound values led to larger displacements near the dredge level, while upper bound values reduced deformation in this region (Figure 4.26a). For E_3 (Layer 3 modulus), the effect was primarily confined to deeper wall segments below the dredge level, with minimal impact on upper wall behaviour (Figure 4.26b). This indicates that the deep passive resistance provided by Layer 3 is sensitive to stiffness changes but does not significantly influence surface-level wall movements.

Overall, the parametric study confirms that:

- ϕ_2 has the highest impact on wall displacement magnitude and profile shape.
- ϕ_1 influences upper wall displacements but to a lesser extent.
- E_2 affects displacement magnitudes near the dredge level, while E_3 primarily influences deeper segments.

This comprehensive evaluation underscores the importance of accurately characterising the friction angle of Layer 2 in future design assessments, as it controls much of the quay wall's deformation behaviour under operational conditions.

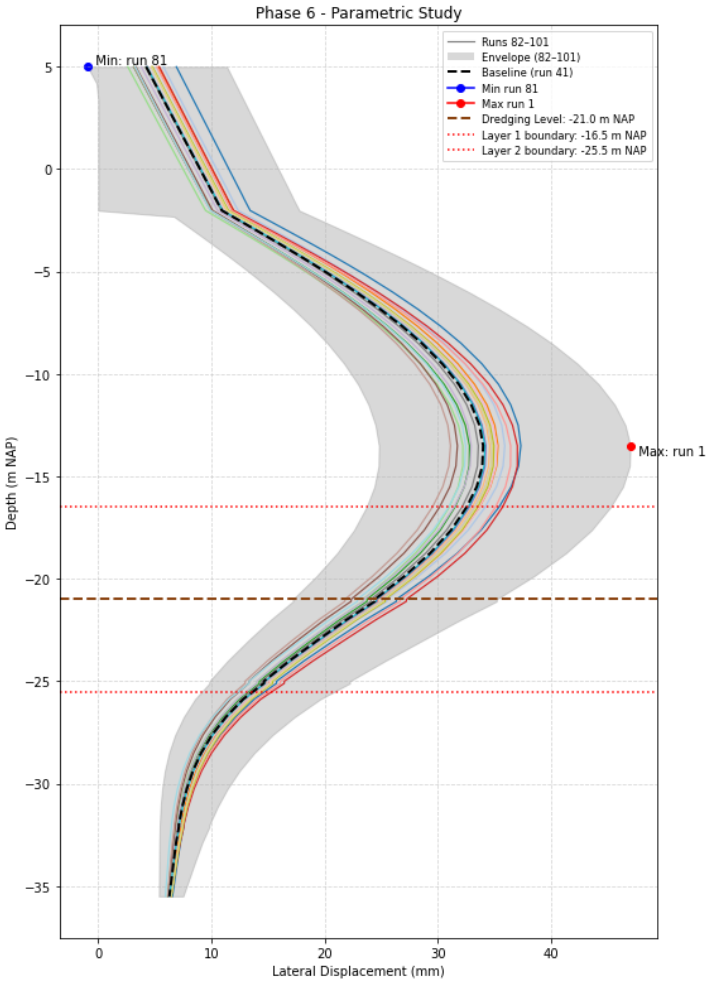

Figure 4.23: Lateral displacements for all soil parameter variations in Phase 6.

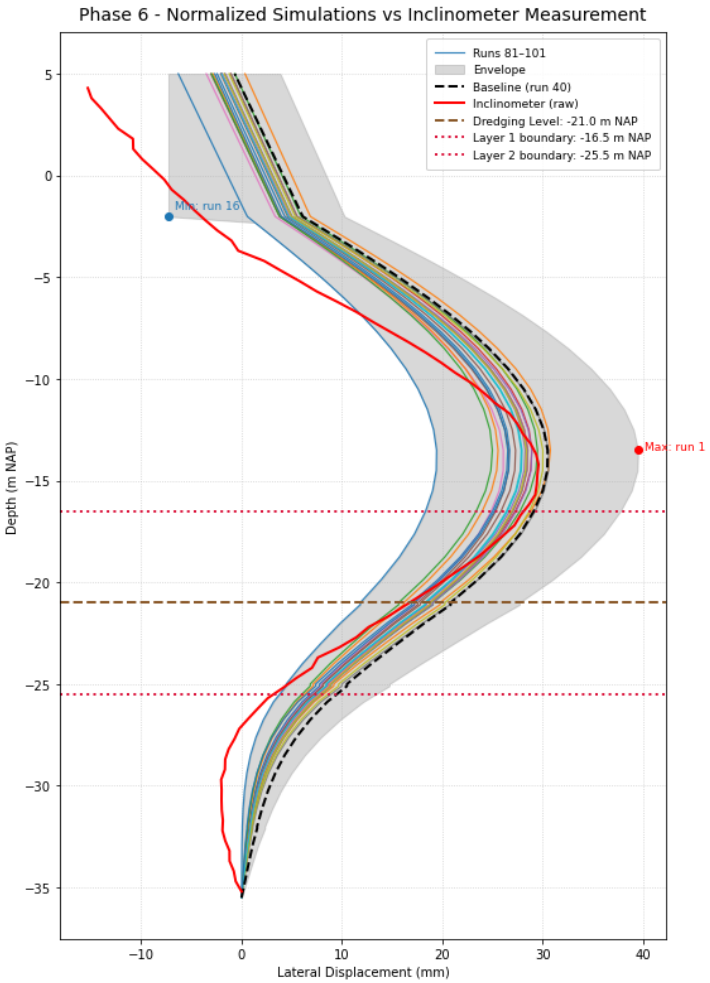

Figure 4.24: Comparison of corrected FEM displacement profiles to inclinometer measurements in Phase 6.

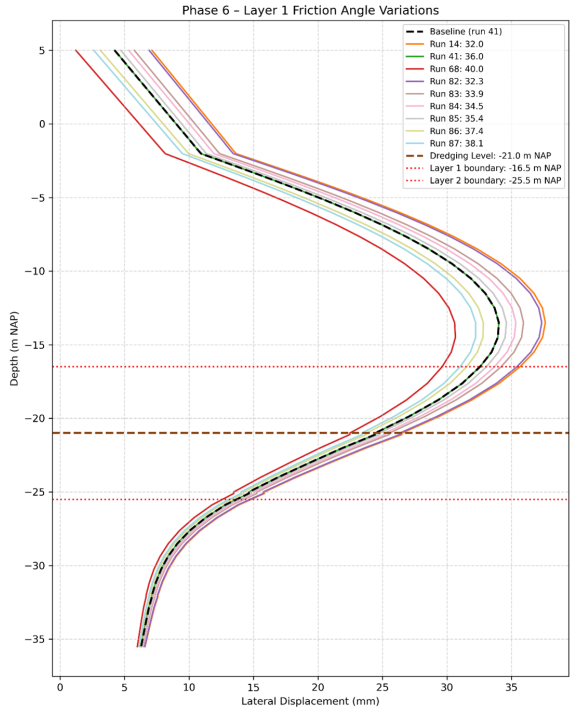

(a) Effect of Layer 1 friction angle (ϕ_1) variation on lateral displacement profile in Phase 6.

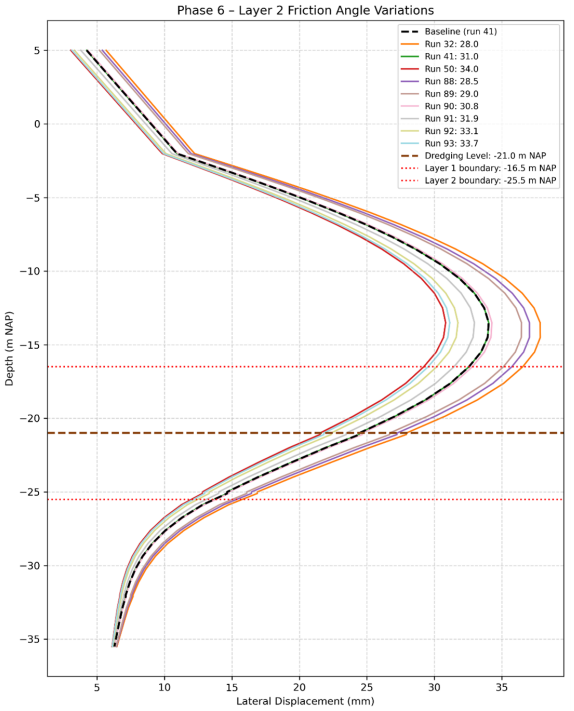

(b) Effect of Layer 2 friction angle (ϕ_2) variation on lateral displacement profile in Phase 6.

Figure 4.25: Effects of friction angle variation for Layer 1 and Layer 2 in Phase 6.

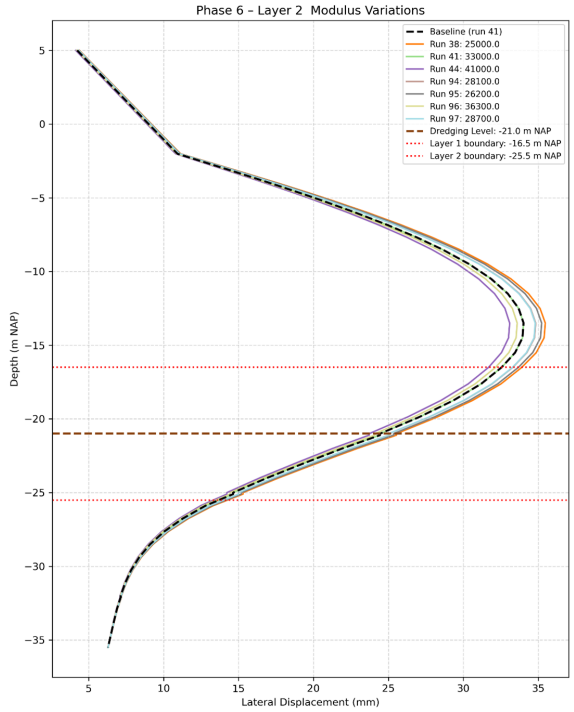

(a) Effect of Layer 2 modulus (E_2) variation on lateral displacement profile in Phase 6.

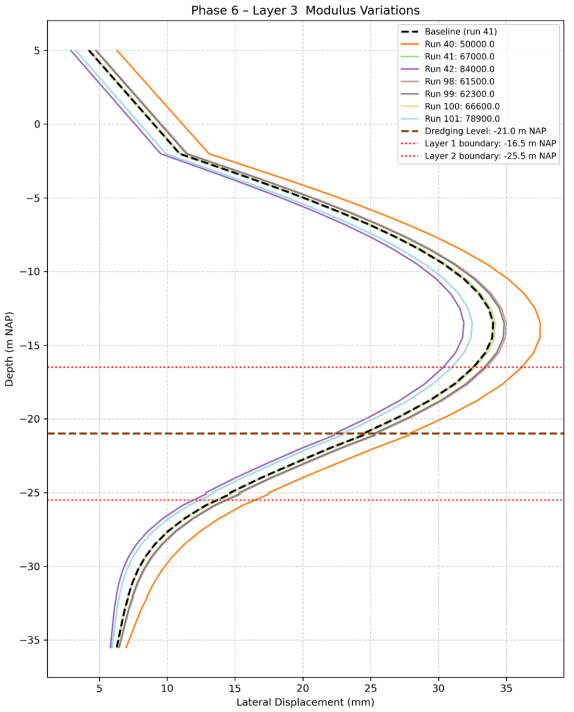

(b) Effect of Layer 3 modulus (E_3) variation on lateral displacement profile in Phase 6.

Figure 4.26: Effects of modulus variation for Layer 2 and Layer 3 in Phase 6.

4.3. Conclusion

This chapter presented a comprehensive analysis of the quay wall behaviour during staged dredging, based on finite element modelling (FEM) and validation against inclinometer measurements. The investigation progressed from the initial FEM model to a calibrated version, followed by a fixed-connection variant, a comparison between the Hardening Soil (HS) and HSsmall constitutive models, and concluded with a parametric study assessing the effects of dredging depth, surcharge loading, and soil property variation.

The calibration process was guided by the grouped sensitivity analysis, which identified the friction angles of Layers 1 and 2 and the stiffness moduli of Layers 2 and 3 as the most influential parameters across dredging phases. These findings shaped the calibration strategy:

- The stiffness of Layer 1 ($E_{50,1}^{ref}$) was reduced to decrease the overestimation of wall stiffness in the upper section observed in the initial model, which resulted in underpredicted displacements in early dredging phases. Its friction angle (ϕ_1) was increased to provide additional shear resistance and maintain overall stability after the stiffness reduction. This combination ensured that displacement magnitudes aligned more closely with inclinometer data while preserving the correct deformation shape.
- For Layer 2, both stiffness ($E_{50,2}^{ref}$) and friction angle (ϕ_2) were reduced, consistent with higher fines content and heterogeneity suggested by CPT results. This reduced the over-stiff behaviour in early phases and improved agreement in the mid-depth displacement profile.
- The stiffness of Layer 3 ($E_{50,3}^{ref}$) was increased to enhance toe restraint and capture deeper-stage behaviour, while minor adjustments to Layer 4 improved lower boundary response without creating excessive rigidity.

These adjustments illustrate the interplay between stiffness and strength. The friction angle (φ) has a more pronounced effect on the ultimate magnitude of wall displacements, as it directly influences the active earth pressure coefficient K_a and therefore the lateral loads acting on the wall during excavation unloading. Even small changes in ϕ can lead to significant differences in K_a, and consequently in the final displacement magnitudes. The calibrated parameter set reflects a balanced optimization between stiffness and strength effects thereby ensuring both realistic deformation shapes and agreement with inclinometer measurements.

The calibrated FEM model significantly improved agreement with inclinometer data, often reducing discrepancies to within the accepted $\pm 30\%$ margin. In several phases, the predicted response was very close to the corrected field data in both magnitude and shape. However, the most consistent agreement was observed at the final dredging stage of each scenario, indicating that the FEM representation captured the cumulative deformation behaviour well, even if intermediate phases showed localised mismatches. These local deviations may be attributed to modelling simplifications, such as the idealised representation of dredging stages. In reality, dredging is not executed as a single-step excavation; rather, it progresses through staged depth increases and may involve temporary slopes or support structures to maintain stability during excavation. Additionally, the simplified stratigraphic profile adopted in the model smooths out local heterogeneities in soil layering and properties, which can affect displacement predictions at certain depths.

The front wall behavior consistently presented a mismatch between model predictions and field measurements. In all FEM models, the front wall exhibited progressive rotation, with landside movement in early phases transitioning to waterside displacement in later stages. Conversely, the inclinometer data suggested a consistent landside displacement throughout dredging. This discrepancy likely arises from modeling simplifications. Firstly, the assumed hinge connection between the combi wall and front wall in PLAXIS may not accurately replicate the actual site conditions. While real-world hinges are designed to allow rotation, they often exhibit some degree of frictional resistance. In contrast, the hinge modelled in PLAXIS is entirely frictionless, potentially altering the rotation behaviour of the front wall. Moreover, the precise location of the hinge in the numerical model may not correspond exactly with the structural detail as constructed on site.

Another plausible explanation involves the modelling of the pre-stressing procedure. According to literature, anchor pre-stressing is sometimes applied in multiple stages to control deformation more

effectively. However, in the current model, the pre-stressing was implemented in a single step, which may contribute to discrepancies between the model predictions and the observed field behaviour, particularly in the responses of the combi wall and front wall.

The fixed-connection model further reduced discrepancies in all phases, particularly for the front wall, where the hinge model had underpredicted landside displacement. By removing the idealized rotational freedom between the combi wall and front wall, this variation more accurately reproduced the measured displacement slope and the location of peak movement. The trade-off was a noticeable increase in anchor loads, with the highest mobilized forces recorded in Phase 6, although these remained well below design limits. In practice, the connection between the front wall and the combi wall is likely neither perfectly hinged nor fully fixed, but exhibits a degree of rotational restraint that lies between these two extremes, an intermediate behaviour that the fixed-connection model approximated more closely than the hinge model.

Finally, the comparison between the HS and HSsmall models demonstrated that small-strain stiffness had limited impact on overall deformation behavior in this case. Due to the relatively high stiffness moduli of the sand layers and the small strain levels induced during dredging, the HS model proved sufficiently accurate and computationally efficient for continued analysis.

The parametric study confirmed that:

1. Increasing dredging depth beyond $-21\ \mathrm{m\ NAP}$ leads to a progressive increase in maximum lateral displacement, with the largest changes occurring between $-22.5\ \mathrm{m}$ and $-24\ \mathrm{m}$ NAP.
2. Surcharge loading above the design value of $40\ \mathrm{kN/m^2}$ also increases wall displacement.
3. Variations in the key soil parameters (ϕ_1, ϕ_2, $E^{ref}_{50,2}$, $E^{ref}_{50,3}$) strongly influence Phase 6 behaviour. The FEM results for different parameter combinations showed trends consistent with the sensitivity analysis, with the corrected inclinometer data used as the benchmark.

Table 4.10 summarises the maximum lateral displacements from the corrected field data and FEM predictions for all three phases across the Initial, Calibrated, and Calibrated with Fixed Connection models. It highlights the progressive improvement achieved through calibration and connection adjustment, with percentage differences generally reduced compared to the initial model.

Overall, the study demonstrates that careful calibration of soil stiffness and strength parameters, guided by sensitivity analysis, can substantially improve the predictive accuracy of quay wall FEM models. Connection detailing between structural elements significantly influences displacement profiles and anchor force development, while dredging depth, surcharge loading, and key soil properties are confirmed as critical factors in wall performance. The findings reinforce the importance of integrating field measurements, and targeted parameter adjustment to achieve reliable predictions for staged dredging operations.

Table 4.10: Comparison of Corrected Field and FEM-Predicted Maximum Lateral Displacements

Model	Dredging Phase	Corrected Field (mm)	FEM Predicted (mm)	Difference (%)
Initial FEM	1	-11	-8.5	22
	3	22	17	22
	6	35	34	3
Calibrated FEM	1	-11	-12	9
	3	22	21	5
	6	35	39	11
Calibrated FEM with Fixed Connection	1	-11	-12	8
	3	22	19	14
	6	35	33	6

5

Conclusion and Recommendations

5.1. Conclusions

This thesis set out to develop, calibrate and validate a finite element model (FEM) of the Amaliahaven quay wall during dredging, using field inclinometer data to ensure predictive accuracy. Four FEM scenarios were compared, initial (uncalibrated), calibrated via inverse analysis which was supported by the sensitivity analysis, fixed-connection variation, and a model variation that compared the HS and the HS-small strain constitutive models.

5.1.1. Main Findings

This study progressed from an initial finite element model (FEM) of the Amaliahaven quay wall to a calibrated model, then to a fixed-connection variant, followed by a comparison between the Hardening Soil (HS) and HSsmall constitutive models, and concluded with a parametric study assessing the effects of dredging depth, surcharge loading, and soil parameter variation.

The grouped sensitivity analysis identified the friction angles of Layers 1 and 2 and the stiffness moduli of Layers 2 and 3 as the most influential parameters across all dredging phases. This informed the calibration strategy:

- Layer 1: Stiffness ($E_{50,1}^{ref}$) was reduced to soften the upper wall response, addressing over-stiffness in early phases, while friction angle (ϕ_1) was increased to reflect cleaner, denser sands inferred from low CPT f_r values. This combination aligned displacement magnitudes and shape with inclinometer data.
- Layer 2: Both stiffness ($E_{50,2}^{ref}$) and friction angle (ϕ_2) were reduced to represent higher fines content and heterogeneity suggested by CPT results, improving agreement in mid-depth displacements.
- Layer 3: Stiffness ($E_{50,3}^{ref}$) was increased to enhance toe restraint and match deeper-stage behaviour. Minor adjustments to Layer 4 improved the lower boundary response.

The friction angle had the most pronounced influence on ultimate displacement magnitude, due to its direct effect on the active earth pressure coefficient K_a and thus on lateral loads during excavation unloading. Stiffness changes, in contrast, primarily adjusted the profile shape and depth distribution.

The calibrated FEM significantly improved agreement with inclinometer data, reducing discrepancies to within the accepted $\pm 30\%$ range in all phases. In several phases, the predicted response was very close to the corrected field data in both magnitude and shape, with the most consistent match occurring in the final dredging stage. Localized mismatches in intermediate phases are attributed to modelling simplifications, such as the idealised representation of dredging (single-step depth changes rather than staged excavation with temporary slopes or supports) and the idealized stratigraphic profile, which omits local heterogeneities.

In all FEM variants, the front wall exhibited progressive rotation, shifting from landside movement in

early phases to waterside displacement in later phases, whereas inclinometer data indicated consistent landside movement. The fixed-connection model, replacing the frictionless hinge between the combi wall and front wall, more accurately reproduced the measured slope and peak location of the displacement profile, reducing maximum errors to 8% (Phase 1), 14% (Phase 3), and 6% (Phase 6). Anchor loads increased under this assumption but remained well below the $2\,200\ \mathrm{kN}$ design limit. These results indicate that the real connection behaviour likely lies between a purely hinged and a fully fixed condition, with partial rotational restraint being more representative.

Switching from the HS to the HSsmall model changed predicted displacements by only 1–3 mm in early phases and had negligible effect in later phases, due to the relatively high stiffness of the sand layers and small strain levels during dredging. Given the increase in computation time for minimal accuracy gain, the HS model was retained as the most efficient choice.

The parametric study confirmed that:

1. Increasing dredging depth beyond $-21\ \mathrm{m\ NAP}$ leads to a progressive increase in maximum lateral displacement, with the largest changes occurring between $-22.5\ \mathrm{m}$ and $-24\ \mathrm{m}$ NAP.
2. Surcharge loading above the design value of $40\ \mathrm{kN/m^2}$ also increases wall displacement.
3. Variations in the key soil parameters (ϕ_1, ϕ_2, $E^{ref}_{50,2}$, $E^{ref}_{50,3}$) strongly influence Phase 6 behaviour. The FEM results for different parameter combinations showed trends consistent with the sensitivity analysis, with the corrected inclinometer data used as the benchmark.

Overall, the study demonstrates that careful calibration of soil stiffness and strength parameters, guided by sensitivity analysis, can substantially improve the predictive accuracy of quay wall FEM models. Connection detailing between structural elements significantly influences displacement profiles and anchor force development, while dredging depth, surcharge loading, and key soil properties are confirmed as critical factors in wall performance. The findings reinforce the importance of integrating field measurements, and targeted parameter adjustment to achieve reliable predictions for staged dredging operations.

5.1.2. Research Sub-Questions

In this section, the research subsections are answered.

- **What are the key structural and geotechnical factors influencing the mechanical behavior of quay walls during dredging activities?**

  Structurally, the bending stiffness (EI) of the quay wall elements, specifically the front wall, and the relieving platform, plays a pivotal role in controlling wall deformation. Increased stiffness generally reduces lateral displacements and bending curvatures but may induce higher anchor forces. Conversely, more flexible systems facilitate load redistribution but may result in displacements that exceed serviceability limits.

  Anchorage systems also exert a critical influence. Their performance depends on installation depth, stiffness, and the level of pre-stressing. Pre-stressed anchors, particularly when installed at appropriate elevations and in phases, effectively reduce wall displacements and stabilize internal force distributions.

  The connection detail between the front wall and combi-wall further shapes system response. Fixed connections transfer both shear and bending moments, creating a stiffer, more continuous system. Hinged connections, typically implemented using cast iron saddles, provide rotational freedom and reduce internal moments, resulting in more statically determinate systems [10]. In practice, such joints often provide partial rotational restraint, lying between idealized hinge and rigid conditions. In this thesis, the fixed connection assumption yielded better agreement with inclinometer measurements than a fully hinged representation.

  Geotechnically, two primary mechanisms govern quay wall deformation during dredging:

  - Reduction in vertical effective stress in the soil in front of the wall, leading to heave and unloading;

- Increased retaining height of the quay wall, which activates greater earth pressure and alters its distribution.

The relative importance of these mechanisms was confirmed through grouped sensitivity analyses, which also guided the calibration process. Friction angles and stiffness moduli were iteratively adjusted to align simulation outputs with inclinometer data, with layer-specific modifications informed by CPT correlations (q_c and f_r values). These provided a robust starting point but required refinement to capture site-specific behavior.

In summary, both structural and geotechnical parameters, particularly wall stiffness, anchor configuration, connection detailing, friction angle, and soil stiffness, are decisive in governing quay wall performance under dredging conditions.

- **What are the calibration and validation methods available to ensure the finite element model accurately represents the mechanical behavior of the quay walls?**

  Calibration and validation are fundamental steps in the development of accurate finite element models (FEM) for geotechnical structures such as quay walls. The aim of calibration is to refine uncertain soil parameters—particularly stiffness and strength—so that the model reproduces observed field behavior. Because soils are inherently heterogeneous and anisotropic, purely deterministic calibration often falls short, and inverse analysis is commonly applied to iteratively improve model accuracy using monitoring data.

  In this study, calibration was carried out iteratively against inclinometer measurements of lateral wall displacements, ensuring that both the magnitude and the shape of deformation profiles were captured. A grouped sensitivity analysis was first performed to identify the parameters with the strongest influence on predicted displacements across dredging phases. Parameters were varied within bounds derived from CPT-based correlations and literature, while others were kept constant, to assess their relative impact. The results highlighted the friction angles of Layers 1 and 2 and the stiffness moduli of Layers 2 and 3 as the most influential. Changes in friction angle primarily controlled the ultimate magnitude of displacements through their effect on active earth pressures, while stiffness variations dictated the curvature and depth distribution of the displacement profile.

  Layer-specific modifications were then introduced based on both CPT correlations and inclinometer response trends. For instance, the friction angle of Layer 1 was increased to 38° to reflect its cleaner, more frictional sand character, while its stiffness was reduced to reproduce the larger early-stage movements observed in the field. Layer 3 parameters were substantially raised, with ϕ increased from 37° to 40° and stiffness values adjusted upward in line with its high q_c (40.6 MPa), low I_c, and high relative density ($D_r \approx 72\%$), consistent with dense sand–gravel deposits. Similar targeted adjustments were applied to Layers 2 and 4, ensuring consistency with site data while improving agreement between model predictions and inclinometer profiles. These adjustments were empirical but grounded in both CPT evidence and observed behavior.

  Validation was performed by comparing the calibrated model predictions against independent inclinometer readings across dredging phases. The deviations were consistently within the commonly accepted margin of ±30%, with errors as low as 11%. This confirmed that the final model provided a robust and reliable representation of the quay wall's mechanical behavior during excavation.

  It is important to acknowledge the limitations of the available data. Direct calibration against laboratory test results was not feasible, as the triaxial consolidated undrained (CU) tests were of poor quality and relied on incorrect assumptions regarding drainage and boundary conditions. Similarly, a fully probabilistic calibration framework was not pursued due to two main constraints: the limited number of CPTs in the study area and the computational effort required for probabilistic simulations.

  For these reasons, the calibration strategy adopted in this thesis occupied an intermediate position between deterministic and semi-probabilistic approaches. A structured sensitivity analysis

was first used to highlight the influence of key parameters and soil layers on lateral wall displacements, after which targeted calibration and validation were performed against inclinometer data. This hybrid approach ensured that the most critical uncertainties were addressed, while avoiding the impracticalities associated with full probabilistic modeling.

In summary, reliable calibration and validation of quay wall FEM models under dredging conditions require the integration of high-quality field monitoring data, refinement of soil parameters guided by CPT-based correlations, and the use of sensitivity analyses to prioritize calibration efforts. The intermediate approach adopted in this study proved effective in strengthening the robustness of the final model despite limitations in laboratory data and the infeasibility of a fully probabilistic framework.

- **How can the Finite Element Method be applied to model the interaction between the quay wall structure and the surrounding soil during dredging?**

  In this thesis, the Finite Element Method proved effective in simulating the interaction between the quay wall and the surrounding soil during dredging. The method captured the main deformation mechanisms and internal forces, showing how unloading in front of the wall and increased earth pressures behind it combine to drive wall movements. Comparison with inclinometer data confirmed that the model reproduced both the size and shape of displacements with good accuracy. Although the approach requires reliable input data and is computationally demanding, FEM provided valuable insights into the behavior of quay walls.

- **Which soil constitutive model will be used to represent soil behavior in the finite element model, and how will its input parameters be derived?**

  In this study, the Hardening Soil (HS) model is employed as the primary constitutive model to represent the mechanical behavior of the soil in the finite element analysis. The HS model is preferred over simpler models such as Mohr-Coulomb due to its ability to account for stress-dependent stiffness, pre-consolidation effects, and the distinction between loading and unloading stiffness, thereby providing a more realistic representation of soil behavior under staged excavation and dredging.

  A supplementary analysis using the Hardening Soil model with small-strain stiffness (HSsmall) was also carried out to evaluate the influence of strain-dependent stiffness on the predicted wall displacements. However, the difference between HS and HSsmall models in this case was found to be minor, with lateral displacement variations generally within 1–3 mm during initial dredging phases and negligible in the final phase. This limited impact is attributed to the relatively high stiffness values derived from Cone Penetration Test (CPT) data, which result in low mobilized shear strains. Consequently, the advantages of the HSsmall model did not substantively enhance the model's predictive capability, and the standard HS model was deemed sufficient for further analysis due to its balance between computational efficiency and accuracy.

  Input parameters for the HS model, particularly stiffness and strength parameters, were initially estimated using empirical correlations with CPT results. The layer-averaged cone resistance (q_c) and friction ratio (f_r) were key indicators used to identify soil behavior and classify stratigraphy. These parameters were further interpreted using the Soil Behavior Type Index (I_c), enabling the subdivision of the soil profile into four distinct layers. While this approach provides a sound basis for parameter estimation, local heterogeneity and variability in CPT results necessitated iterative calibration to align model outputs with observed field measurements, especially inclinometer data.

  The calibration process involved adjustments to both stiffness and strength parameters. For instance, Layer 1, initially characterized by a low friction ratio indicating clean, dense sand, was assigned a higher friction angle, but its stiffness was reduced to match observed deformations. In contrast, Layer 2, with higher f_r values suggesting greater fines content, received reductions in both stiffness and strength. Layers 3 and 4 were refined based on their respective trends in CPT

data, ensuring consistency with expected behavior. These adjustments were validated through comparison with inclinometer records and contributed to improved model reliability.

To support the CPT-based parameter derivation, laboratory tests, specifically Consolidated Undrained (CU) triaxial tests, were analyzed. Although these tests were intended to provide supplemental stiffness and strength data, their interpretation proved challenging. Several inconsistencies were observed: the reported undrained shear strengths, stiffness moduli, and friction angles were uncharacteristically high for fine-grained soils. Moreover, saturation ratio such as Skempton's B-values were borderline or slightly below acceptable thresholds, raising questions about sample quality and the reliability of test results.

Further investigation using sieve analysis revealed that the tested samples, originally classified as clay, actually consisted primarily of medium to fine sand with limited fines content. This re-classification supports the earlier CPT-based interpretation and further justifies the reliance on CPT data for defining the global stratigraphy. While the triaxial tests provided some validation for strength parameters, especially friction angles, which aligned well with CPT-derived estimates—their stiffness results were considered less reliable due to possible sample disturbance, incomplete saturation, and inappropriate test type selection.

In summary, the HS model was selected as the most suitable constitutive model for this study due to its ability to simulate non-linear, stress-dependent soil behavior under staged loading. Input parameters were primarily derived from CPT-based empirical correlations, and refined through inverse analysis and comparison with field data. Laboratory tests provided supplementary validation but were interpreted cautiously due to quality concerns. The combination of CPT interpretation, model calibration, and selective laboratory data usage ensured a robust representation of soil behavior within the finite element framework.

5.1.3. Research Main Question

The aim of this research is to develop, calibrate, and validate a reliable finite element model (FEM) for a quay wall in the Amaliahaven Project in the Port of Rotterdam, using field measurement data collected during the dredging construction phase. The main research question that is based on this objective is:

How can a finite element model be developed, calibrated, and validated to accurately simulate the behavior of a quay wall in the Port of Rotterdam?

This research showed that a reliable FEM of the quay wall can be achieved when calibration is guided by sensitivity analysis and validated against field measurements. The results demonstrated that the hinge or fixed assumption at the wall connection significantly affects predicted displacements, with the real behavior likely lying in between. Sensitivity analyses further revealed that a 10% change in soil friction angle can cause large differences in wall displacement, highlighting the critical influence of strength parameters. Calibration reduced prediction errors to within 6–14%, confirming that the FEM could reproduce the magnitude and shape of observed displacements with good accuracy. The parametric study showed that deeper dredging and higher surcharge loads lead to substantial increases in wall movement, while soil stiffness mainly affects the deformation profile.

Overall, the study confirmed that FEM is a powerful tool for understanding quay wall performance during dredging, provided that key parameters are carefully calibrated. The findings underline the importance of accurate soil characterization and realistic structural assumptions, as even small parameter variations can strongly influence predicted displacements.

5.2. Recommendations

Based on the findings and limitations identified in this study, several recommendations are proposed to improve the reliability and applicability of finite element modelling for assessing quay wall performance during dredging activities.

The observed mismatch between FEM-predicted and measured front wall displacements, particularly in the rotation pattern, suggests that the simplified hinge assumption does not fully capture the actual connection behaviour. Given that the fixed-connection model produced better agreement with inclinometer data, future analyses should explore semi-rigid connection modelling to more accurately represent the partial rotational restraint likely present in reality. This adjustment could improve accuracy in predicting landside displacement trends.

The sensitivity analysis in this study showed that the most important factors were the friction angles of Layers 1 and 2 and the stiffness of Layers 2 and 3. Using sensitivity analysis at the start of future projects is recommended, as it helps focus calibration on the parameters that matter most. This makes the process more efficient, avoids spending time on less important inputs, and ensures that changes in parameters can be directly linked to improvements in model performance.

While the calibration method used in this study reduced displacement differences to within acceptable engineering limits, it did not capture the uncertainty of the final soil parameters. Future work should use probabilistic approaches, such as Bayesian updating, to provide not only best-fit values but also confidence ranges. This would be especially useful in areas like the Port of Rotterdam, where soil conditions are highly variable.

This study focused mainly on quay wall behaviour during dredging. However, long-term performance is also important. Effects such as tidal cycles, temperature changes, anchor load relaxation, and corrosion were not included in the analysis. Adding these factors into FEM models, together with long-term monitoring and inspections, would allow better assessment of serviceability and durability over the entire design life.

The FEM developed here proved useful as a predictive tool. With proper calibration and validation, it can be applied to study the impact of future changes such as heavier crane loads, deeper dredging, or climate-related effects. The parametric study showed that dredging depth, surcharge loading, and soil properties strongly affect quay wall behaviour. These factors should be included in predictive assessments to support safer design and better operational planning.

In conclusion, improving how wall connections are modelled, combining sensitivity analysis with calibration, enhancing monitoring, accounting for long-term effects, and using FEM for scenario testing will make future quay wall performance assessments more reliable and robust.

Bibliography

[1] ArcelorMittal. (2019, June 4). *Steel Combined Wall Systems*. Informational brochure on foundation solutions for quay walls and marine infrastructure. ArcelorMittal Projects Europe, Heijningen, Netherlands.

[2] G. B. Baecher and J. T. Christian, *Reliability and Statistics in Geotechnical Engineering*. John Wiley & Sons, 2003.

[3] Brinkgreve, R. B. J., Engin, E., & Engin, H. K. (2010). Validation of empirical formulas to derive model parameters for sands. In T. Benz & S. Nordal (Eds.), *Numerical Methods in Geotechnical Engineering (NUMGE 2010)* (pp. 137–142). CRC Press.

[4] Brinkgreve, R. B. J. (2019). *PLAXIS Scientific Manual*. PLAXIS BV, Netherlands.

[5] Brinkgreve, R. B. J. (2019a), *PLAXIS 2D 2019 Reference Manual*, Bentley Systems; CUR (2003), *Geotechnical Design: Handbook for the Design of Retaining Walls* (CUR Publication 166), CUR/PBV; Obrzud, R., & Truty, A. (2018), *The Hardening Soil Model: A Practical Guidebook with Examples*, ZSoil.PC, Lausanne.

[6] Brinkgreve, R. B. J. (2021, February 24). *The Hardening Soil Model*. Bentley Systems Blog. Retrieved from `https://blog.bentley.com/software/the-hardening-soil-model/`

[7] Burton, G. J., & Airey, D. W. (2003). Strain rate calculation in consolidated undrained triaxial testing and implications on design strengths. *Centre for Geotechnical and Materials Modelling, University of Newcastle, and Centre for Geotechnical Research, University of Sydney*.

[8] B. M. Das and N. Sivakugan, *Principles of geotechnical engineering* (10th ed.). Cengage Learning, 2021.

[9] den Adel, N. (2018). *Load testing of a quay wall: An application of Bayesian Updating*. MSc Thesis, Delft University of Technology.

[10] *Quay Walls* (2nd ed.). Boca Raton, FL: CRC Press.

[11] Douglas Partners. (2023). *How Inclinometers Assist Geotechnical Monitoring*. Retrieved from `https://www.douglaspartners.com.au/knowledge-sharing/how-inclinometers-assist-geotechnical-monitoring/`

[12] Duffy, K., Gavin, K., Korff, M., de Lange, D., & Roubos, A. (2024). Influence of installation method on the axial capacity of piles in very dense sand. *Journal of Geotechnical and Geoenvironmental Engineering, American Society of Civil Engineers (ASCE)*.

[13] Gumucio, J. P. L. (2013). *Design and economic evaluation of relieving quay wall structures*. Delft University of Technology. Retrieved from http://repository.tudelft.nl/

[14] D. V. Griffiths and G. A. Fenton, *Bearing capacity of spatially random soil: The undrained clay Prandtl problem revisited*, Géotechnique, vol. 51, no. 4, pp. 351–359, 2001.

[15] International Information Center for Geotechnical Engineers. (n.d.). *Slope Inclinometers*. Geoengineer.org. Retrieved from `https://www.geoengineer.org/education/instrumentation/slope-inclinometers`

[16] Huang, J., Kelly, R., & Sloan, S. W. (2016). *Enhanced data interpretation: combining in-situ test data by Bayesian updating*. In Geotechnical and Geophysical Site Characterisation 5 – Lehane, Acosta-Martínez & Kelly (Eds), Australian Geomechanics Society, Sydney, Australia, ISBN 978-0-9946261-2-7.

[17] Kulhawy, F. H., & Mayne, P. W. (1990). *Manual on estimating soil properties for foundation design* (No. EPRIEL-6800). Electric Power Research Institute, Palo Alto, CA; Cornell University, Ithaca, NY, Geotechnical Engineering Group.

[18] Korff, M. (2023). *Reader Deep Excavations: CIEM2000 Unit 3 – Design, Execution and Monitoring of Deep Excavations with Retaining Walls*. Delft University of Technology.

[19] S. Lee, *Uncertainty Quantification in Geotechnical Engineering*, Number Analytics Blog, June 11, 2025. Available at: https://www.numberanalytics.com/blog/uncertainty-quantification-in-geotechnical-engineering

[20] Mayne, P. W., Cargill, E., & Greig, J. (2023). *The Cone Penetration Test: Better Information, Better Decisions – A CPT Design Parameter Manual* (Rev. 1.1). ConeTec.

[21] NEN 5117. (1991). *Geotechnics – Determination of shear resistance and deformation parameters of soil – Triaxial test*. Nederlands Normalisatie-Instituut, 1e druk, December 1991.

[22] K. K. Phoon and F. H. Kulhawy, "Characterization of geotechnical variability," *Canadian Geotechnical Journal*, vol. 36, no. 4, pp. 612–624, 1999. https://doi.org/10.1139/t99-038

[23] PIANC/KIVI. (2023, September 14). *Panama Canal Expansion Program*. Presentation at PIANC/KIVI event. Rotterdam, Netherlands.

[24] PORR. (n.d.). *Grouted anchors*. In PORR's Special Civil Engineering Wiki. Retrieved from https://porr.de/wiki-special-civil-engineering/grouted-anchors/

[25] Port of Rotterdam. (2024). *Quay wall construction Amaliahaven*. Retrieved from https://www.portofrotterdam.com/en/building-port/ongoing-projects/quay-wall-construction-amaliahaven

[26] Robertson, P. K., & Cabal, K. L. (2010, May). Estimating soil unit weight from CPT. In *2nd International Symposium on Cone Penetration Testing* (pp. 2–40).

[27] R. K. Rowe and S. K. Ho, "Continuous wall deflections and lateral earth pressures due to compaction," *Canadian Geotechnical Journal*, vol. 34, no. 3, pp. 409–418, 1997. https://doi.org/10.1139/t97-004

[28] Roubos, A. A., Schweckendiek, T., Brinkgreve, R. B. J., Steenbergen, R. D. J. M., & Jonkman, S. N. (2020). *Reliability assessments of quay walls using FEM*. Georisk: Assessment and Management of Risk for Engineered Systems and Geohazards, 15(3), 165–181. DOI: 10.1080/17499518.2020.1756344

[29] SAALG Geomechanics, *Managing Geotechnical Uncertainty in Extreme Terrain Conditions*, SAALG Blog, Dec. 10, 2024. Available at: https://www.saalg.com/post/managing-geotechnical-uncertainty-in-extreme-terrain-conditions-1

[30] Schanz, T., Vermeer, P. A., & Bonnier, P. G. (1999). The hardening soil model: formulation and verification. In *Beyond 2000 in Computational Geotechnics* (pp. 281–296).

[31] Schouten, O. (2020). *Optimising the functionality of smart quay walls using measurement data obtained during the construction process: A case study in the port of Rotterdam: HHTT-quay*. Delft University of Technology. Retrieved from http://repository.tudelft.nl/

[32] H. B. Seed and R. V. Whitman, "Design of earth retaining structures for dynamic loads," in *ASCE Specialty Conference on Lateral Stresses in the Ground and Design of Earth Retaining Structures*, pp. 103–147, 1970.

[33] Seo, S., Park, J., Ko, Y., Kim, G., & Chung, M. (2023). *Geotechnical factors influencing deformation during excavation*. Frontiers in Earth Science. DOI: 10.3389/feart.2023.1263997

[34] I. M. Smith and D. V. Griffiths, *Programming the Finite Element Method*, 4th ed., John Wiley & Sons, Ltd., 2004.

[35] Tolba, E. R., Abd Ellah, S., Galal, E. M., Sallam, E. A., & Kamal, M. A. (2020). *Comparative analyses of quay wall case study using Plaxis 3D*. IJASR, 3(2), March–April. ISSN: 2581-7876.

[36] TU Delft. (2024, October 30). *15536_Proefbelasting RWG kade*. Presented during the meeting on test loading of the RWG quay wall. Delft, Netherlands.

[37] Wolters, P., Bakker, K. J., & de Gijt, J. G. (2012). *Real-world complexities in FEM quay wall modeling*. Geotechnical Engineering Journal.

References.tex [heading=bibintoc,title=References]

A

Parametric Study

Phase	Parameter	Param Value	Value Type	Run ID	Max Disp (mm)	Depth at Max (m NAP)	Diff (%)
Phase 3	phi_1	32	Lower	14	19.7	-11.5	18.1
Phase 3	phi_1	40	Upper	68	13.9	-12.5	-16.8
Phase 3	phi_1	32.3	Intermediate	82	19.4	-11.5	16.6
Phase 3	phi_1	33.9	Intermediate	83	18.5	-12.5	11.1
Phase 3	phi_1	34.5	Intermediate	84	17.7	-12.5	6.5
Phase 3	phi_1	37.4	Intermediate	86	15.6	-12.5	-6.0
Phase 3	phi_1	38.1	Intermediate	87	15.2	-12.5	-9.0
Phase 3	phi_2	28	Lower	32	19.1	-12.5	14.6
Phase 3	phi_2	34	Upper	50	15.1	-11.5	-9.5
Phase 3	phi_2	28.5	Intermediate	88	18.4	-12.5	10.5
Phase 3	phi_2	29	Intermediate	89	18.0	-12.5	8.3
Phase 3	phi_2	33.1	Intermediate	92	15.6	-12.5	-6.5
Phase 3	phi_2	33.7	Intermediate	93	15.2	-11.5	-8.7
Phase 3	E50_2	25000	Lower	38	18.0	-12.5	8.0
Phase 3	E50_2	41000	Upper	44	15.8	-12.5	-5.0
Phase 3	E50_2	26200	Intermediate	95	17.8	-12.5	6.7
Phase 3	E50_3	50000	Lower	40	18.1	-12.5	9.0
Phase 3	E50_3	84000	Upper	42	15.8	-12.5	-5.2
Phase 6	phi_1	32	Lower	14	37.6	-13.5	10.6
Phase 6	phi_1	40	Upper	68	30.7	-14.5	-9.9
Phase 6	phi_1	32.3	Intermediate	82	37.4	-13.5	9.8
Phase 6	phi_1	33.9	Intermediate	83	35.9	-13.5	5.6
Phase 6	phi_1	38.1	Intermediate	87	32.2	-13.5	-5.3
Phase 6	phi_2	28	Lower	32	37.8	-14.5	11.2
Phase 6	phi_2	34	Upper	50	30.8	-13.5	-9.4
Phase 6	phi_2	28.5	Intermediate	88	37.0	-14.5	8.9

Phase 6	phi_2	29	Intermediate	89	36.5	-13.5	7.1
Phase 6	phi_2	33.1	Intermediate	92	31.7	-13.5	-6.7
Phase 6	phi_2	33.7	Intermediate	93	31.1	-13.5	-8.5
Phase 6	E50_3	50000	Lower	40	37.5	-13.5	10.2
Phase 6	E50_3	84000	Upper	42	31.9	-13.5	-6.3

run	phi_1	phi_2	E50_2	EOedRef_2	EURRef_2	E50_3	EOedRef_3	EURRef_3
1	32	28	25000	25000	75000	50000	50000	150000
2	32	28	25000	25000	75000	67000	67000	201000
3	32	28	25000	25000	75000	84000	84000	252000
4	32	28	33000	33000	99000	50000	50000	150000
5	32	28	33000	33000	99000	67000	67000	201000
6	32	28	33000	33000	99000	84000	84000	252000
7	32	28	41000	41000	123000	50000	50000	150000
8	32	28	41000	41000	123000	67000	67000	201000
9	32	28	41000	41000	123000	84000	84000	252000
10	32	31	25000	25000	75000	50000	50000	150000
11	32	31	25000	25000	75000	67000	67000	201000
12	32	31	25000	25000	75000	84000	84000	252000
13	32	31	33000	33000	99000	50000	50000	150000
14	32	31	33000	33000	99000	67000	67000	201000
15	32	31	33000	33000	99000	84000	84000	252000
16	32	31	41000	41000	123000	50000	50000	150000
17	32	31	41000	41000	123000	67000	67000	201000
18	32	31	41000	41000	123000	84000	84000	252000
19	32	34	25000	25000	75000	50000	50000	150000
20	32	34	25000	25000	75000	67000	67000	201000
21	32	34	25000	25000	75000	84000	84000	252000
22	32	34	33000	33000	99000	50000	50000	150000
23	32	34	33000	33000	99000	67000	67000	201000
24	32	34	33000	33000	99000	84000	84000	252000
25	32	34	41000	41000	123000	50000	50000	150000
26	32	34	41000	41000	123000	67000	67000	201000
27	32	34	41000	41000	123000	84000	84000	252000
28	36	28	25000	25000	75000	50000	50000	150000
29	36	28	25000	25000	75000	67000	67000	201000
30	36	28	25000	25000	75000	84000	84000	252000
31	36	28	33000	33000	99000	50000	50000	150000
32	36	28	33000	33000	99000	67000	67000	201000
33	36	28	33000	33000	99000	84000	84000	252000
34	36	28	41000	41000	123000	50000	50000	150000
35	36	28	41000	41000	123000	67000	67000	201000
36	36	28	41000	41000	123000	84000	84000	252000
37	36	31	25000	25000	75000	50000	50000	150000
38	36	31	25000	25000	75000	67000	67000	201000
39	36	31	25000	25000	75000	84000	84000	252000
40	36	31	33000	33000	99000	50000	50000	150000
41	36	31	33000	33000	99000	67000	67000	201000
42	36	31	33000	33000	99000	84000	84000	252000
43	36	31	41000	41000	123000	50000	50000	150000

44	36	31	41000	41000	123000	67000	67000	201000
45	36	31	41000	41000	123000	84000	84000	252000
46	36	34	25000	25000	75000	50000	50000	150000
47	36	34	25000	25000	75000	67000	67000	201000
48	36	34	25000	25000	75000	84000	84000	252000
49	36	34	33000	33000	99000	50000	50000	150000
50	36	34	33000	33000	99000	67000	67000	201000
51	36	34	33000	33000	99000	84000	84000	252000
52	36	34	41000	41000	123000	50000	50000	150000
53	36	34	41000	41000	123000	67000	67000	201000
54	36	34	41000	41000	123000	84000	84000	252000
55	40	28	25000	25000	75000	50000	50000	150000
56	40	28	25000	25000	75000	67000	67000	201000
57	40	28	25000	25000	75000	84000	84000	252000
58	40	28	33000	33000	99000	50000	50000	150000
59	40	28	33000	33000	99000	67000	67000	201000
60	40	28	33000	33000	99000	84000	84000	252000
61	40	28	41000	41000	123000	50000	50000	150000
62	40	28	41000	41000	123000	67000	67000	201000
63	40	28	41000	41000	123000	84000	84000	252000
64	40	31	25000	25000	75000	50000	50000	150000
65	40	31	25000	25000	75000	67000	67000	201000
66	40	31	25000	25000	75000	84000	84000	252000
67	40	31	33000	33000	99000	50000	50000	150000
68	40	31	33000	33000	99000	67000	67000	201000
69	40	31	33000	33000	99000	84000	84000	252000
70	40	31	41000	41000	123000	50000	50000	150000
71	40	31	41000	41000	123000	67000	67000	201000
72	40	31	41000	41000	123000	84000	84000	252000
73	40	34	25000	25000	75000	50000	50000	150000
74	40	34	25000	25000	75000	67000	67000	201000
75	40	34	25000	25000	75000	84000	84000	252000
76	40	34	33000	33000	99000	50000	50000	150000
77	40	34	33000	33000	99000	67000	67000	201000
78	40	34	33000	33000	99000	84000	84000	252000
79	40	34	41000	41000	123000	50000	50000	150000
80	40	34	41000	41000	123000	67000	67000	201000
81	40	34	41000	41000	123000	84000	84000	252000
82	32,3	31	33000	33000	99000	67000	67000	201000
83	33,9	31	33000	33000	99000	67000	67000	201000
84	34,5	31	33000	33000	99000	67000	67000	201000
85	35,4	31	33000	33000	99000	67000	67000	201000
86	37,4	31	33000	33000	99000	67000	67000	201000
87	38,1	31	33000	33000	99000	67000	67000	201000
88	36	28,5	33000	33000	99000	67000	67000	201000
89	36	29	33000	33000	99000	67000	67000	201000

90	36	30,8	33000	33000	99000	67000	67000	201000
91	36	31,9	33000	33000	99000	67000	67000	201000
92	36	33,1	33000	33000	99000	67000	67000	201000
93	36	33,7	33000	33000	99000	67000	67000	201000
94	36	31	28100	28100	84300	67000	67000	201000
95	36	31	26200	26200	78600	67000	67000	201000
96	36	31	36300	36300	108900	67000	67000	201000
97	36	31	28700	28700	86100	67000	67000	201000
98	36	31	33000	33000	99000	61500	61500	184500
99	36	31	33000	33000	99000	62300	62300	186900
100	36	31	33000	33000	99000	66600	66600	199800
101	36	31	33000	33000	99000	78900	78900	236700